國 立 交 通 大 學
電機與控制工程學系

博 士 論 文

以自迴歸模型為基礎之禪坐腦電波隨時空變異之頻譜分析

Time-varying Spatio-spectral Analysis of Zen-meditation EEG

based on Autoregressive Models

研 究 生：廖憲正

指導教授：羅佩禎 博士

中 華 民 國 九 十 六 年 六 月

以自迴歸模型為基礎之禪坐腦電波隨時空變異之頻譜分析

Time-varying Spatio-spectral Analysis of Zen-meditation EEG

based on Autoregressive Models

研 究 生：廖憲正　　　　　　　　　　Student：Hsien-Cheng Liao

指導教授：羅佩禎　　　　　　　　　　Advisor：Pei-Chen Lo

國 立 交 通 大 學

電機與控制工程學系

博 士 論 文

A Dissertation

Submitted to Department of Electrical and Control Engineering

College of Electrical and Computer Engineering

National Chiao Tung University

In Partial Fulfillment of the Requirements

For the Degree of

Doctor of Philosophy

in

Electrical and Control Engineering

June 2007

Hsinchu, Taiwan, Republic of China

中華民國九十六年六月

獻給我的父母

廖方觀先生與廖李時女士

To my parents

Fang-Du Liao and Li-Shih Liao

以自迴歸模型為基礎之禪坐腦電波隨時空變異之頻譜分析

學生：廖憲正　　　　　　　　　　　　　指導教授：羅佩禎 博士

國立交通大學電機與控制工程研究所

摘要

　　本論文主要利用單變數（univariate）與多變數（multivariate）之自迴歸模型（autoregressive model）來分析探討禪坐腦電波時間與空間之特性。在第一章的背景簡介之後，第二章提出了一個可程式化的方法 Subband-AR EEG Viewer 來進行腦電波的分析，該方法主要是追蹤禪坐中腦電波隨時間變化的頻譜特性，繼而可以提供禪坐腦電波的總覽。為了達到這樣的目的，禪坐腦電波首先會經由樹狀的濾波器組（filter banks）分解成子頻帶成份（subband components）。然後每個子頻帶成份再利用二階的自迴歸模型求出其主要頻率，利用求出來的主要頻率可以針對所欲解決的問題來設計演算法。根據 Subband-AR EEG Viewer，我們發展了兩個特別用來研究禪坐中的視覺感知能力與禪坐腦電波時空特性的演算法。這些演算法在實際應用上不需要繁複決定參數的程序，並且因為採用了二階自迴歸模型而大大的降低了運算量。因此這個方法非常適合用來進行長時間的腦電波分析與即時處理。

　　在禪坐的視覺誘發電位（visual evoked potentials）研究中常會遇到一個問題就是無法得知可以作為參考的實際禪坐狀態來給予刺激，為了讓每一個視覺誘發電位取得時的大腦狀態盡量維持一致，我們選擇在前額α波出現時給予閃光刺激，這是因為前額α波被發現在禪坐的過程中會有顯著的增加，因此，我們根據第二章所述的 Subband-AR EEG Viewer 設計出一個即時的α波偵測器，如此一來，每一個視覺誘發電位便會是在類似的背景腦電波下所取得。然後我們再利用α波下之視覺誘發電位（alpha-dependent F-VEPs）來研究禪坐中大腦對於刺激的動態變化。根據實驗設計所得出的結果顯示出禪坐組與控制組有顯著的差異，與控制組在休息狀態下的比較下，禪坐組在禪坐中，特別是在 Cz 和 Fz 的視覺誘發電位 P1-N2 和 N2-P2 的振幅上有明顯的增加。因此，我們推測禪坐會導致主要視覺皮質層以及其相關區域對於閃光刺激產生較大振幅的反應。

　　另一個由 Subband-AR EEG Viewer 演繹過來的演算法為一個結合多重解析度（multi-resolution）技術與自迴歸模型的腦電波解讀器，它可以辨別出腦電波的低振幅波(ϕ), δ, θ, χ, α, 和 β 波，另外，對於常見的雜訊如基準線飄移（baseline drift）和肌電圖干擾（electromyograph interference）也可以被這個解讀器所偵測出來。這個解讀器擁有高效率的計算能力以及容易以硬體實現的特性，因此非常適合用來作為長時間的腦電波解讀以及即時的腦電波處理，它也可以對於大量的腦電波記錄提供一個快速的總覽。

因此，禪坐腦電波階段性的變化就可經由不同灰階值表示不同的腦電波特徵所構成的圖表顯示出來。實驗結果顯示了禪坐組與控制組在時間與空間的腦電波節律特徵上有很大的不同，特別是禪坐中 β 節律在大腦上的傳遞現象。

除了單變數的自迴歸模型外，在這論文的最後，我們也提出了殘餘共變異矩陣（residual covariance matrix），係根據多變數的自迴歸模型所發展出來的一個評估腦電波時空一致性的指標：LSTS（local spatiotemporal synchronization）指標。LSTS 指標針對大腦局部區域上相鄰腦電波頻道間一致性的程度進行估測。利用 QR 分解，LSTS 指標可以有效率的被計算出來。另外，我們也提供了自迴歸模型階數與相鄰頻道形態選擇的策略。根據初期的結果顯示腦電波頻道間一致性的降低（去一致性）會使得 LSTS 指標的數值增加。爲了評估這個指標的有效性，我們設計了一個由外部指示（externally-paced）的手指運動實驗，結果顯示在主要運動區所產生的去一致性成功的反應出較高數值的 LSTS 指標。 因此，LSTS 指標或許可被用來研究如禪坐等尚未被完全了解的心智活動下大腦的動態變化。在我們的初步結果中，當禪坐中的低振幅波出現時，LSTS 指標顯示了整體腦電波一致性的增加，而這個現象被推測爲與在深層禪坐中較不被環境刺激所影響的狀態有關。

Time-varying Spatio-spectral Analysis of Zen-meditation EEG

based on Autoregressive Models

Student: Hsien-Cheng Liao   Advisor: Dr. Pei-Chen Lo

Institute of Electrical and Control Engineering

National Chiao-Tung University

Abstract

This dissertation reports the study on EEG (electroencephalograph) spatiotemporal characteristics under Zen meditation. Univariate and multivariate AR models were applied. Following the background introduction, Chapter 2 presents a computerized scheme *Subband-AR EEG Viewer* that provides a comprehensive view of the meditation EEG record. The scheme was mainly designed to trace the varying spectral characteristics in meditation EEG. To accomplish this task, a meditation EEG signal was first decomposed into subband components by tree-structured filter banks. The second-order autoregressive model was then applied to each subband component to estimate its root frequency. Based on the estimated root frequencies and sound logic, specific criterion can be deduced for a particular problem-domain application. Two algorithms were developed to investigate the visual perception under meditation and to explore the spatiotemporal characteristics of EEG rhythms. These algorithms do not require exhausting work at determining appropriate parameters in implementation. Further, due to the second-order autoregressive model adopted, the computation load is greatly reduced. This approach is practically favorable to long-term EEG monitoring and real-time processing.

In the study of evoked response potential during Zen meditation, one issue encountered was the inaccessibility to the actual meditation level or stage as a reference. By modifying *Subband-AR EEG Viewer*, an alternative strategy was proposed for dealing with this problem. To secure a consistent condition of the brain dynamics when applying stimulation, a scheme of recording flash visual evoked potentials (F-VEPs) was designed, with main idea of applying flash stimuli during a constant background EEG (electroencephalograph) – frontal α-rhythm dominating activity. This particular activity was found increasing during Zen meditation. Thus the flash-light stimulus was to be applied upon emergence of the frontal α-rhythm. The alpha-dependent F-VEPs were then employed to inspect the effect of Zen meditation on brain dynamics. Based on the experimental protocol proposed, considerable differences between experimental and control groups were obtained. Our results showed that

amplitudes of P1-N2 and N2-P2 on Cz and Fz increased significantly during meditation, contrary to the F-VEPs of control group at rest. We thus suggest that Zen meditation results in acute response on primary visual cortex and the associated parts.

Another algorithm deduced from *Subband-AR EEG Viewer* was a unique interpreter that combined a multi-resolution scheme with autoregressive modeling to identify the EEG patterns including the flat wave (ϕ), δ, θ, χ, α, and β activities. In addition, such artifacts as the baseline drift and EMG (electromyograph) interference were identifiable in the scheme. With the merits of high computational efficiency and easy hardware realization, the method proposed is feasible for long-term EEG monitoring and online EEG processing. It also allows a quick overview of an enormous amount of EEG data and the meditation scenario can be illustrated by a running gray-scale chart with each gray tone coding a particular EEG rhythmic pattern. Moreover, results of applying the proposed scheme to an experimental group (Zen meditation practitioners) and a control group (normal, healthy subjects) revealed significant distinction in spatiotemporal characteristics of EEG rhythmic patterns, especially the spatial propagation of the β rhythm during meditation sessions.

Besides univariate AR model, this dissertation finally presented our study on a parameter called the local spatiotemporal synchronization index (LSTS index), mainly based on residual covariance matrix of a multivariate autoregressive (mAR) model. Analysis of The LSTS index measures the degree of synchronization among neighboring channels of a local brain area. By using the QR factorization, the index can be efficiently calculated. A strategy for determining the AR model order and the array of neighboring channels was also proposed. According to preliminary results, a reduction of synchronization (or, significant desynchronization) of evaluated brain areas was quantified by a relatively high index. An externally-paced finger-movement experiment was designed to evaluate the proposed method. The LSTS index estimated successfully reflected the spatiotemporal desynchronization in the primary motor area. Accordingly, the LSTS measurement could be considered as a potential approach for investigating the spatiotemporal synchronization of unknown brain dynamics under particular mental process, such as the Zen meditation. In the preliminary findings, the LSTS index of meditation EEG revealed an increasing global synchrony for the extremely low power EEG activities (to be called the 'flat' waves), that had been hypothesized as a *detached* state of sensory perception during deep meditation.

誌　　謝

Contents

List of Tables

List of Figures

Chapter 1－

Introduction

The sages did not treat those who were already ill; they instructed

those who were not yet ill. They did not want to rule those who were

already rebellious; they guided those who were not yet rebellious.

~ 《*Huang Ti Nei Ching*》

A rapid increase in the use of CAM (complementary and alternative medicine) across the Western World has aroused attention of researchers. Zen meditation, classified as the category of *mind-body intervention* in CAM [National Center for Complementary and Alternative Medicine 2002], has been widely practiced on a daily basis for maintaining good health. However, it still has not yet been completely understood by people in CAM or in mainstream Western medicine. Our research group has been attending to how meditation enhanced the mind capacity for maneuvering our bodily functions, emotions and even mental activities. For investigation into brain dynamics during meditation, we thus began the researches on Zen meditation, mostly based on Electroencephalograph (EEG), in 1998. EEG was favored due to not only its ability of exploring brain functions via neuro-electrophysiological basis but its advantage of easily recording implementation and high temporal resolution.

1.1. Background

Over the past four decades, much research has been devoted to investigating meditation benefits to humans. To know more about its benefit to our body, a lot of researches have been devoted to the study of meditation process and phenomena, mostly in the physiological and psychological aspects. Scientific exploration has corroborated the effectiveness of meditation practice on the health promotion which includes regulation of the hormone-level and blood pressure, moderation of stress and anxiety, reduction of chronic pain, etc [Wallace 1970, Wallace et al. 1971, Woolfolk 1975, Elson et al. 1977, Wallace 1986, Jevning et al. 1992, Travis 2001]. According to the experienced practitioners, meditation facilitates a greater sense of calmness, empathy, and compassion. As Western medical practitioners begin to understand the role of mind in health and disease, there has been more interest in both employing meditation in medicine and exploring brain dynamical phenomena during meditation.

EEG has been of great interest in monitoring brain dynamical phenomena during meditation. Although many research studies have been conducted since the 1960s [Wallace 1970, Banquet 1973, Woolfolk 1975, Pagano et al. 1976, Elson et al. 1977, Hebert and Lehmann 1977, West 1980, Aftanas and Golocheikine 2001, Zhang et al. 1988, Travis 2001], there are still a wide spectrum of queries about the brain electrical phenomena (recorded in the form of EEGs) corresponding to various transcendental-consciousness states. In recent years, we have been investigating the Zen meditation EEG in multi-faceted aspects. According to our long-term interactions with the experienced practitioners for several years, the Zen meditation process involves experience of transcending various physiological, mental, and conscious states as follows. A meditator would first attenuate their physical and mental sensors via particular mind-focusing technique, leave off the message transmission from outside world, and keep subconsciousness tranquil during meditation. Moreover, meditators often experience unusual perceptions, for example, loss or distortion of space and time perceptions, sensation

of aureola-surroundings, etc. Especially, in the deeper meditation state, many meditators have experienced the *perception* of inner light [Lo et al. 2003]. Few experienced practitioners may attain the spiritual realm (defined by Zen doctrine). Variations in EEG temporal and spatial activities have been presumed to be associated with the meditation stages, a comprehensive review was published recently [Cahn B.R., Polich 2006]. A scientific approach to exploring the brain behavior under such states of consciousness becomes a matter of significance in understanding the meditation scenario and in advancing neuro-cognitive science.

1.2. Aims of this work

In our meditation studies, each EEG recording has lasted more than 30 minutes for a complete monitoring of the meditation process, so over the years, we have accumulated an enormous amount of data. Analysis of such a large amount of raw EEG data becomes a significant problem. Thus an EEG interpreter capable of providing a fast overview is of acute need. For reducing the complexity of analyzing the long-term EEGs, a number of techniques have been proposed. In general, segmentation methods are used first to break down the EEGs into stationary segments, and then classification schemes are applied to the segmented epochs. Segmentation methods applied to the EEG analysis are mostly based on an autocorrelation function [Michael and Houchin 1979], parametric modeling [Jansen et al. 1981, Amir and Gath 1989], nonlinear energy operator[Agarwal and Gotman 1999], statistical properties [Brodsky et al. 1999], AIC (Akaike Information Criterion) [Inouye et al. 1995], cross-spectrum [Gath and Michaeli 1989], etc. Problems of the methods mentioned above include: difficulty of determining the appropriate implementing parameters and requirement for continual update of parameters [Michael and Houchin 1979, Creutzfeld et al. 1985, Amir and Gath 1989, Inouye et al. 1995, Agarwal et al. 1998, Agarwal and Gotman 1999, Brodsky et al. 1999] which is practically unfeasible for long-term meditation EEG monitoring. Similarly,

most classification schemes, like the artificial neural network approach [Vuckovic et al. 2002], need a particular learning strategy to adjust classifier parameters. In consideration of long-term EEG monitoring, this kind of intensive, time-consuming approach is thus impractical for real-time applications.

The results of previous papers [Banquet 1973, Hebert and Lehmann 1977, West 1980] allow us to hypothesize that one key feature in meditation EEG is the frequency composition. The EEG is a low-frequency signal ranging between DC to 30 Hz or higher. It is commonly classified into delta (0–4Hz), theta (4–8Hz), alpha (8–14Hz), and beta (14–30Hz) rhythms. Conventional spectral analysis uses Fourier Transform to estimate frequency components. However, FFT has had limited application to characterizing low-frequency EEGs and requires numerous data to get acceptable frequency resolution. Moreover, the spectrum estimated this way is often contaminated by noise and low frequency components, which is an inevitable and severe problem in EEGs. Accordingly, spectral analysis based on Fourier Transform may not be feasible for long-term EEG analysis. Another method for examining time-varying frequency activity is the autoregressive (AR) spectral estimation, from which more accurate estimate with better resolution is attainable [Hayes 1996, Pardey et al. 1996, Güler et al. 2001]. Nevertheless, the AR estimates of low frequencies are less reliable than those for high frequencies. However, EEGs are low-frequency signals in the range between DC and 30 Hz (this number is research-oriented and may be higher). The meditation EEG, in particular, may contain substantial amounts of theta and delta activities for some experimental subjects (meditators). The AR method often fails to provide accurate estimate of low-frequency spectral components. To solve this problem, we can use a higher order AR model to estimate the spectrum, but this is at the cost of a heavy computation load.

To deal with the problems mentioned above, we developed a computerized scheme, combining a multiresolution concept with the AR spectrum estimation to facilitate long-term meditation EEG analysis. The main idea of the proposed scheme is to establish an adequate

criterion for classifying the windowed segment, based on the characteristic frequency extracted from subband components, and for eventually identifying different EEG rhythms and then providing an overview of the entire meditation EEG record. The scheme provides more accurate estimates with better resolution and less computation complexity [Liao and Lo 2006]. Moreover, results of EEG overview provided an efficient way of scrutinizing the spatiotemporal characteristics of meditation EEG.

In addition to the EEG rhythmic characteristics, synchronization among different brain regions also provides an alternative way to inspect brain dynamics. According to the assumption of oscillation model [Klimesch 1996, Pfurtscheller and Lopes da Silva 1999], different neuronal networks may oscillate with different frequencies during various mental activities. Various event-related desynchronizations on different brain areas thus provide information for exploring the behavior of neuronal network under particular mental task.

There have been several studies about event-related desynchronization and synchronization (ERD/ERS), in which band power changes were used to evaluate synchrony in specific frequency bands [Pfurtscheller and Lopes da Silva 1999]. Sensory processing and motor behavior might result in focal EEG power suppression in certain rhythms, particularly in the alpha band. Based on the ERD/ERS phenomenon, the scheme of brain–computer interface (BCI) becomes feasible [Wolpaw et al. 2002, Pfurtscheller et al. 2006]. On the other hand, coherence analysis has been employed in quantifying the degree of EEG spatial synchronism for investigating the Alzheimer disease, memory, anxiety, intelligence, sleep, etc. [Locatelli et al 1998, Weiss and Rappelsberger 2000, Duckrow and Zaveri 2005, Knyazev et al. 2005, Thatcher et al. 2005].

In addition to the methods described above, Franaszczuk and Bergey proposed a new measure of synchronization of multichannel ictal and interictal EEG signals based on multivariate autoregressive model [Franaszczuk and Bergey 1999]. Multivariate autoregressive model has been applied to EEG classification [Anderson et al. 1998, Peters et al. 2001, Pei

and Zheng 2004] and coherence analysis [Ding et al. 2000, Möller et al. 2001, Kuś et al. 2004]. In Franaszczuk's work, residual covariance matrix of a multivariate autoregressive model was used to measure the relative level of synchronization between channels. The measure could be interpreted in both the stochastic and the deterministic frameworks. They found, as expected, the increasing synchronization during ictal periods. Moreover, the level of synchronization remains higher after a seizure for a prolonged period.

We further modified Franaszczuk's method of synchronization measure to derive the local spatiotemporal synchronization (LSTS) index that gives a quantitative description of the event-related spatiotemporal synchronization of the brain. Based on the quantified residuals of the multivariate autoregressive model, LSTS index is capable of measuring the degree of temporal synchronization among neighboring channels in a local brain area. Computation efficiency of the method is further improved with the QR factorization used in computing the residual covariance matrix of the multivariate autoregressive model.

The LSTS index was demonstrated to be effective in studying the EEG spatiotemporal behavior in an externally-paced finger-movement experiment. We then utilized this quantitative approach to explore the meditation EEG. Estimated index provides us new insight into particular EEG spatiotemporal behavior observed during meditation process.

1.3. Organization of the dissertation

This dissertation consists of six chapters presenting methods for meditation-EEG research based on univariate and multivariate AR models. Figure 1-1 illustrates the hierarchy associating different chapters.

In the beginning, this chapter makes an introduction to this study and describes the main aim. Chapter 2 reports a computerized scheme *Subband-AR EEG Viewer* that provides a comprehensive view of the meditation EEG record. The scheme is mainly designed to trace

the time-varying spectral characteristics in meditation EEG and could be modified for specific requirements or applications. Two algorithms are introduced for slow α-rhythm detection and meditation EEG interpretation.

```
                    ┌─────────────────┐
                    │    Chapter 1    │
                    │  Introduction   │
                    └─────────────────┘
        univariate AR model  │  multivariate AR model
                    ┌─────────────────┐
                    │    Chapter 2    │
                    │   Subband-AR    │
                    │   EEG Viewer    │
                    └─────────────────┘

┌──────────────┐   ┌──────────────┐   ┌──────────────┐
│  Chapter 3   │   │  Chapter 4   │   │  Chapter 5   │
│ Online α-rhythm│  │ Meditation EEG│  │ Spatiotemporal│
│  detection   │   │ interpreter  │   │synchronization│
└──────────────┘   └──────────────┘   └──────────────┘

              ┌────────────────────────┐
              │       Chapter 6        │
              │ Discussion and Conclusion│
              └────────────────────────┘
```
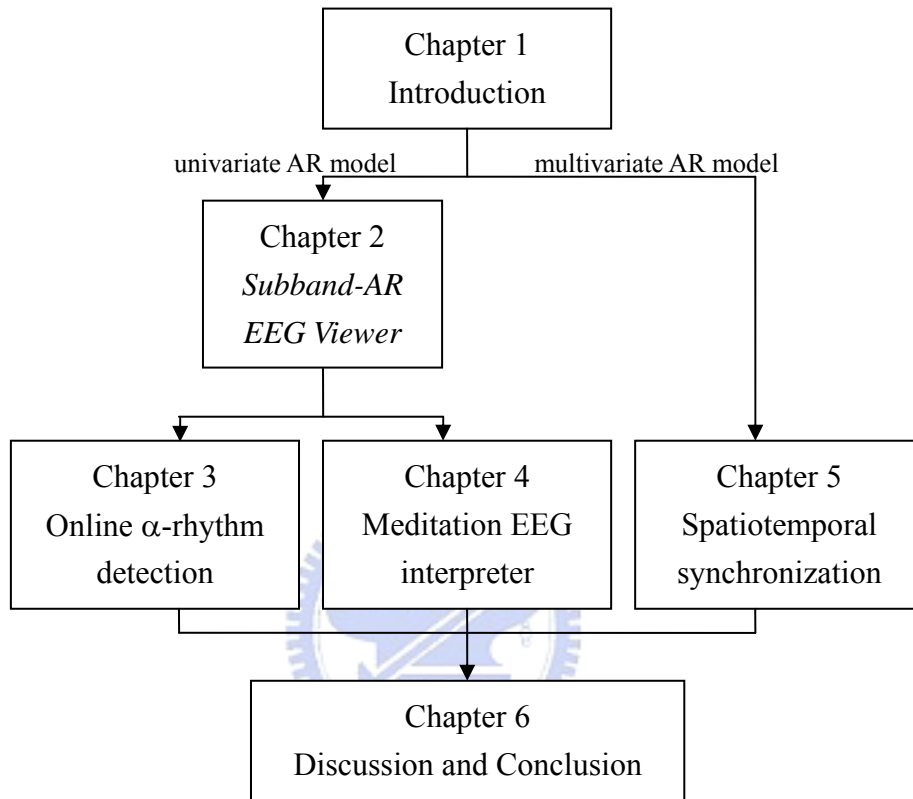
Figure 1-1: Chapter hierarchical structure.

A method for α-rhythm detection was implemented in a real-time manner in Chapter 3. In addition, an alternative strategy was proposed to investigate the human brain in response to external flash stimuli during Zen meditation course. The flash-light stimulus was to be applied upon emergence of the frontal α-rhythm. This study was developed and conducted for further understanding the effect of Zen meditation on human perception.

Chapter 4 describes a software system "meditation EEG interpreter" based on the second algorithm presented in Chapter 2. This interpretation system can identify such EEG patterns like the flat wave (ϕ), δ, θ, χ, α, and β activities. Moreover, it possesses noise screening capa-

bility, especially for rejecting the artifacts like the baseline drift and EMG (electromyograph) interference. It also allows a quick overview of an enormous amount of EEG data.

Besides the univariate AR model employed in meditation EEG research, Chapter 5 focuses on the multivariate autoregressive (mAR) model feasible for quantitative study of spatiotemporal behavior in multichannel EEG. The spatiotemporal synchronization index based on residual covariance matrix of mAR model was proposed. The index measures the degree of synchronization among neighboring channels of a local brain area. A reduction of synchronization (or, significant desynchronization) in the brain areas results in a relatively high index. It might provide a quick inspection of spatiotemporal characteristics for various meditation scenarios.

Significant differences in EEG rhythmic patterns, meditation scenarios, spatiotemporal characteristics, and visual evoked potentials have been observed between experimental and control groups. The last chapter makes a summary of the results obtained from previous chapters.
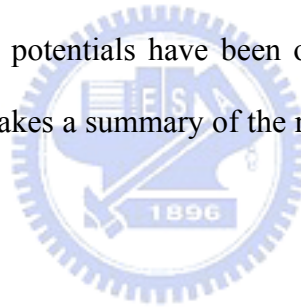
Chapter 2－

Meditation EEG Overview Based on Subband Features Quantified by AR Model

Measurement does not necessarily mean progress. Failing the possibility of measuring that which you desire, the lust for measurement may, for example, merely result in your measuring something else - and perhaps forgetting the difference - or in your ignoring some things because they cannot be measured.

~ George Udny Yule

This chapter reports a computerized scheme *Subband-AR EEG Viewer* that provides a comprehensive view of the meditation EEG record. The scheme was mainly designed to trace the varying spectral characteristics in meditation EEG. Following sections illustrate the main ideas and the methods adopted in the scheme. Two algorithms modified from the scheme are introduced for particular applications. An on-line implementation of the *Subband-AR-EEG Viewer* is also drawn in the end of this chapter.

2.1. Subband-AR-EEG Viewer

The scheme is focused on monitoring the time-varying characteristic frequency in medi-

tation EEG. The AR model is applied to the subband component to quantify the characteristic frequency. Consider that the EEG signal, $x[n]$, is generated by an autoregressive ($AR(p)$) process driven by unit-variance white noise [Theodoridis and Koutroumbas 1999]. A pth order all-pole model is formulated by

$$x[n] + \sum_{k=1}^{p} a_p[k]x[n-k] = w[n] \tag{2-1}$$

where p is the order of the AR model. Based on this model, the spectrum of the EEGs can be obtained if the coefficients $a_p[k]$ are known. Several techniques have been proposed to estimate parameters $a_p[k]$. We apply the autocorrelation method in which the AR coefficients $a_p[k]$ are determined by solving the autocorrelation normal equations

$$\begin{bmatrix} \gamma_x[0] & \gamma_x^*[-1] & \cdots & \gamma_x^*[-p] \\ \gamma_x[1] & \gamma_x[0] & \cdots & \gamma_x^*[-p+1] \\ \vdots & \vdots & \ddots & \vdots \\ \gamma_x[p] & \gamma_x[p-1] & \cdots & \gamma_x[0] \end{bmatrix} \begin{bmatrix} 1 \\ a_p[1] \\ \vdots \\ a_p[p] \end{bmatrix} = \begin{bmatrix} \varepsilon \\ 0 \\ \vdots \\ 0 \end{bmatrix} \tag{2-2}$$

where ε is the modeling error and $\gamma_x[k]$ is the estimated autocorrelation function defined below:

$$\gamma_x[k] = \begin{cases} \dfrac{1}{N} \sum_{n=0}^{N-|k|-1} x[n]x[n+|k|], & |k| \leq N-1, \\ 0 & \text{otherwise,} \end{cases} \tag{2-3}$$

As addressed previously, a higher model order (for example, p ranges from 6 to 14) is normally required to better estimate the low-frequency component in EEGs. According to (2-2), the coefficients of the AR(6) model are determined by $\{\gamma_x[k] \mid 0 \leq k \leq 6\}$. As demonstrated in Table 2-1, the values of the autocorrelation function $\gamma_x[0]$ - $\gamma_x[6]$ for θ and δ rhythms are too close to distinguish between each other, whereas the coefficients for α and β exhibit significant deviation.

10

Table 2-1: Values of autocorrelation function, $\gamma_x[0]$ - $\gamma_x[6]$, computed for δ, θ, α, and β rhythms.

	$\gamma_x[0]$	$\gamma_x[1]$	$\gamma_x[2]$	$\gamma_x[3]$	$\gamma_x[4]$	$\gamma_x[5]$	$\gamma_x[6]$
δ	1.000	0.986	0.948	0.891	0.822	0.746	0.665
θ	1.000	0.985	0.946	0.889	0.823	0.752	0.676
α	1.000	0.946	0.792	0.562	0.287	−0.0004	−0.271
β	1.000	0.872	0.553	0.166	−0.155	−0.323	−0.324

In fact, even increasing the model order to $p=12$ cannot discriminate δ rhythm from θ rhythm. The dominant pole pairs for δ and θ modeled by AR(12) are $0.964\angle\pm0.131$ and $0.959\angle\pm0.129$, respectively, which results in a close estimate of the spectral frequencies (symbol '$\angle$' denotes the phase in radian). In addition, the computational time required by AR(12) becomes four-fold compared with that for AR(6).

A downsampling process ensures the AR modeling better characterizes the low frequency activities. This is revealed by the autocorrelation function values $\gamma_x[0]$ - $\gamma_x[6]$ estimated for δ and θ rhythms downsampled by 8:

$$\gamma_x[k]_\delta: \{1.00, 0.48, -0.18, -0.48, -0.39, -0.03, 0.06\}, \tag{2-4a}$$

$$\gamma_x[k]_\theta: \{1.00, -0.16, 0.26, 0.06, -0.42, 0.02, -0.23\}. \tag{2-4b}$$

Moreover, according to Gabor's uncertainty principle [Oppenheim et al. 1998], downsampling operation improves frequency resolution which is desired for narrow-band EEG. We accordingly employed subband-filtering prior to the frequency analysis by AR modeling.

In summary, EEG signals are firstly decomposed into different subband components by downsampling and filtering. Then the characteristic frequency (root frequency) of each subband component is estimated by the AR(2) model. The entire scheme is called the *Subband-AR EEG Viewer* and it can be illustrated by the tree-structured filter banks shown in Fig.

2-1. In the *Subband-AR EEG Viewer*, a linear-phase lowpass FIR filter $H(z)$ with cutoff frequency 30Hz is used as an anti-aliasing filter before the downsampling operation. Then the AR(2) model is applied to the decimated signal. The filtering-and-downsampling process is repeated until the equivalent cutoff frequency equals 1.875Hz.

Differing from the wavelet decomposition, the *Subband-AR-EEG-Viewer* only employs the lowpass linear-phase filter. A nonlinear-phase filter which is commonly employed in wavelet analysis [Vaidyanathan 1993] would distort the temporal information of EEG and consequently affect the AR model coefficients estimated by the autocorrelation method.

The *Subband-AR-EEG-Viewer* structure (Fig. 2-1) can be rearranged into a six-channel filter banks shown in Fig. 2-2 with decimation ratios which are powers of two. Fig. 2-3 shows the frequency responses of the lowpass filters in the filter banks. The cutoff frequencies of $H_1(z)$, …, $H_5(z)$ are, respectively, 30Hz, 15Hz, 7.5Hz, 3.75Hz, and 1.875Hz (sampling rate: 200Hz).
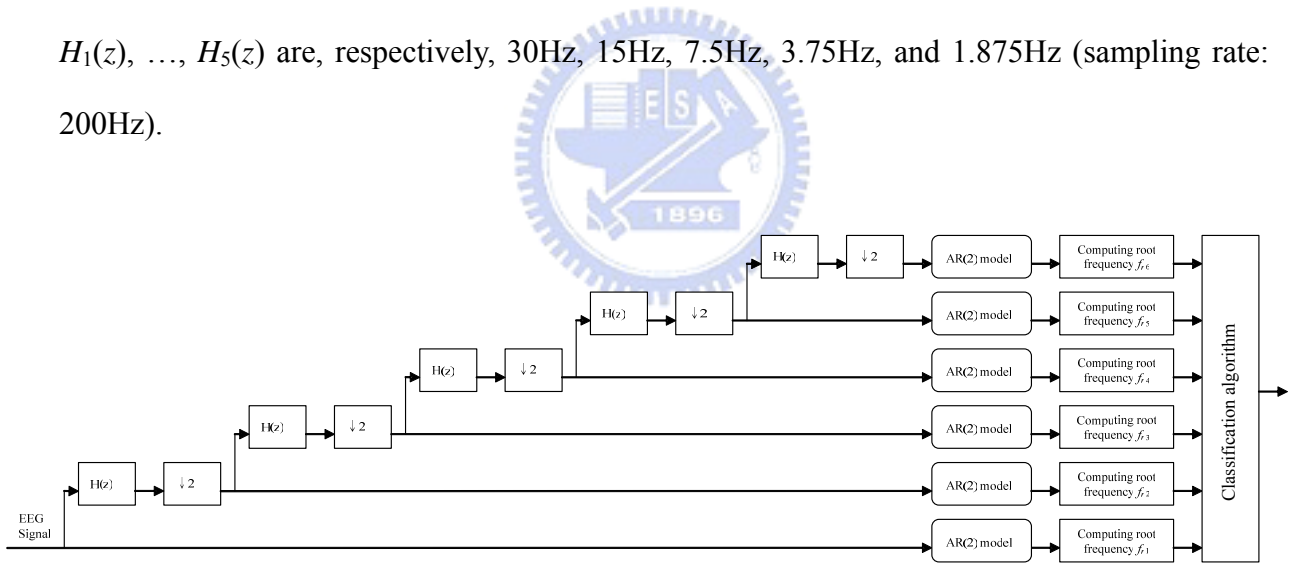
Figure 2-1: The structure for the *Subband-AR-EEG-Viewer*.
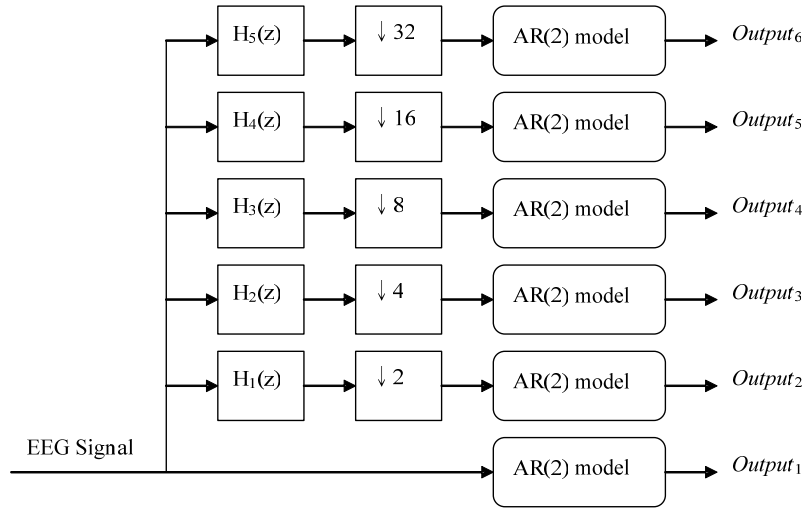
Figure 2-2: The equivalent six-channel system of the subband filter bank.
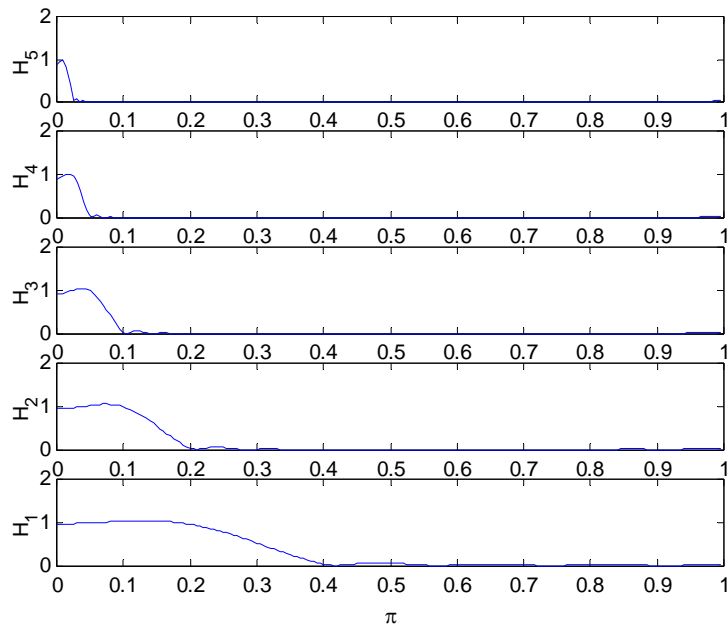
Figure 2-3: The frequency responses of $H_1(z)$, …, $H_5(z)$.

It should be noted that the cutoff frequencies approximate the upper boundaries of the four well-known EEG rhythms— β (14–30Hz), α (8–13Hz), θ (4–7Hz), and δ (below 3Hz). Therefore, changes of the characteristic frequency in meditation EEG can be traced by quantifying the root frequency (f_r) of each subband filtered component. For example, when f_rs of

output$_1$, *output*$_2$ and *output*$_3$ are all within the range 8–13 Hz, the dominant pattern of this windowed segment is identified, to a great degree, as the α rhythm. When *f$_r$*s of *output*$_1$ and *output*$_2$ are greater than 15Hz and *f$_r$* of *output*$_4$ is between 4Hz and 7Hz, the particular segment most likely contains θ intermixed with β rhythm.

After the subband decomposition, the AR(2) model coefficients are computed. An AR(2) model can be expressed as

$$x[n] + a_2[1]x[n-1] + a_2[2]x[n-2] = w[n] \tag{2-5}$$

The model coefficients are directly computed by

$$a_2[1] = -\left(\frac{\gamma_x[1]}{\gamma_x[0]}\right) + \left(\frac{\gamma_x[1]}{\gamma_x[0]}\right)\left(\frac{\gamma_x[0]\gamma_x[2] - \gamma_x[1]^2}{\gamma_x[0]^2 - \gamma_x[1]^2}\right) \tag{2-6}$$

and

$$a_2[2] = -\left(\frac{\gamma_x[0]\gamma_x[2] - \gamma_x[1]^2}{\gamma_x[0]^2 - \gamma_x[1]^2}\right) \tag{2-7}$$

where $\gamma_x[k]$ is the autocorrelation function estimated by (2-3).

The characteristic frequency, also called the root frequency, of *output$_i$* can be estimated from the phase of the pole, or the root of the model equation (2-5) expressed in the frequency domain. After obtaining the model coefficients, the conjugated pole pair is

$$-\frac{a_2[1]}{2} \pm j\frac{\sqrt{4a_2[2] - a_2^2[1]}}{2} \tag{2-8}$$

Therefore, the root frequency f_r can be formulated as

$$f_r = \sin^{-1}\left(\frac{\sqrt{\frac{4a_2[2] - a_2^2[1]}{4}}}{\sqrt{a_2[2]}}\right) \tag{2-9}$$

$$= \sin^{-1}\left(\sqrt{1 - \frac{a_2^2[1]^2}{4a_2[2]}}\right) \approx \sqrt{1 - \frac{a_2^2[1]}{4a_2[2]}}$$

Because the root frequency is much smaller than the sampling frequency, the result of

$\sin^{-1}x$ can be approximated by x. For example, the α rhythm having a higher frequency of 13Hz results in a normalized radian frequency of 0.13π (assume $f_s = 200$Hz). The approximation only causes a 2.8% deviation from the true value. It should be noted that $output_2$-$output_6$ are the results of downsampling (Fig. 2-2), the root frequency $f_{r,i}$ should be further divided by 2^{i-1}. According to equations (2-6) to (2-9), root frequency of each subband component depends on $\gamma_x[0]$, $\gamma_x[1]$, and $\gamma_x[2]$. Tracking the root frequency of each subband component provides an efficient way to illustrate the time evolution of the characteristic frequency in meditation EEG.

2.2. Experimental setup and protocol

The meditation EEG signals were recorded using 8-channel SynAmps amplifiers (manufactured by NeuroScan, Inc.) connected to the Pentium MMX-166 (MHz) PC. Due to hardware limitation, we observed EEG characteristics in different regions with the 8-channel, unipolar recording montage involved the electrode sites at O1, O2, Oz, Cz, Pz, F3, F4 and Fz (Fig. 2-4). The common reference was the linked M1-M2 (mastoid electrodes). The EEG signals were pre-filtered by a bandpass filter with passband 0.3–30 Hz, and digitized at 200 Hz sampling rate. Each recording lasted for 45 minutes, which consisted of the first 5-minute background EEG (the subject sat in a normal relaxed position with eyes closed) and the 40-minute meditation EEG. During the meditation session, the subject sat, with eyes closed, in the full-lotus or half-lotus position. Each hand formed a special mudra (called the Grand Harmony Mudra), laid on the lap of the same side. The subject focused on the Zen Chakra and the Dharma Eye Chakra (also known as the "Third Eye Chakra") in the beginning of meditation till transcending the physical and mental realm. The Zen Chakra is located inside the third ventricle, while the Dharma Eye Chakra is located at the hypophysis [Lo et al. 2003].
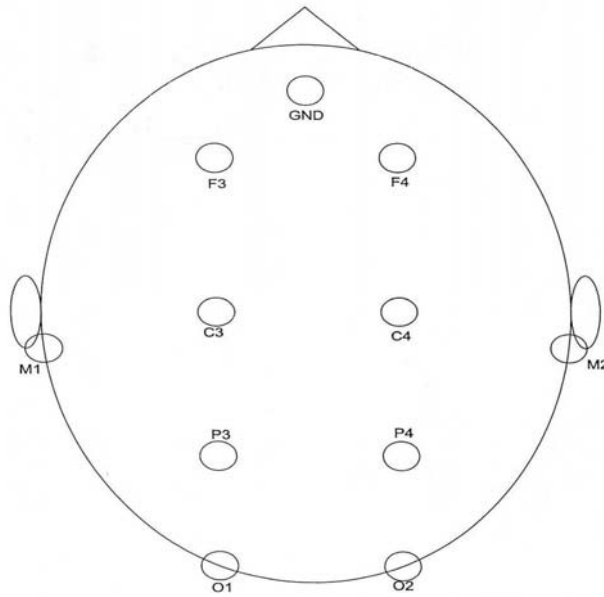
Figure 2-4: 8-channel recording montage.

2.3. Slow alpha rhythm detection (SARD) algorithm

The slow α-rhythm in meditation EEG was found to be related to the early stage of meditation. The first algorithm was designed particularly to detect the slow α-rhythm in the long-term meditation EEG record. The ideas and methods proposed can be implemented in different ways, oriented towards a specific purpose.

2.3.1. The algorithm

Frequency of the α-rhythm ranges from 8Hz to 13Hz. The slow α-rhythm is a particular pattern, normally below 10Hz, that was observed in some experimental subjects at the mind-focusing stage of meditation. The *Subband-AR-EEG-Viewer* can be reduced to the structure (Fig. 2-5(a)) for tracking the slow α-rhythm and the slow alpha rhythm detection (SARD) algorithm is illustrated in Fig. 2-5(b). According to analytical reasoning and practical

experience, *output*₁ in combination with *output*₃ highly enhances the effectiveness of slow α-rhythm detection. Note that $f_{r,1}$ acts as an index to screen out the high-frequency component, and $f_{r,3}$ is employed in the classification as a major reference. The SARD algorithm depicts that the slow α-rhythm pattern is detected when both root frequencies satisfy the following criteria:

$f_{r,1}$ < 14Hz, and

8Hz < $f_{r,3}$ <10Hz.

2.3.2. Simulation

While only examining *output*₁ (up to 30Hz) with the criterion 8Hz < $f_{r,1}$ <10Hz, it often fails to identify the noise-contaminated slow α-rhythm. Figure 2-6 demonstrates the noise-immunization capability of our scheme. When a pure 9Hz sinusoid (Fig. 2-6(a)) was partially contaminated by uniformly distributed random noise (Fig. 2-6(b)), the AR model did not recognize the noise-contaminated slow α-rhythm segment based on the criterion 8Hz<$f_{r,1}$<10Hz (Fig. 2-6(c)). The results in Fig. 2-6(d) show that the SARD algorithm successfully detected the slow α-rhythm under poor environment (SNR=8dB).

To verify the performance, we first analyzed a simulated signal of 4-sec duration. The signal shown in Fig. 2-7(d) was generated by connecting three short-duration, amplitude-modulated sinusoids, respectively, with frequencies 9Hz, 15Hz, and 5Hz (Figs. 2-7(a)-(c)). The window length is 0.5 sec (100 samples), moving at a step of 0.25 sec. As shown in Fig. 2-7(d), the SARD algorithm effectively detected the slow α-rhythm pattern.
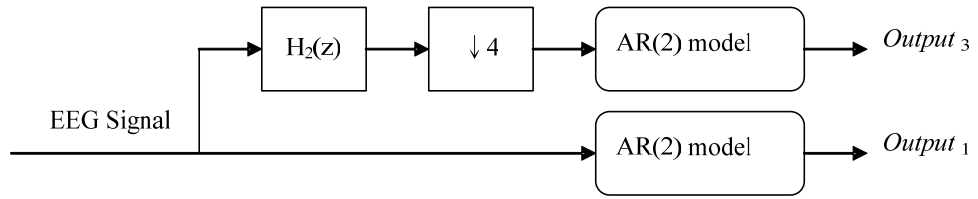
(a)
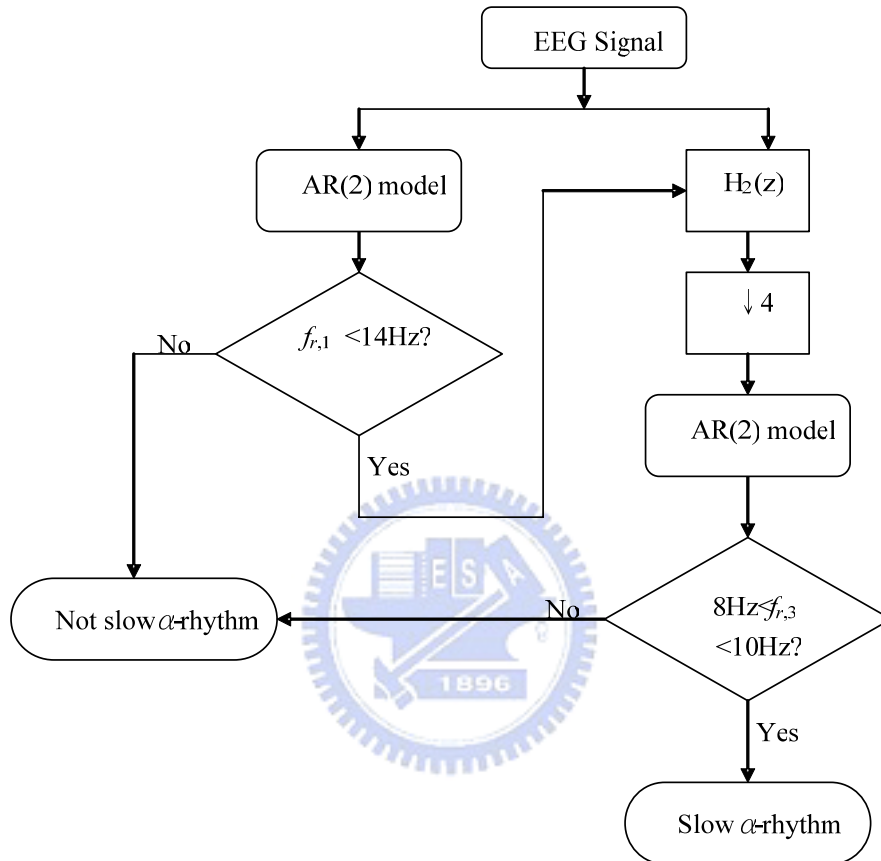
(b)

Figure 2-5: The *Subband-AR-EEG-Viewer* modified for slow α-rhythm detection: (a) structure and (b) algorithm.
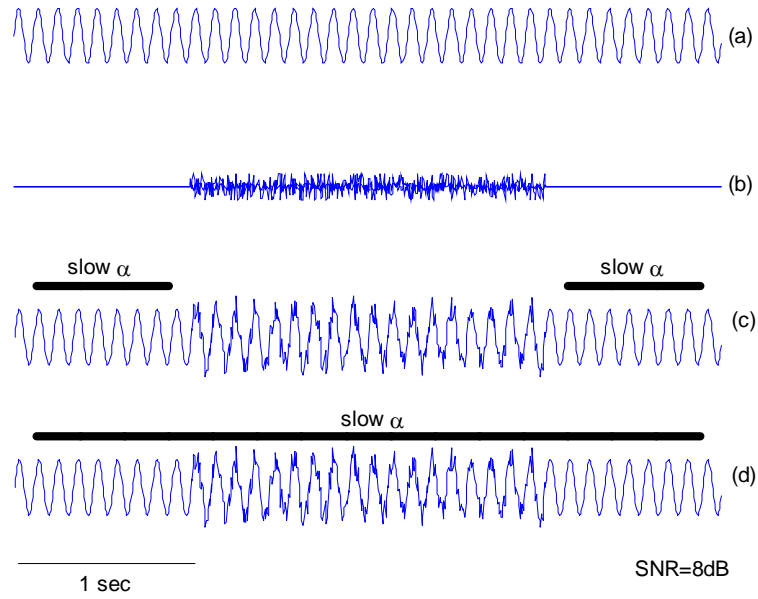
Figure 2-6: Capability of noise immunization of slow α-rhythm detector. The black bold lines mark epochs identified as slow α-rhythm.
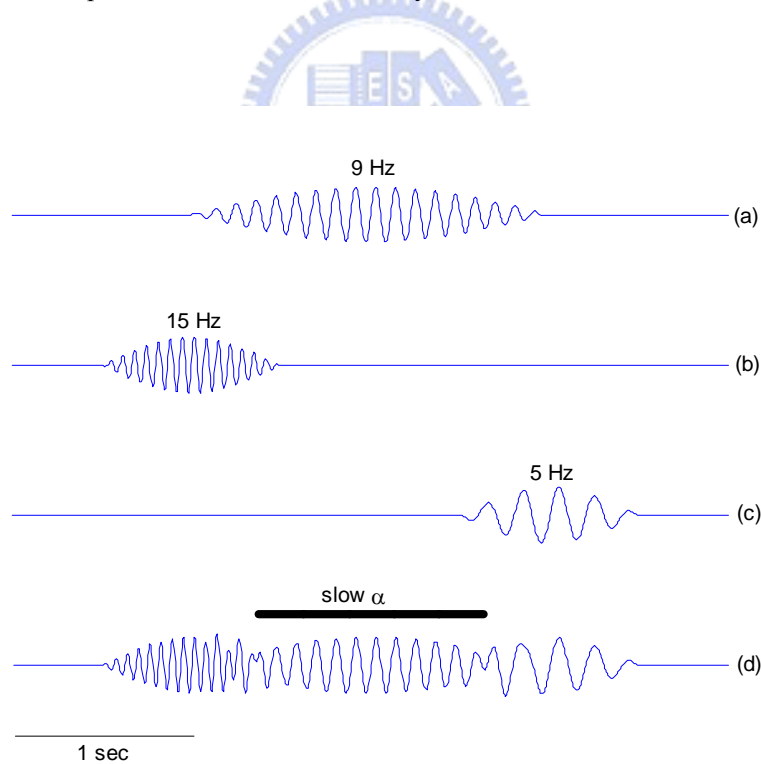
Figure 2-7: Slow α-rhythm detection from the time-varying rhythmic activities. The signal in (d) is simulated by adding three short-duration, amplitude-modulated sinusoids with frequencies (a) 9Hz, (b) 15 Hz, and (c) 5 Hz.

2.3.3. Identification of slow alpha rhythm

Next, the SARD algorithm was applied to the meditation EEGs (channel O1). A 10-second segment shown in Fig. 2-8 was analyzed with the same implementing parameters as used in Fig. 2-7. Bold lines above the signal indicate the slow α-rhythm detection. As shown in Fig. 2-8(a), amplitude variation often affects the recognizability of slow α-rhythm. It results in a crack in the first bold line. On the other hand, a transient slow α-rhythm may be of little significance. We thus designed a post-processor to further refine the result. It removed segments shorter than 0.3 sec and fused cracks shorter than 0.3 sec (Fig. 2-8(b)).
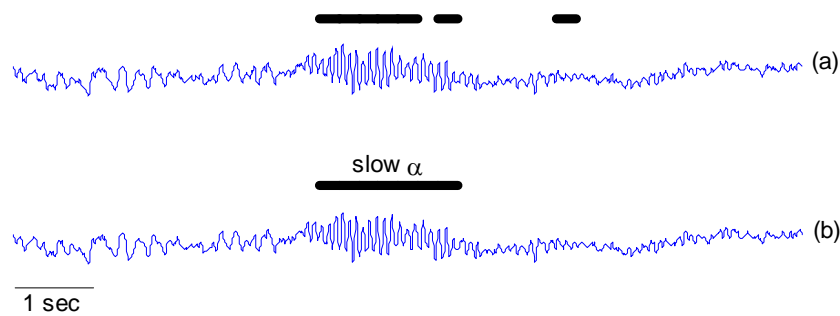
Figure 2-8: Detection of slow α-rhythm in meditation EEG (Channel O1). Bold lines above the signal indicate the slow α-rhythm detection. (a) A crack in the first bold line is caused by variation of the α amplitude. (b) A post-processor removes the second lines with duration shorter than 0.3 sec (insignificant activity) and fuses the crack shorter than 0.3 sec.

Detection of specific EEG patterns is important in identifying various meditation states. In addition, it may serve as a preprocessing stage in such tasks like the EEG segmentation or interpretation. Based on the *Subband-AR-EEG-Viewer*, we devised a strategy for meditation EEG interpretation. Details are illustrated below.

2.4. Long-term meditation EEG interpretation (MEEGI) algorithm

Changes of the characteristic frequency in meditation EEG may be a key feature for understanding various states of consciousness during meditation. We therefore developed a logical strategy implemented in the computerized MEEGI algorithm to segment the EEG into sections with different frequencies. The results, illustrated as a running gray-scale chart, clearly reveal the evolution of a characteristic frequency during meditation.

2.4.1. The algorithm

In the following, we present interpretation results of the meditation EEG based on five spectral features frequently observed during meditation: (1) The χ features which is a slow waveform intermixing with high-frequency rhythms, (2) δ, (3) θ, (4) α, and (5) β features. The χ feature mostly appears at the transition from one EEG rhythm to another. To provide a long-term visual record, the five spectral features are displayed by different gray tones. The gray tones from the darkest to the lightest indicate, respectively, the χ, δ, θ, α, and β features. In this task, the structure of *Subband-AR-EEG Viewer* can be reduced to that shown in Fig. 2-9.
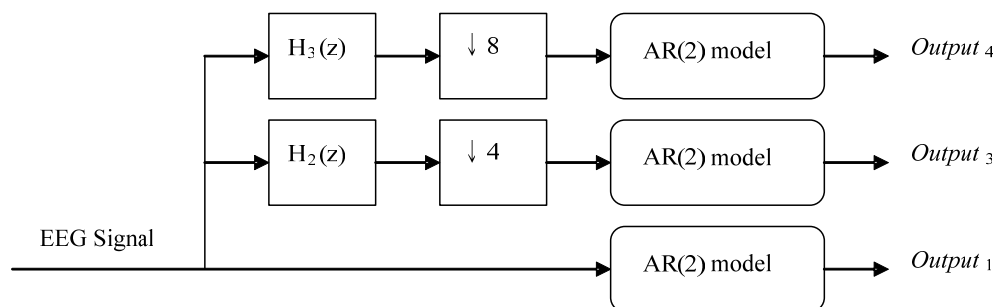
Figure 2-9: The *Subband-AR-EEG Viewer* modified for meditation EEG interpretation.

The MEEGI algorithm examines each windowed segment to check the following criteria in order:

Criterion-χ: $f_{r,3} < 7\text{Hz} < f_{r,1}$ and $|p_3| > 0.8$;

Criterion-δ: $f_{r,1} < 7\text{Hz}$ and $f_{r,4} < 3.5\text{Hz}$;

Criterion-θ: $f_{r,1} < 7\text{Hz}$;

Criterion-α: $7\text{Hz} < f_{r,1} < 14\text{Hz}$ and $7\text{Hz} \leq f_{r,3}$;

Criterion-β: $7\text{Hz} \leq f_{r,1}$;

where p_3 is the AR(2) pole of *output*$_3$. The criteria checkup is ordered according to a sound logic realizing the subband filtering method. The root frequency $f_{r,1}$ is used to differentiate between 0-7Hz and 7-30Hz EEG bands, while the $f_{r,3}$, $f_{r,4}$ and $|p_3|$ is employed in the subsequent discrimination process. The length of p_3 can be considered as an indication of the significance of the root frequency. Because the χ wave represents an intermixed signal composed of both low- and high-frequency components, we impose restrictions on the range of $|p_3|$ to ensure the significance of the low frequency component. The flowchart of the MEEGI algorithm is shown in Fig. 2-10.

2.4.2. Simulation

To verify the effectiveness of feature recognition, the MEEGI algorithm was first applied to a simulated signal. As displayed in Fig. 2-11(e), the signal was formed by connecting five segments of δ, θ, χ, α, and β patterns. We assumed the sampling rate is 200Hz. This signal can be simulated by the pole placement method, that is, by placing each pole in the corresponding frequency band (Table 2-2) and adding Gaussian noise. The transition from θ to β normally results in a compound pattern like χ. The running gray-scale chart (Fig. 2-11(e)) above the simulated sequence successfully signals the temporal patterns.
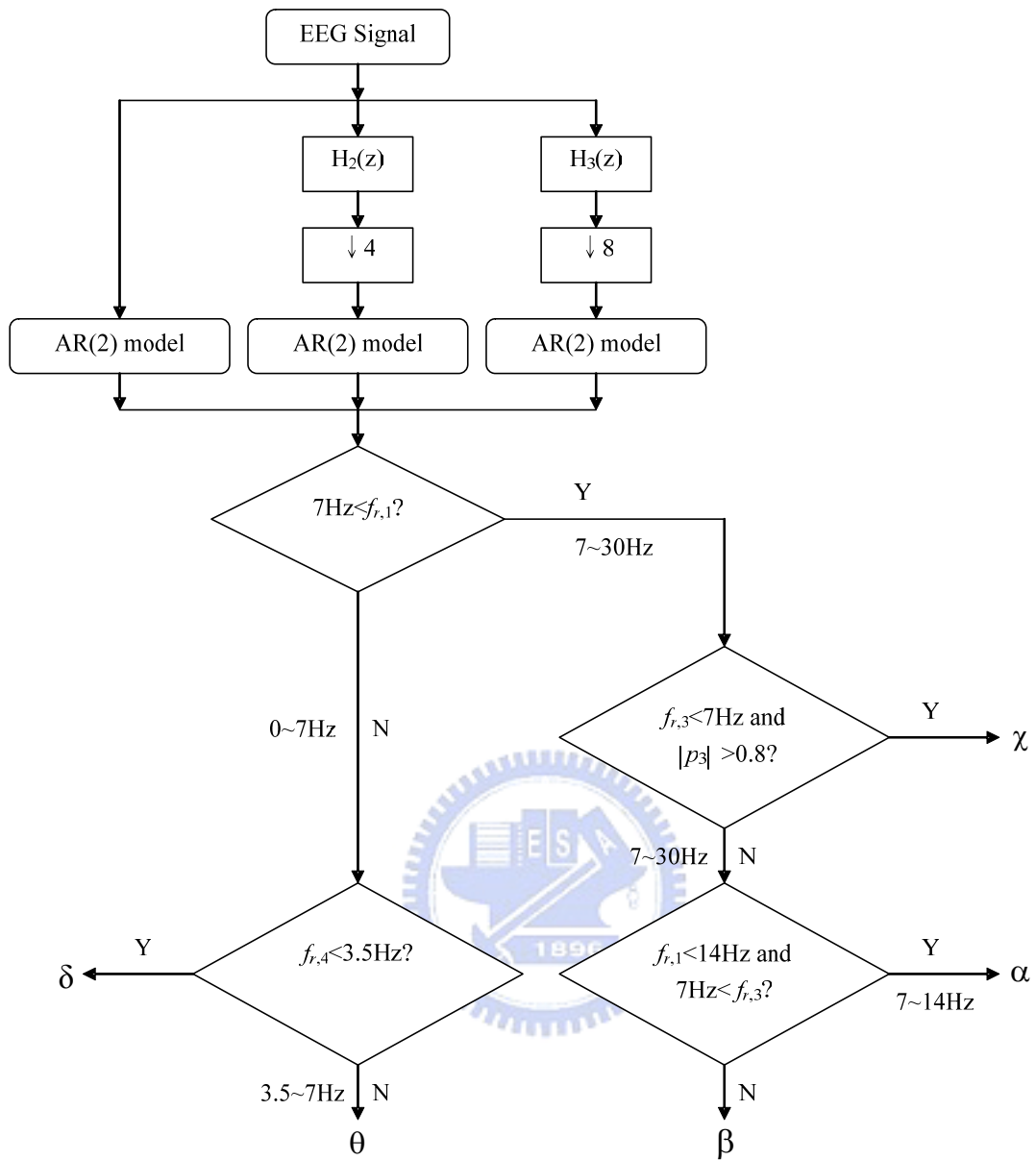
Figure 2-10: Meditation EEG interpretation (MEEGI) algorithm.

(1) χ, (2) δ, (3) θ, (4) α, and (5) β.
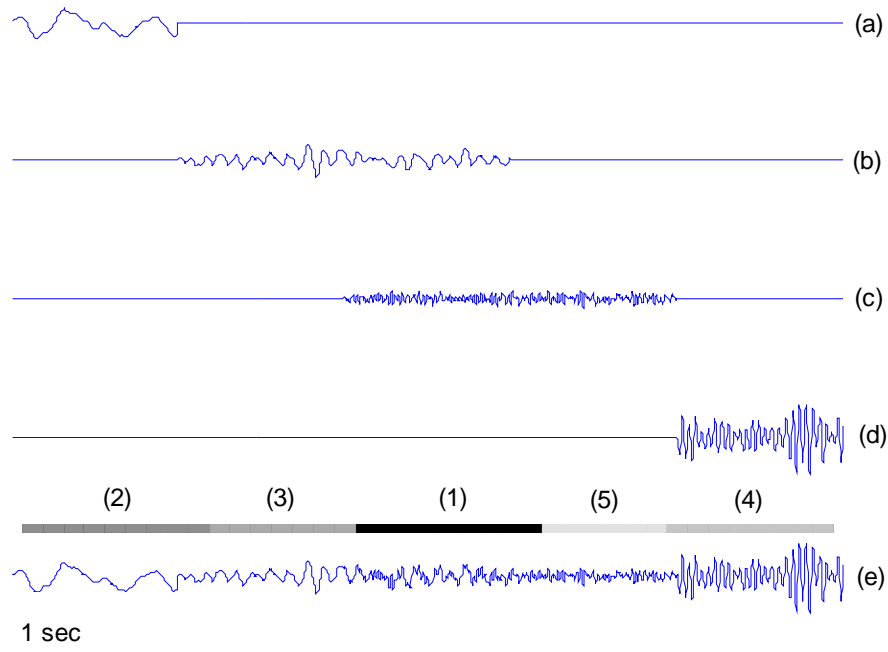
Figure 2-11: Simulation results (a) δ activity (b) θ activity (c) β activity (d) α activity (e) simulated signal and classification results.

Table 2-2: Locations of poles of the simulated signal

	δ	θ	α	β
Pole locations	$0.98\angle 0.04$	$0.98\angle 0.16$	$0.98\angle 0.4$	$0.88\angle 0.63$

The above simulation demonstrates the feasibility of the scheme and algorithm in Fig. 2-9 and 2-10 for automatically identifying different EEG rhythms and revealing time-varying schema of the simulation. In empirical data, as more complex rhythmic patterns are involved, discrepancies between experienced EEG interpreters may occur. Methodology development thus focused on reliable recognition of some key features in meditation EEG analysis. Figure 2-12 demonstrates the robustness of the *Subband-AR-EEG Viewer* for identifying even the little jittering of β rhythms embedded in the high-amplitude slow activity.

(1) χ, (2) δ, (3) θ, (4) α, and (5) β.
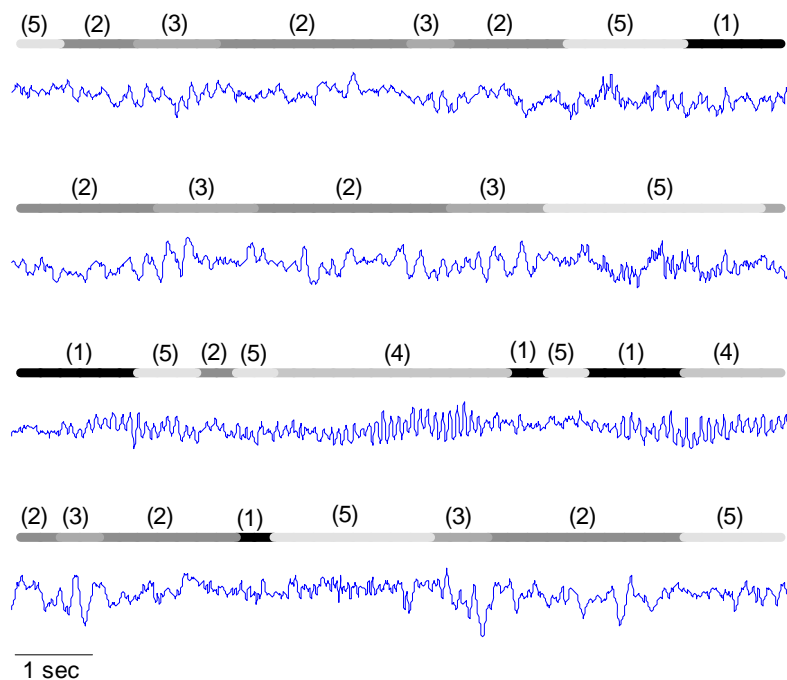
Figure 2-12: *Subband-AR-EEG Viewer* applied to the EEG signal for feature recognition.
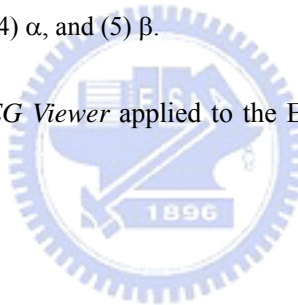
2.4.3. Long-term meditation EEG interpretation

When applied to the long-term meditation EEG, this algorithm is particularly robust for automatic interpretation with no need to determine the implementing parameters. Fig. 2-13 displays three running gray-scale charts for two experimental subjects (Fig. 2-13(a) and (b)) and one control subject (Fig. 2-13(c)). Since Watts [Watts 1957] has reported the variation of alpha amplitude and frequency in the frontocentral region during meditation, we thus selected channel F3 for further analysis. The error rate was approximately 8.7% in comparison with the results of naked-eye examination by an experienced EEG interpreter. Both meditators have been practicing Zen Buddhist meditation for more than eight years. The control subject sat in a normal, relaxed position with the eyes closed. During the meditation session, the two

meditators exhibited different meditation scenarios. Meditation EEG of subject 2k1019p was apparently dominated by β rhythm, sometimes transforming into a short-duration α rhythm. According to the post-experimental interview, the subject did not always stay in the Alaya consciousness and occasionally went back to normal consciousness.

The chart in Fig. 2-13(a) reveals this scenario for 20-minute. In Fig. 2-13(b), subject 2k0830a exhibited a large portion of χ activities. In our meditation EEG experiment, EEG signals of some meditators indeed were found to be characterized by large-amplitude, slow-drifting rhythms interwoven with high-frequency tiny jiggles. Meditators with this kind of EEG characteristic normally have their meditation process wandering among normal consciousness, subconsciousness (subliminal consciousness), and Alaya consciousness [Lo et al. 2003]. Compared with the experimental group, EEGs collected from the control subject are normally dominated by α rhythm, as illustrated in Fig. 2-13(c). Note that this subject was drowsy in the experiment, resulting in occurrence of θ and δ rhythms.

2.4.4. On-line implementation of the Subband-AR-EEG Viewer

Due to its simplicity, the algorithms provides a robust tool for on-line processing required for meditation EEG interpretation as well as the biofeedback scheme in the BCI (brain-computer interface) research. Currently, we have implemented the MEEGI algorithm under Simulink (MathWorks, Inc., Natick, MA) with Real-Time Workshop on a Pentium-M 1.4 (GHz) notebook (Fig. 2-14(a)). By generating a real-time code with Real-Time Workshop, the algorithm can be downloaded to the kernel and run in a real-time manner under Windows [Guger 2001]. The classification results were displayed on a monitor. As shown in Fig. 2-14(b), the height of each bar reflects the power percentage of the corresponding EEG rhythm within a 2-sec frame. We can thus monitor the meditator's state in a real-time manner that enables the development of a more subtle correlation between the EEG characteristics

and the meditation scenario.
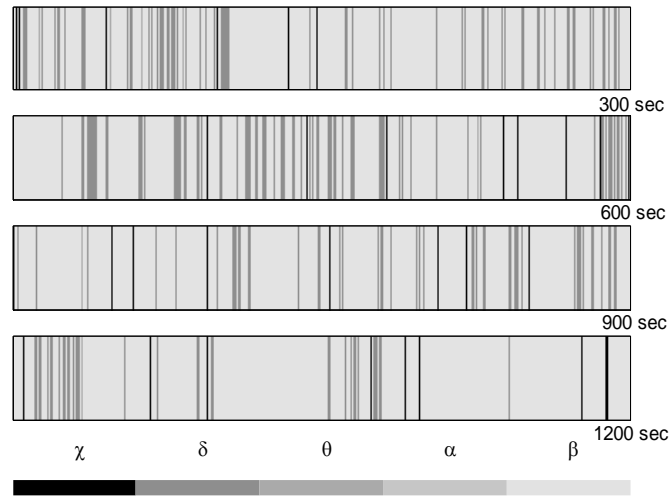
(a)
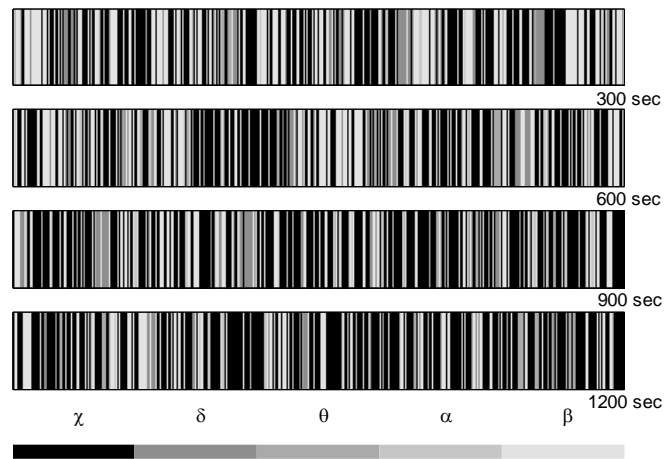
(b)
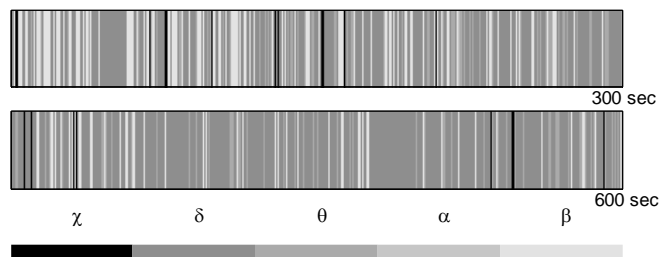
(c)

Figure 2-13: Running gray-scale charts (Channel F3) for two meditators (a) subject 2k1019p, and (b) subject 2k0830a, and (c) one non-meditator (control) subject 2k1007p.
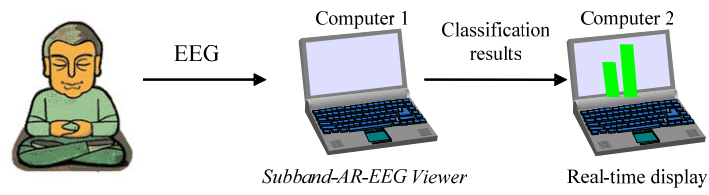
(a)
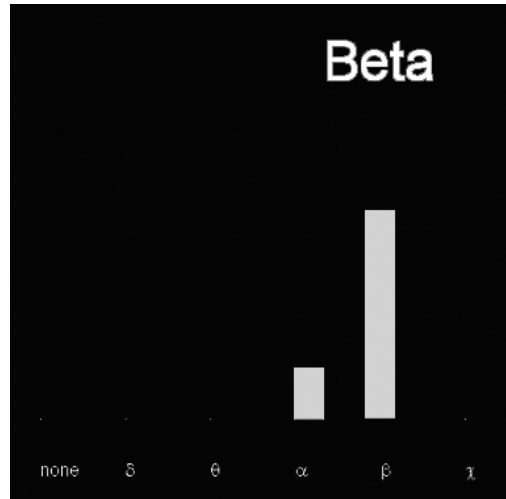
(b)
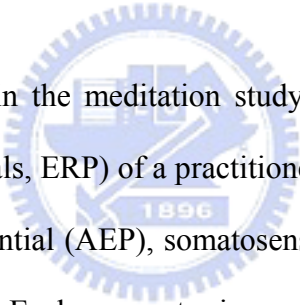
Figure 2-14: On-line implementation of the *Subband-AR-EEG Viewer*. (a) Computer 1 executes the MEEGI algorithm (**Fig. 2-10**), and Computer 2 displays the classification results, as illustrated in (b). The height of each bar reflects the power percentage of the corresponding EEG rhythm within a 2-sec frame.

Chapter 3－

Investigation of Visual Perception under Zen-Meditation

If the brain were so simple we could understand it, we would be so simple we couldn't.

~Lyall Watson

O ne topic of interest in the meditation study is the evoked potentials (EP) (or event-related potentials, ERP) of a practitioner under meditation, which includes auditory evoked potential (AEP), somatosensory evoked potential (SEP), visual evoked potential (VEP), and so on. Each parameter is meaningful to the respective perception function. Due to unusual perceptions often experienced during meditation, human brain in response to external flash stimuli during Zen meditation drew our attention. Recording of VEPs provides a means of characterizing the visual pathway and visual function. VEPs can be recorded by applying either patterned or non-patterned stimulus that results in various VEP waveforms [Odom et al. 2004]. Since practitioners must close their eyes during meditation, we employed non-patterned flashes in the VEP recording.

3.1. Why EEG-triggered F-VEP?

In Zen-meditation EEG study, increased alpha activity over the frontal regions of the brain has been observed during meditation [Kasamatsu and Hirai 1966, Takahashi et al. 2005]

and so has the increased frontal alpha coherence [Murata 2004]. Kasamatsu and Hirai found an increase in alpha amplitude at the beginning of meditation, which then spread frontally [Kasamatsu and Hirai 1966]. Furthermore, Takahashi et al. observed that the increased frontal alpha power correlated with the enhancing internalized attention [Takahashi et al. 2005]. Thus increased frontal alpha activity was hypothesized as a result of Zen-meditation process. All the observations have led into further understanding of the function-correlated, spatial characteristics of the brain affected by meditation.

In another aspect, Zhang et al. [Zhang et al. 1993] claimed that the amplitudes of F-VEPs (VEPs under flash stimuli) of Qigong meditators increased under meditation. In Xu et al.'s research [Xu et al. 1998], the amplitude of F-VEP increased while the latency decreased. They suggested that concentration and attention may be the reason of altering the evoked potentials. One problem encountered in the F-VEP study is to determine the appropriate timing for applying the flash-light stimulus. To our knowledge it has not been reported in regard to this issue. In our previous study, stimulus was applied at the mid-section of meditation at which subjects might undergo various physiological and mental states. In that case, F-VEPs were not able to reveal different experimental courses such as the section before, during, and after meditation [Liu and Lo 2005]. To assure that all F-VEPs are acquired under a consistent condition, a rational experimental setup is to apply the stimulus based on a controllable factor. To gain access to particular brain states, one approach is to ask the subject to signal the attainment of the meditation state by finger movement [Newberg et al. 2001, Lo et al. 2003, Takahashi et al.2005]. However, it often causes meditators to break off from the meditation state.

To investigate the ERP activities in a given brain state defined by EEG, we thus conceive the idea of *EEG-triggered F-VEP* scheme, that is, the flash-light stimulus is applied under specific oscillatory features of the EEG. In this preliminary study, we intuitively selected the frontal α-rhythm as the F-VEP triggered signal based on the results reviewed previously and our empirical observations these years. The following section illustrates the methods for de-

tecting the frontal α-rhythm and the experimental setup. Significant results obtained are presented at the end of this chapter.

3.2. Alpha-dependent F-VEP

According to the description in 3.1, the flash-light stimulus is to be applied upon emergence of the frontal α-rhythm. The scheme, *Subband-AR EEG Viewer*, proposed in Chapter 2 [Liao and Lo 2006] provides more accurate estimate with better resolution [Hayes 1996, Güler et al. 2001] and, in particular, allows on-line α-rhythm detection within a very small time frame. Modification of the scheme for on-line α-rhythm detection is described below.

3.2.1. Online α-rhythm detection

For online α-rhythm detection, the SARD algorithm described in Chapter 2 was slightly modified. Because cutoff frequency of the bandpass filter is different (to be explained in next section) for VEP recording, the tree structural filter bank in Fig. 2-5 was adjusted as shown in Fig. 3-1. As presented in Chapter 2, an AR(2) model can be expressed as

$$x[n] + a_2[1]x[n-1] + a_2[2]x[n-2] = w[n]. \tag{3-1}$$

The model coefficients $a_2[k]$ can be determined by solving the autocorrelation normal equations [Hayes 1996]. After the model coefficients have been obtained, the conjugated pole pair is determined as,

$$-\frac{a_2[1]}{2} \pm j\frac{\sqrt{4a_2[2] - a_2{}^2[1]}}{2}. \tag{3-2}$$

Thus the root frequency of the signal can be obtained from Eq. (3-2)

$$f_{r,i} = \angle\left(-\frac{a_{2,i}[1]}{2} + j\frac{\sqrt{4a_{2,i}[2] - a_{2,i}{}^2[1]}}{2}\right) \tag{3-3}$$

where i denotes the ith decomposition level. The filtering-and-downsampling process is reit-

erated to attain good accuracy in discriminating between α and δ/θ rhythms. The equivalent

cutoff frequency is 15Hz. We designed a criterion based on the root frequency to detect the

α-rhythm. The algorithm examines each windowed segment to check whether it meets the

following criterion.

Criterion-α: $f_{r,1}$<14Hz and 7Hz<$f_{r,2}$.

The root frequency $f_{r,1}$ is used to differentiate EEG rhythms in 0–14Hz from those in 14–30Hz.

Next, root frequency $f_{r,2}$ is examined to screen out δ/θ rhythms.

Note that *output*$_1$ and *output*$_2$ are the results of downsampling (Fig. 3-1), the root fre-

quency $f_{r,i}$ should be further divided by 2^i. This experiment employed a window length of 1

second, with a moving step of 0.5 second.
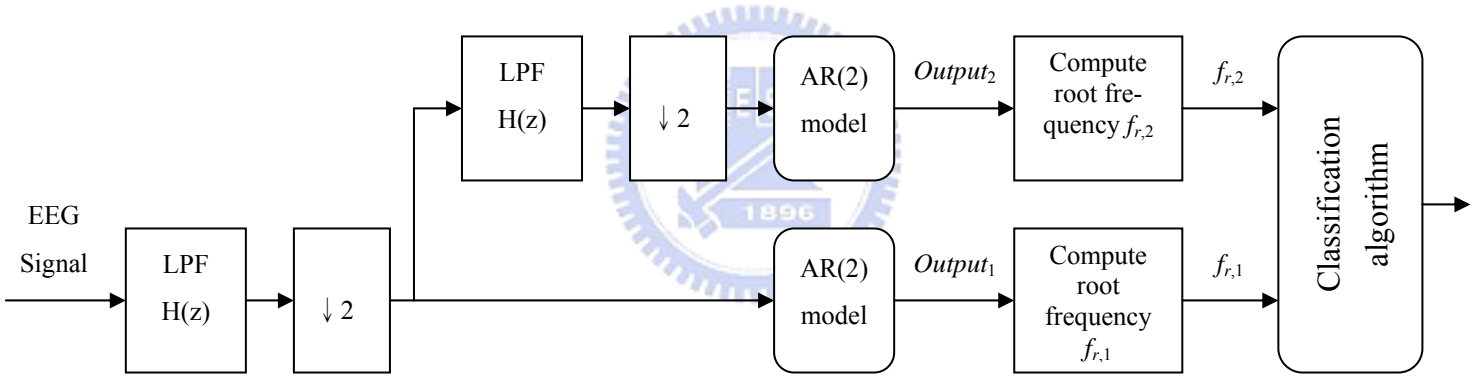
Figure 3-1: Tree structural filter bank for the Subband-AR EEG Classifier. *H*(*z*) is de-

signed by least-squares error minimization with cutoff frequency 30Hz.

3.2.2. Simulation

To verify the effectiveness of the α-rhythm detection algorithm, the algorithm was firstly

applied to a simulated signal. We assumed a sampling rate of 128Hz. The signal can be simu-

lated by the pole placement method, that is, by placing each pole in the corresponding fre-

quency band (Table 3-1) and adding Gaussian noise. As displayed in Fig. 3-2(e), the simu-

lated 10-second signal was formed by connecting four segments of δ, θ, α, and β-rhythm pat-

terns. Detection result in Fig. 3-2(e) is illustrated by two gray scales, with dark (light) gray indicating the α (non-α) pattern. The result clearly justified the effectiveness of the algorithm in α detection.

Table 3-1: Locations of poles of the simulated signal

	δ	θ	α	β
Poles' location	$0.98\angle 0.04$	$0.98\angle 0.16$	$0.98\angle 0.4$	$0.88\angle 0.63$
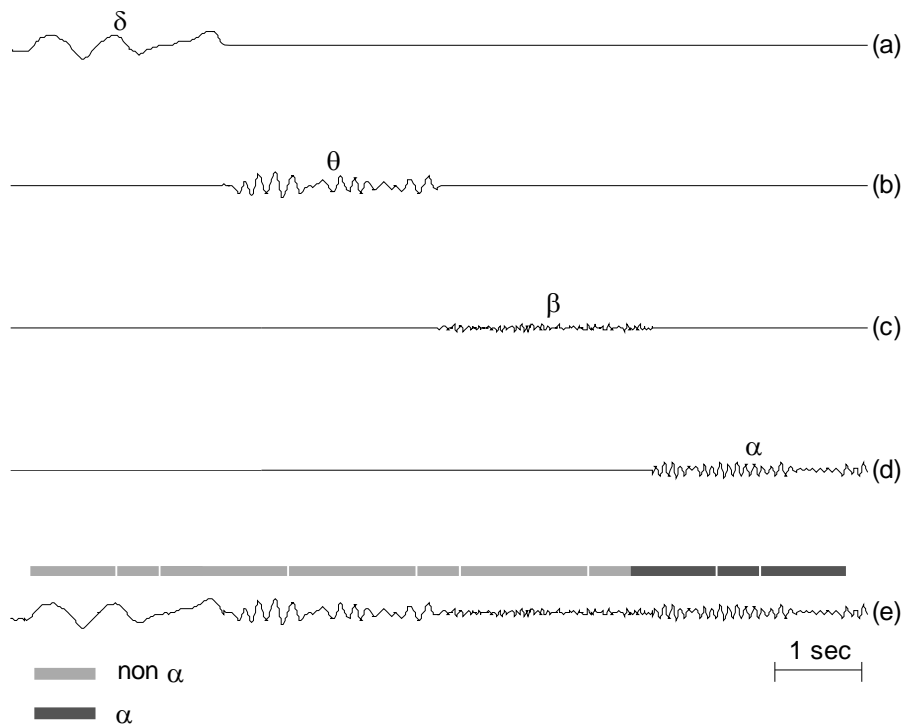
Figure 3-2: Classification result of the simulated signal. Different grays are used to illustrated the α and non-α patterns.

3.2.3. Off-line alpha detection

Empirical EEGs often exhibit highly complex, irregular rhythmic patterns that make the recognition of specific EEG pattern more difficult. Our algorithm is robust in dealing with this

kind of complication. Figure 3-3 displays the result of α detection. The error rate, estimated from the results of identifying 780 alpha candidates, was approximately 7.2% (4.6% false negative and 2.6% false positive rate) in comparison with the results of naked-eye examination by an experienced EEG interpreter.
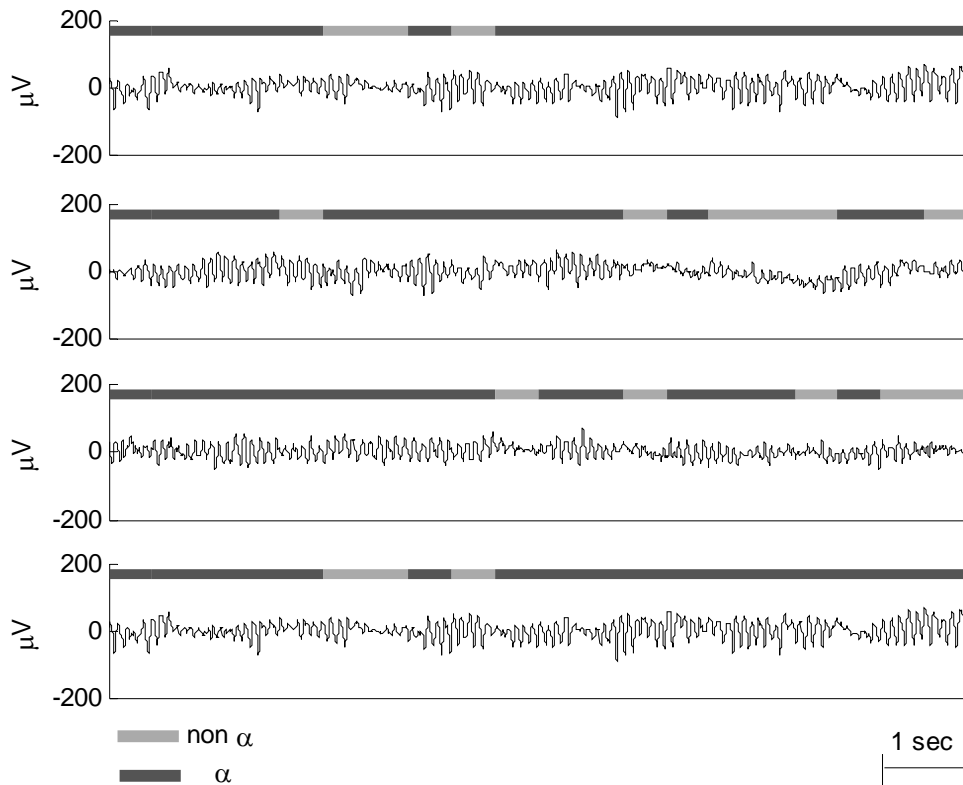
Figure 3-3: Result of α detection for real EEG signal.

3.2.4. F-VEP

The F-VEP consists of a series of negative and positive peaks, denoted respectively by N and P followed by a number. The number is referred to as the order (or time) of occurrence of that particular peak from the stimulus. The F-VEP source is located in the occipital lobe. Normally, the event-related brain potentials propagate via neural network toward the nearby regions. The phase differences among different channels are caused by the time delays of

34

brain-wave propagation [Hughes et al. 1992]. Figure 3-4 shows typical F-VEPs recorded on Fz, Cz, and Oz with corresponding peak labels. In this study, peaks of significance including N2, P2, N3, and P3 are to be analyzed. Note that F-VEPs of different channels have phase deviation.

Researchers inferred that the noticeable negative peak N2 of Oz was generated in lamina IV cb [Kraut 1985, Ducati 1988], then the following positive peak P2 might reflect the inhibition activity within lamina. This study is mainly based on the hypothesis that Zen meditation affects visual neural pathway that can be revealed on the F-VEPs.

3.3. Experimental setup and protocol

3.3.1. Subjects

This study involved 11 meditators and 11 control subjects. In the experimental group, 4 females and 7 males at the mean age of 27.5 ± 3.2 years participated. Their experiences in Zen-Buddhist practice span 5.5 ± 4.3 years. The control group included 3 female and 8 male students with an average age of 23.6 ± 3.3 years.

3.3.2. Apparatus

The EEG signals and F-VEPs were recorded at standard 10/20 positions (Fig. 3-5) with 32-channel SynAmps amplifiers (manufactured by NeuroScan, Inc.) connected to a Pentium-4 (1.5 GHz) PC. Common reference of linked M1-M2 (mastoid electrodes) was used. EEG signals, after amplification, were pre-filtered by a bandpass filter with passband 0.3–50 Hz, and digitized at 1000 Hz sampling rate. A 60-Hz digital notch filter was applied to the data to remove artifacts from power line or the surroundings.
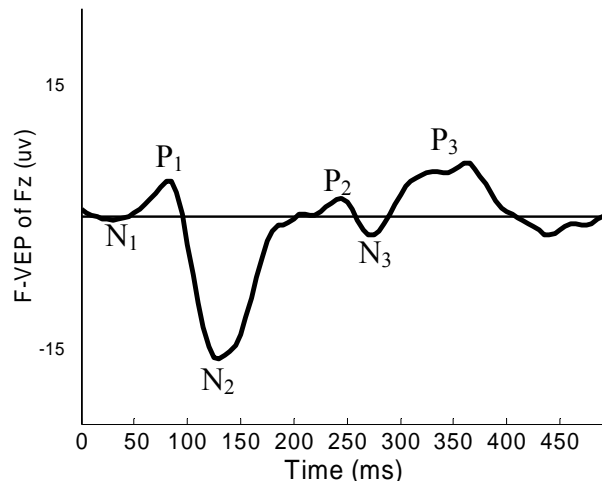
(a): F-VEP of Fz
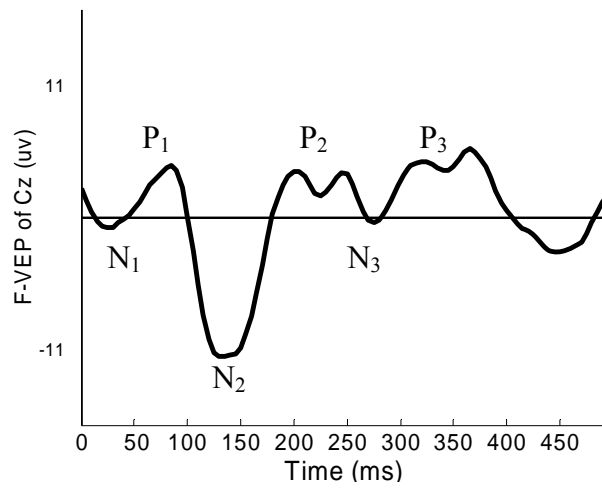
(b): F-VEP of Cz
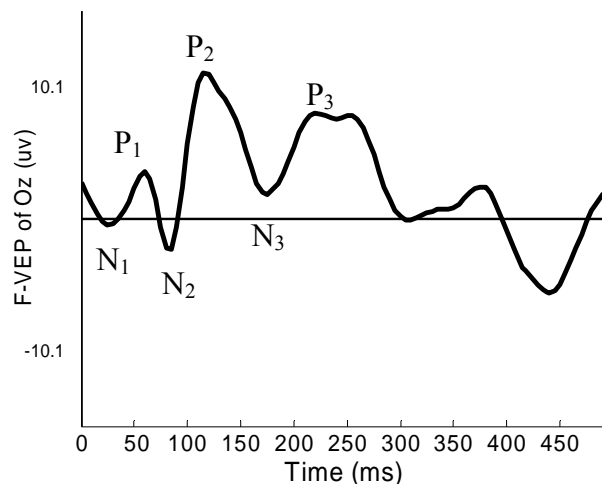
(c): F-VEP of Oz

Figure 3-4: Profile of F-VEPs on (a) Fz, (b) Cz, and (c) Oz with corresponding peaks

labeled.
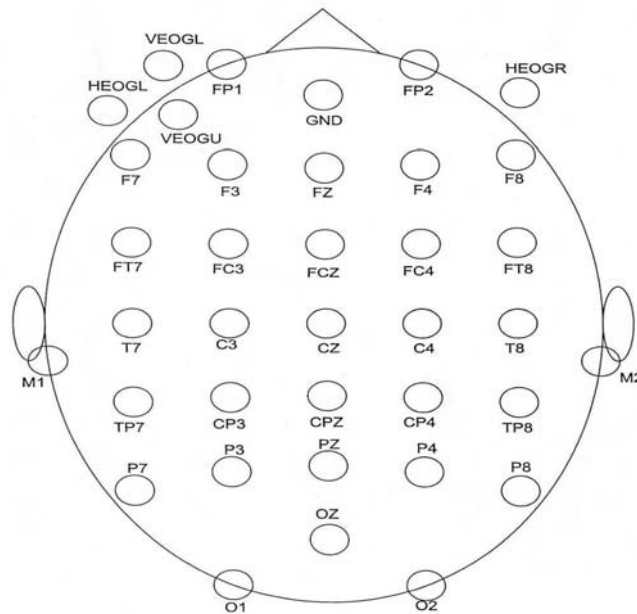
Figure 3-5: 32-channel recording montage.

We developed an online α-detection algorithm that was implemented by using g.BSamp with g.RTsys (manufactured by Guger Technologies, Inc.) connected to a Pentium-M (1.4 GHz) notebook. g.BSamp is a stand-alone biosignal amplifier and g.RTsys is a biosignal acquisition and real-time analysis system for notebook implementation. To facilitate the real-time α detection, channel-Fz EEG was pre-filtered by a bandpass filter with passband 0.5–30 Hz, and digitized at a lower rate of 128 Hz. The α-detection algorithm was implemented on Simulink (MathWorks, Inc., Natick, MA) with Real-Time Workshop. By generating real-time code with Real-Time Workshop, the algorithm can be downloaded to the kernel and run in a real-time manner under Windows [Guger et al. 2001]. The experimental setup is shown in Fig. 3-6. The subject stayed in an isolated space. A CCD camera positioned in front of the subject was used to monitor the entire procedure. The 32-channel EEG signals were recorded by an EEG recording system. Another computer read channel Fz simultaneously to identify the occurrence of frontal-α rhythm. Once the frontal-α was ascertained, the computer

triggered the flash light controller to generate flash stimuli.
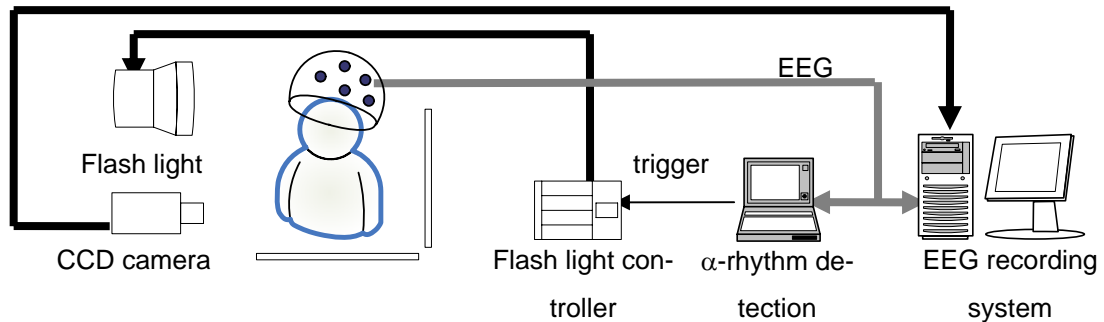
Figure 3-6: Experimental setup for α-dependent F-VEP recording.

3.3.3. Experimental paradigms

During the experiment, subjects sat in a separated space in the laboratory. Each recording lasted for about 60 minutes, including three sections: two 10-minute background EEG recordings (section I and III) before and after a 40-minute recording (section II, the "main section") of EEG under meditation (experimental subject) or rest (control subject). The control subject sat in a normal, relaxed position with eyes closed, while the meditators practiced Zen-Buddhist meditation during the 40-minute main section. In Zen meditation, the subject sat, with eyes closed, in the full-lotus or half-lotus position. Each hand formed a special mudra (called the Grand Harmony Mudra), laid on the lap of the same side. The subject focused on the Zen Chakra and the Dharma Eye Chakra (also known as the "Third Eye Chakra") in the beginning of meditation till transcending the physical and mental realm. The Zen Chakra locates inside the third ventricle, while the Dharma Eye Chakra locates at the hypophysis [Lo et al. 2003].

The term "alpha-dependent F-VEPs" was used because we recorded F-VEPs upon the detection of frontal α rhythms. One run of alpha-dependent F-VEPs were recorded in each of the three sections (Fig. 3-7). Each run consisted of 50 alpha-dependent flash stimuli. The in-

terval between two consecutive stimuli was longer than 1 sec. The flash light, with a 10μs duration, was produced by a xenon lamp that was placed 60 cm in front of the subjects' eyes. Alpha-dependent F-VEPs were acquired from midline channels Oz, Cz and Fz, with the linked-mastoid electrode as the reference. Since we employed the mastoid-referenced unipolar montage, alpha activities could be found in the frontal channels of all subjects [Niedermeyer and Lopes da Silva 2004]. However, more frontal alpha activities were detected during meditation, that reduced the time required for collecting 50 alpha-dependent F-VEPs.
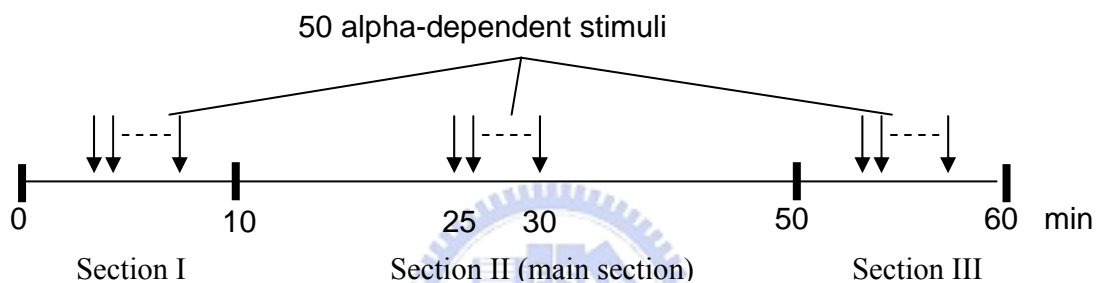
Figure 3-7: Scheduling of the F-VEP recording procedure.

3.4. Modulation of F-VEP amplitudes due to Zen-Meditation process

As shown in Fig. 3-8, different codes were used to indicate the stimuli presented in different sections. The stimuli in section I, II, and III are marked by code 128, 64, and 32, respectively. And the marker at the upper left of each code indicates the time of flash stimulation. A concluding F-VEP of each section was derived by averaging 50 raw tracings in one run.
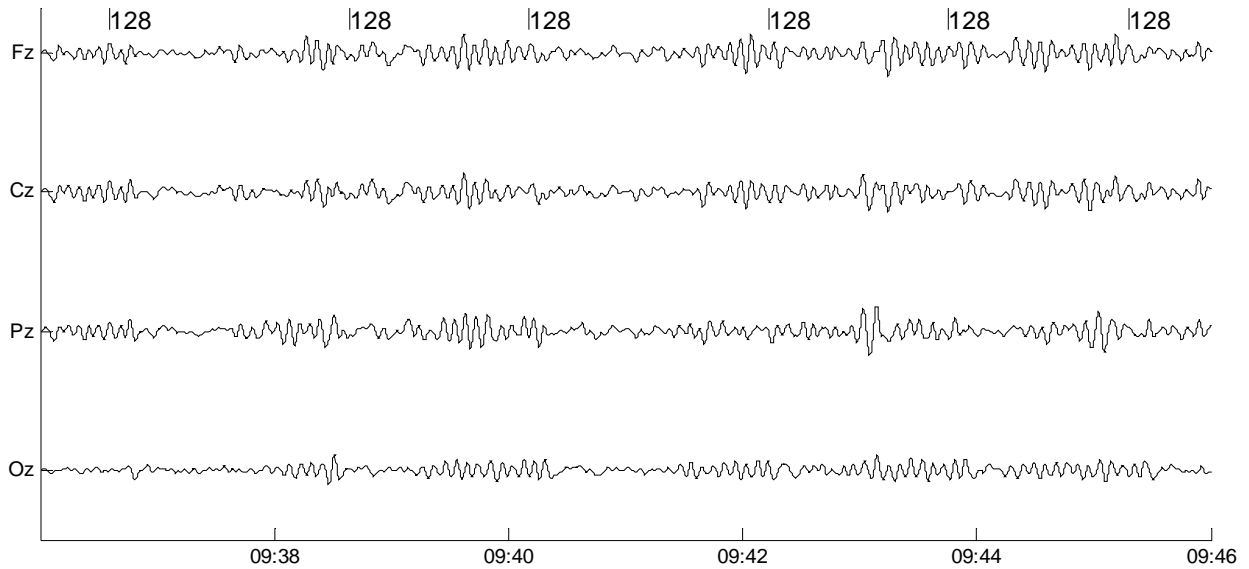
Figure 3-8: Display format of selected channels (Fz, Cz, Pz, and Oz) for α-dependent

F-VEP recording. The vertical bar at the upper left of mark '128' indicates the time of

applying flash stimulus.

Inter-subject variations of human VEP under the open experimental environment are

complicated. We thus investigated the intra-subject differences among various sections con-

ducted in one experiment. We measured the amplitude and latency of the average F-VEP, and

quantified the difference between various sections. Our results presented quite different trends

between two groups. Figure 3-9 plots an example of the F-VEPs at Fz, Cz and Oz (from the

top) for one subject. The solid lines represent the F-VEPs in the section I, and the dash and

dot ones stand for those in the section II and III.
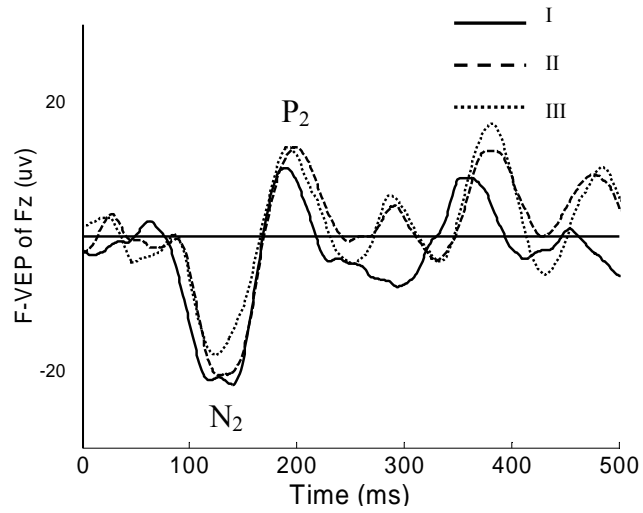
(a): F-VEP of Fz
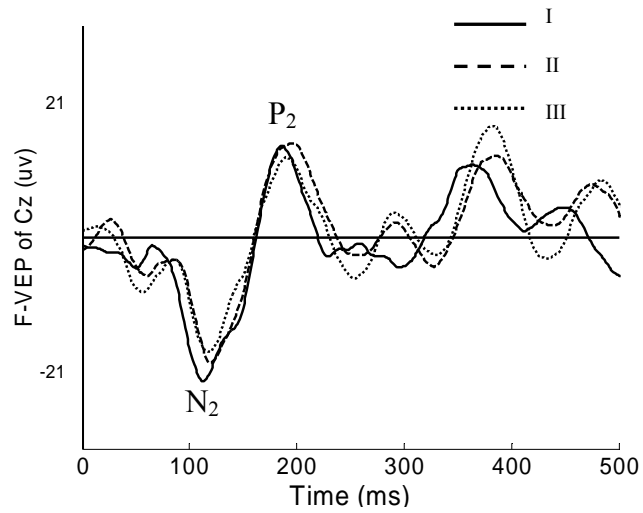
(b): F-VEP of Cz
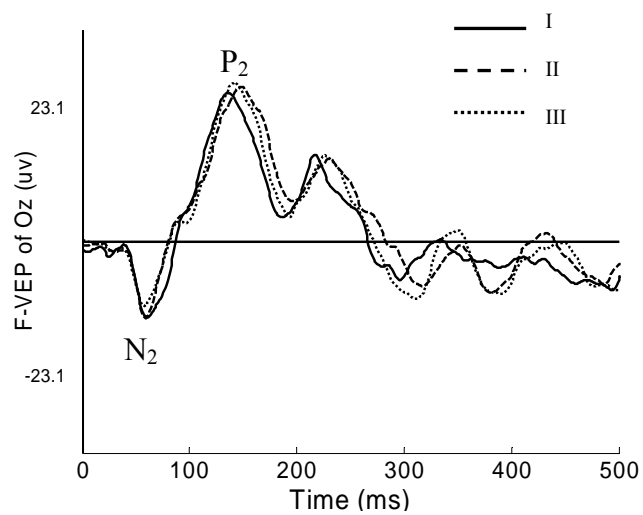
(c): F-VEP of Oz

Figure 3-9: The α-dependent F-VEPs of one meditator recorded on (a) Fz, (b) Cz, and

(c) Oz.

Table 3-2: The changes in the peak amplitudes of specific F-VEP components.

Item		Exp group			Ctrl group			t-test	
		II/I (%)	III/II (%)	P value (paired t-test)	II/I (%)	III/II (%)	P value (paired t-test)	II/I	III/II
	P1-N2	95.09	114.40	NS	141.63	114.31	NS	**0.013***	NS
	N2-P2	101.41	101.44	NS	121.07	103.60	NS	**0.010***	NS
Oz	P2-N3	107.10	102.77	NS	112.20	122.49	NS	NS	NS
	N3-P3	117.33	106.86	NS	90.59	114.25	NS	NS	NS
	P3-N4	121.35	104.18	NS	112.71	81.89	NS	NS	**0.035***
	P1-N2	106.25	76.33	**0.057**	81.20	87.08	NS	**0.043***	NS
Cz	N2-P2	120.10	89.18	**0.00037***	93.64	102.01	NS	**4.78E-05***	NS
	P2-N3	134.73	103.43	NS	124.25	135.75	NS	NS	NS
	N1-P1	126.68	97.03	NS	104.30	125.79	NS	NS	NS
Fz	P1-N2	119.20	86.72	**0.056**	87.02	95.01	NS	**0.043***	NS
	N2-P2	115.70	92.76	**0.040***	88.77	110.03	**0.052**	**0.0025***	**0.045***
	P2-N3	143.35	128.01	NS	99.77	119.34	NS	NS	NS

I: section I, II: section II (main section), III: section III,

*: P<0.05,

NS: Not Significant

From our results we found that latencies of all components exhibit no significant differ-
ence among all sections in both groups. However, the variations of amplitudes show differ-
ences in some components between two groups. Table 3-2 presents, for each F-VEP compo-
nent, ratios of the group average amplitudes of different sections. The p value is calculated by
paired t-test (compared with selves in different phases) and *t-test* (compared to the other
group in the same phase). Amplitudes of P1-N2 and N2-P2 on Cz and Fz increased signifi-
cantly during meditation, yet, decreased during relaxation in the control group. On the other
hand, N2-P2 amplitude on Fz decreased after meditation (experimental group) but increased
after rest (control group). Apparently, the transit from one to another section caused F-VEP

amplitudes on Cz and Fz to vary in opposite directions for both groups. We also observed significant differences between two groups in P1-N2 and N2-P2 amplitudes (Oz). P1-N2 amplitude (Oz) decreased during meditation but increased during rest. N2-P2 amplitude increased in the control group, but had little change in the experimental group. Contrary to the earlier peaks P1-N2 and N2-P2, N3-P3 amplitude (Oz) in the control group slightly decreased, whereas this peak amplitude increased in the experimental group.

Among all the F-VEP components, the most noticeable difference between two groups was the N2-P2 of Cz and Fz. Figure 3-10 plots the variations of N2-P2 amplitudes at Cz and Fz. Each bar represents the percentage of F-VEP varying from section I to section II $\left(\frac{\text{II} - \text{I}}{\text{I}} \times 100\%\right)$ for one subject (white: experimental subject, gray: control subject). Significant distinction is observed between two groups. Most meditation practitioners had their N2-P2 amplitudes increasing by an average rate of 20.1% (standard deviation among 11 subjects was 15.12%). Control subjects, on the contrary, exhibited a decreasing trend (average rate: −6.36%, standard deviation: 7.78%).
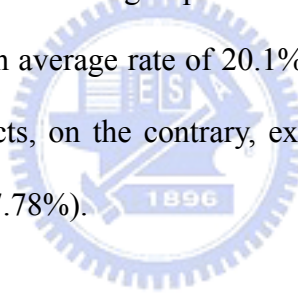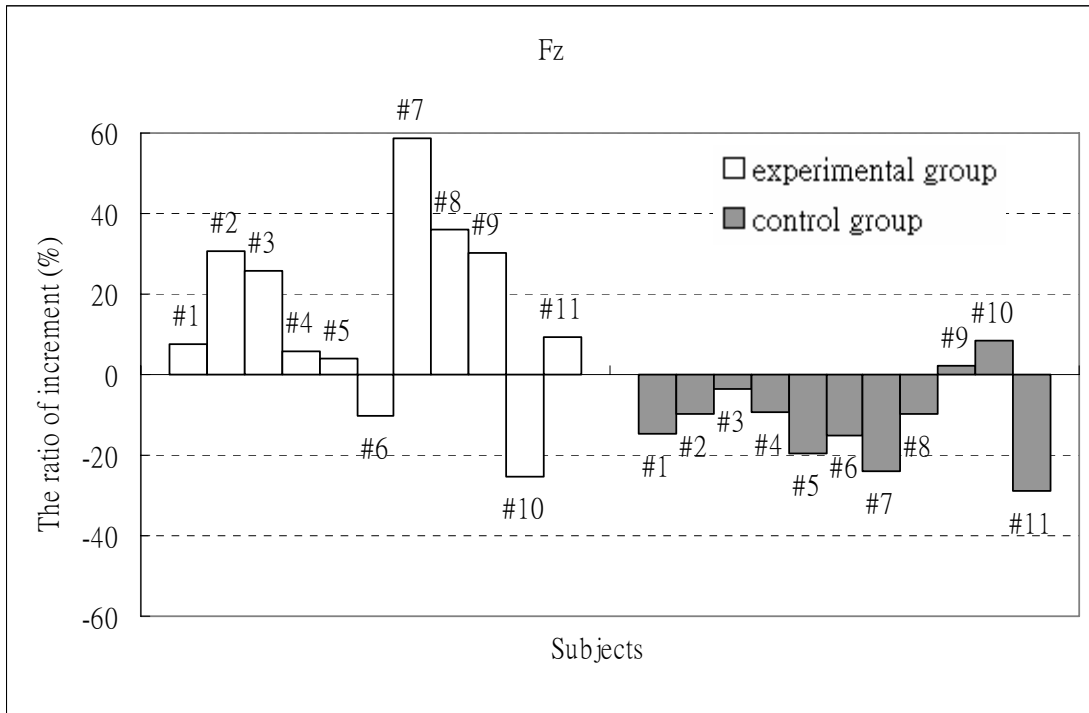
(a): Fz
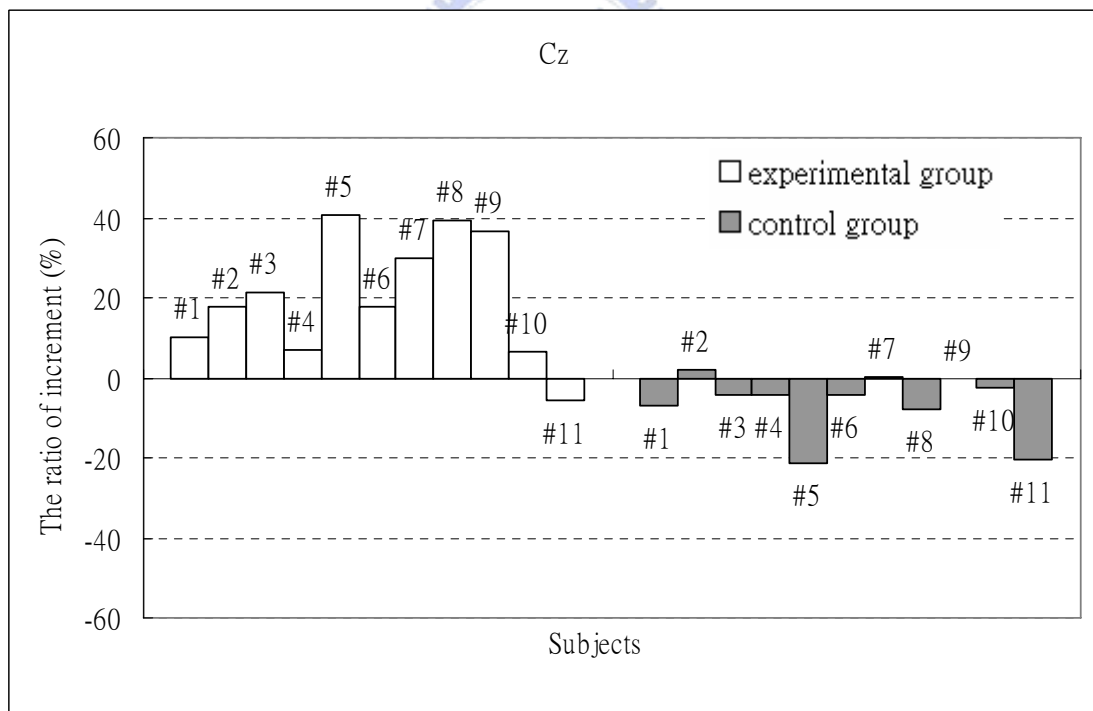
(b): Cz
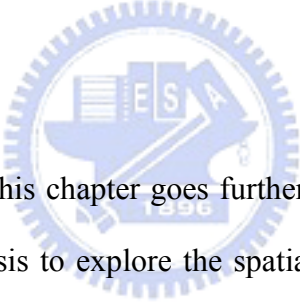
Figure 3-10: Variations of N2-P2 amplitudes at (a) Fz and (b) Cz. Each bar represents

the percentage of F-VEP varying from section I to section II $\left(\dfrac{\text{II}-\text{I}}{\text{I}}\times 100\%\right)$ for each

individual subject (white: experimental subject, gray: control subject).

Chapter 4－

Investigation on Spatiotemporal Characteristics of Zen-Meditation EEG Rhythms

Mathematics compares the most diverse phenomena and discovers the secret analogies that unite them.

~ Joseph Fourier

The work presented in this chapter goes further with a focus on the multi-channel meditation EEG analysis to explore the spatial-spectral behavior of Zen meditation EEG. We will report the findings of the spatiotemporal behaviors of meditation-EEG spectra based on the analyzed results of 30-channel EEGs. To deal with such an enormous amount of EEG data, we developed a novel system, *meditation EEG interpreter*, that was modified from the MEEGI algorithm described in Chapter 2. This interpreter is capable of identifying various EEG activities and detecting the artifacts.

4.1. The meditation EEG interpreter

Artefacts occur every now and then during EEG recording. To identify artifact-interfered EEG, the MEEGI algorithm was further enhanced to facilitate the long-term meditation EEG analysis and to eventually provide an overview of the entire meditation EEG record.

4.1.1. The algorithm

The meditation EEG interpreter is able to identify six wave patterns and two artifacts often appearing in meditation EEG. The six wave patterns include: (1) low-power, almost flat wave (denoted by 'ϕ'), (2) multi-frequency activities with approximate power (denoted by 'χ'), and (3) δ, (4) θ, (5) α, and (6) β activities. Wave pattern ϕ refers to the EEG activity with amplitude no larger than $20\mu V$. Wave pattern χ mostly appears at the transition from one EEG rhythm to another, accordingly, no dominant rhythmic pattern can be justified for the segment. In addition to the six patterns above, the interpreter can detect two artifacts: baseline-drift (denoted by 'B') and EMG (electromyograph) interference (denoted by 'I').

Each windowed segment of the EEG is examined by the following criteria in order (Fig. 4-1):

Criterion-ϕ: Amplitude$<20\mu V$,

Criterion-χ: $f_{r,3}<7\text{Hz}<f_{r,1}$ and $|p_3|>0.8$,

Criterion-δ: $f_{r,1}<7\text{Hz}$ and $f_{r,4}<3.5\text{Hz}$,

Criterion-θ: $f_{r,1}<7\text{Hz}$,

Criterion-α: $7\text{Hz}<f_{r,1}<14\text{Hz}$ and $7\text{Hz}<f_{r,3}$,

Criterion-β: $f_{r,1}>7\text{Hz}$,

where p_3 is the AR(2) pole of *output*$_3$. The length of p_3 is closely related to the amplitude and reflects the significance of the root frequency $f_{r,3}$. In the criterion, the major root frequency of each segment ($f_{r,1}$) is used to differentiate between 0–7Hz and 7–30Hz EEG rhythms. A segment is identified as the χ activity if its $f_{r,1}$ is higher than 7 Hz and its $f_{r,3}$ is lower than 7Hz with $|p_3|$ larger than a given threshold. Then the $f_{r,4}$ is used to discriminate δ activity from θ activity. The pattern excluded by the α-criterion, yet, with $f_{r,1}$ higher than 7Hz is classified as β activity. EEG segments with the above characteristics exhibit no particularly dominant EEG rhythm. According to the oscillations assumption for the brain dynamics, dif-

ferent neuronal networks may start to oscillate with different frequencies during mental activity [Klimesch 1996, Pfurtscheller and Lopes da Silva 1999]. It is thus reasonable to recognize this as the β activity.

After identifying the six patterns from the meditation EEG record, the algorithm further scrutinizes the interpretation to detect the segments of baseline drift and EMG interference possibly leaked to the categories of normal EEG patterns.

4.1.2. Baseline drift detection

EEG signals very often are affected by baseline drift caused by eye movement, breathing, etc. Some methods have been proposed to remove this baseline drift [Philips 1996, Lo and Leu 2001]. In this proposed algorithm, the baseline drift component is detected and marked without being removed from the record. Due to the low-frequency characteristic of baseline drift, the criterion for detecting baseline drift is focused on the delta band (1–3Hz) as described below.

(1) A segment of EEG which has been classified as δ and is longer than 1.25 s.

(2) Amplitude of the signal exceeding $80\mu V$.

(3) Number of zero-crossing events of the segment is less than 3 within 1 s.

The baseline drift is symbolized by 'B'. Generally speaking, a lower (higher) threshold results in more false-positive (false-negative) B segments. Threshold selection needs to be done experimentally to achieve better performance.
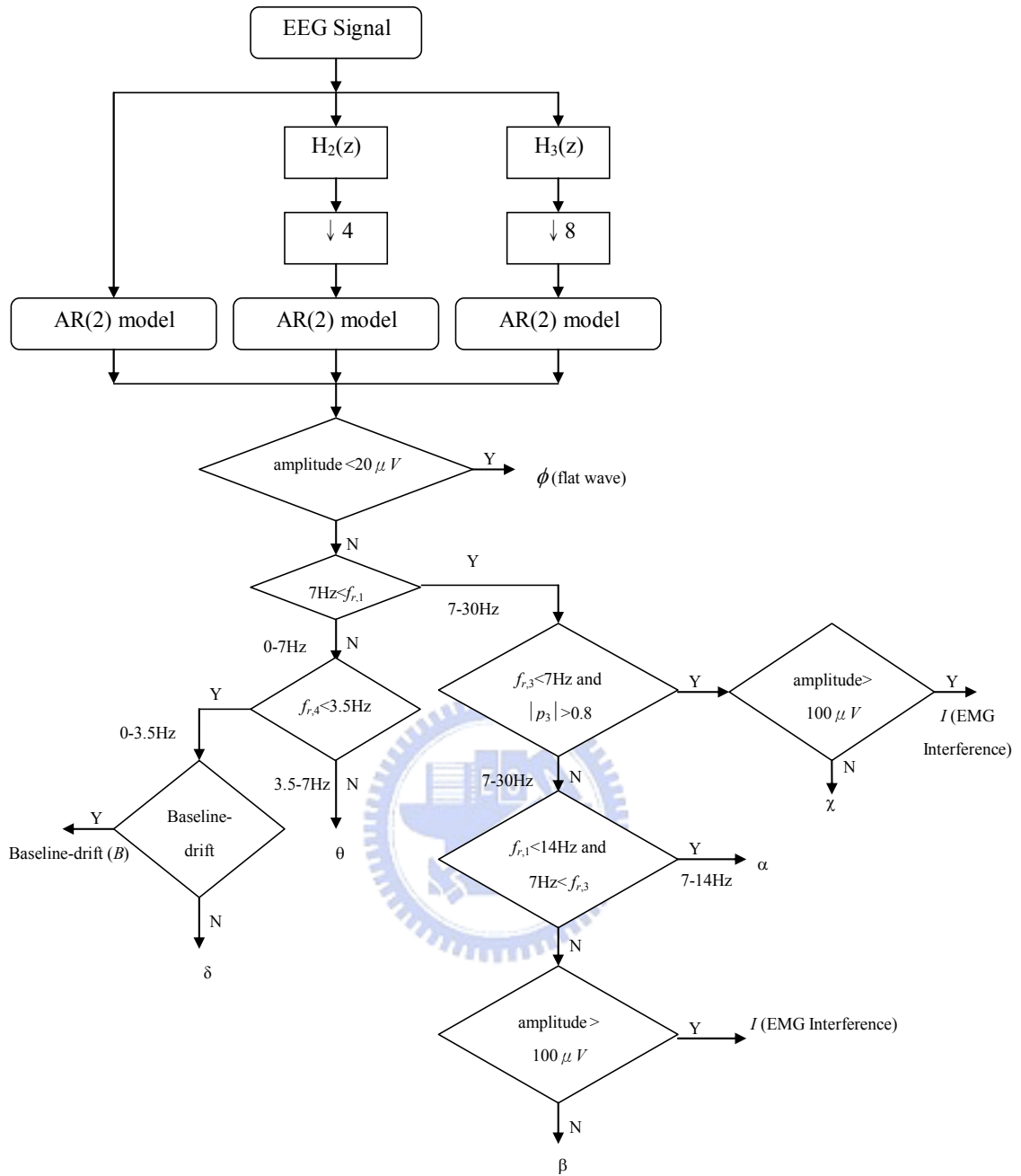
Figure 4-1: The scheme of the meditation EEG interpreter algorithm.

4.1.3. EMG interference detection

EMG interference often caused by muscle contraction is characterized by high frequency and large amplitude. Based on the six patterns first identified by the algorithm, β- and χ-patterns are firm candidates in consideration of frequency. These two patterns are further screened by the criterion of an amplitude larger than $100\mu V$ to determine the EMG interfer-

ence (denoted by 'I').

(a)

(b)
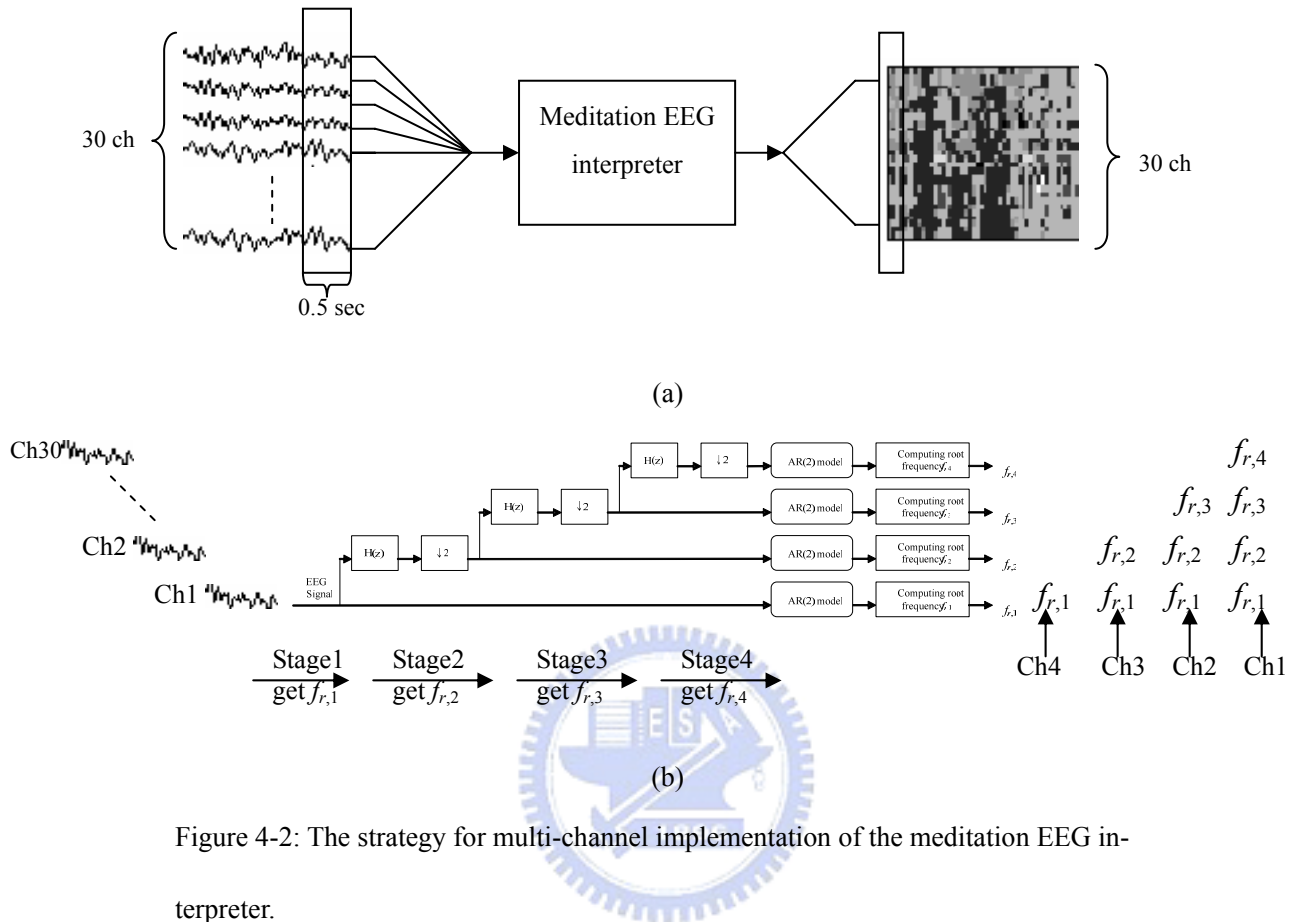
Figure 4-2: The strategy for multi-channel implementation of the meditation EEG in-

terpreter.

In sum, EEG signals are first decomposed into different subband components by succes-

sive downsampling and filtering. Root frequency of each subband component is then esti-

mated by the AR(2) model. Based on a set of logical criteria, the algorithm is capable of iden-

tifying six distinct EEG patterns and two artifacts. Figure 4-1 illustrates the complete scheme

of the proposed algorithm. Figure 4-2 displays the strategy for multi-channel implementation.

All the 30-channel windowed epochs are fed into the meditation EEG interpreter (Fig. 4-2(a)).

The running window moves at a step size of 0.25 s. The interpretation results are illustrated

by a two-dimensional gray-scale image with the vertical and horizontal axes representing the

spatial (channel) and temporal factor, respectively. Various gray scales are used to denote the

six patterns and two artifacts (cf. figures in chapter 2). Fig. 4-2(b) shows the scheduling process of the sequential queue implemented in the meditation EEG interpreter. With appropriate design of the buffer and latch, the architecture in Fig. 4-2(b) can process multi-channel EEGs in a real-time manner.

4.2. Experimental material

The meditation EEG signals were recorded using 30-channel SynAmps amplifiers (manufactured by NeuroScan, Inc.) connected to a Pentium4 1.5 (GHz) PC. A 30-channel recording montage was used, with the linked M1-M2 (mastoid electrodes) as the common reference (Fig. 4-3). The analog EEGs were pre-filtered by a band-pass filter with passband 0.3–30 Hz, and digitized at 200 Hz sampling rate. Each recording lasted for 40 minutes, including the first 10-minute background EEG (the subject sat in a normal, relaxed position with eyes closed) and the rest 30-minute meditation EEG.
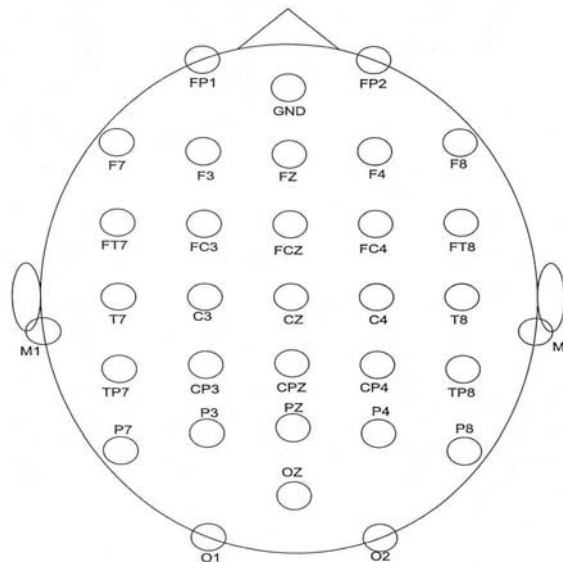
Figure 4-3: 30-channel recording montage.

During the meditation session, the experimental subject sat, with eyes closed, in the

full-lotus or half-lotus position. Each hand formed a special mudra (called the Grand Harmony Mudra) and was laid on the lap on the same side. The subject focused on the Zen Chakra (third ventricle) and the Dharma Eye Chakra (hypophysis) [Lo et al. 2003] at the beginning of meditation until the physical and mental consciousness was transcended. The control subject, on the other hand, sat in a normal, relaxed position with eyes closed [Liao and Lo 2003].

This study involved 8 meditators and 8 control subjects. The experimental group had 1 female and 7 males (mean age: 34.7 ± 7.5 years). Their experiences in Zen Buddhist practice spanned 11.1 ± 1.8 years. The control group included 8 males (mean age: 27.3 ± 1.3 years).

4.3. Simulation

To verify the performance of the algorithm, we first generated a simulated signal by connecting five patterns (ϕ, δ, θ, α, and β in Fig. 4-4(a)–(e)) in series as shown in Fig. 4-4. We note that pattern χ emerges when θ and β overlap each other so that a transition is identified as χ. Assuming a sampling rate of 200Hz, each pattern can be simulated by simply placing the pole in the appropriate frequency band (Table 4-1) and adding Gaussian noise. Fig. 4-4(f) displays the interpretation result that uses different gray scales to represent different patterns. The gray-scale bar chart correlates well with the EEG pattern evolution. It thus confirms the feasibility of the meditation EEG interpreter algorithm.

To demonstrate the efficacy in artifact detection, the baseline drift and EMG-interference artifacts were simulated by mixing a β pattern (Fig. 4-5(a)) with two components, a low-frequency, large-amplitude sinusoid component (Fig. 4-5(b)) and a high-frequency, large-amplitude random noise component (Fig. 4-5(c)). The interpretation result is shown in Fig. 4-5(d). The first artifact with low frequency and large amplitude is recognized as the baseline drift; while the lagging one with high-frequency randomness is classified as the

EMG interference. These two artifacts often contaminate the EEG.
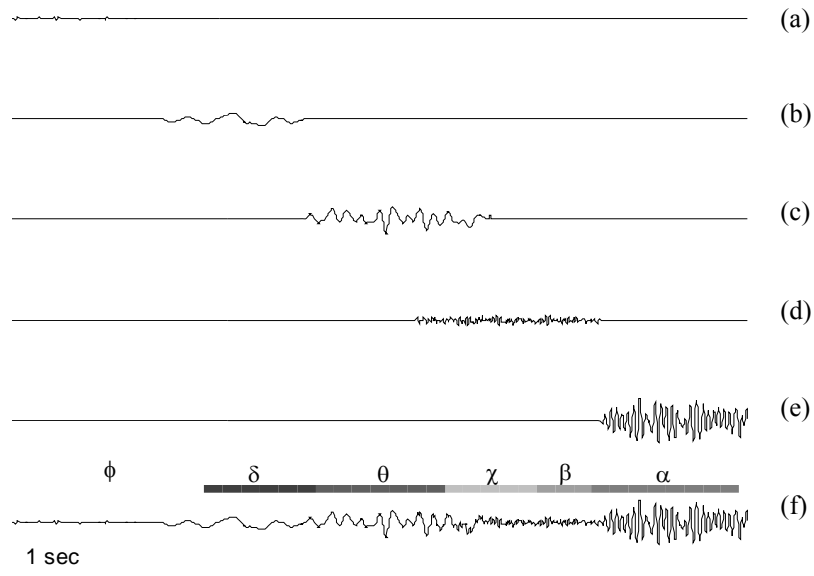
Figure 4-4: Simulation results (a) φ, (b) δ, (c) θ, (d) β, (e) α, and (f) simulated signal
and interpretation results represented by gray-scale bar chart.

Table 4-1: Poles (magnitude (normalized) and phase (radian)) designed to simulate the
four well-known EEG rhythms.

	δ	θ	α	β
Pole locations	$0.98 \angle 0.04$	$0.98 \angle 0.16$	$0.98 \angle 0.4$	$0.88 \angle 0.63$

Finally, interpretation accuracy was evaluated by comparison with the result of a na-
ked-eye examination by an experienced EEG interpreter. The error rate is approximately
10.7%. Figure 4-6 displays a partial segment of interpretation results.
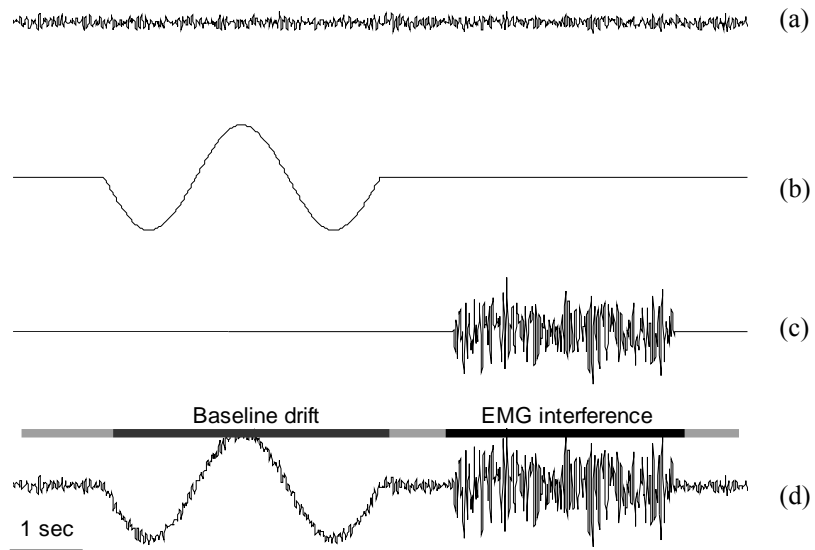
Figure 4-5: Simulation of the baseline drift and EMG-interference artifacts by mixing (a) β activity (b) low-frequency, large-amplitude sinusoid, and (c) high-frequency, large-amplitude random noise, and (d) the artifacts and interpretation result.
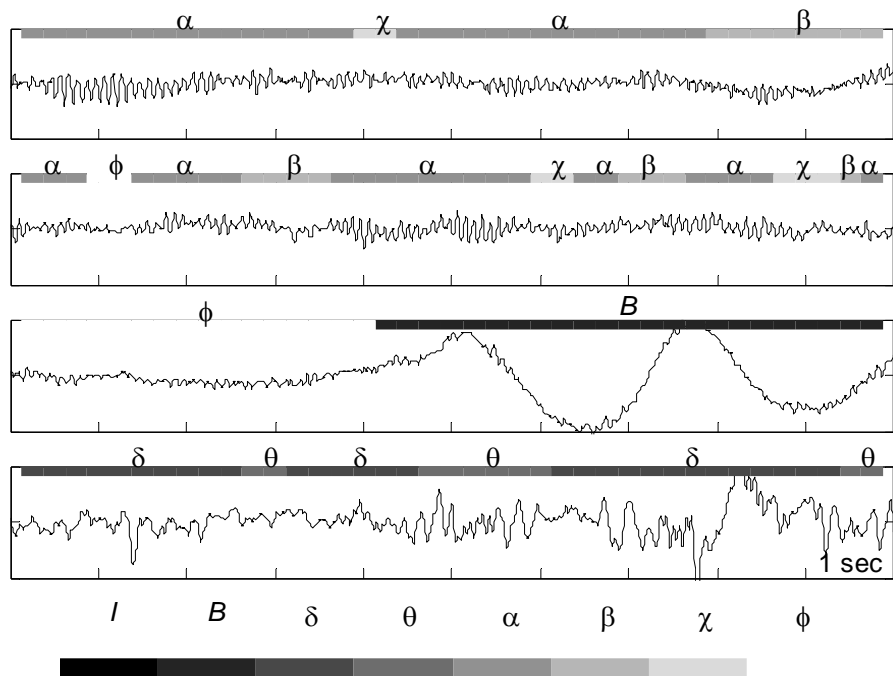
Figure 4-6: Interpretation results illustrated by gray-scale bar chart.

4.4. Meditation EEG interpretation

4.4.1. Pattern-distribution histogram of Zen-meditation EEG

The 20-minute meditation/relaxation EEG in the mid-recording session was examined by the meditation EEG interpreter using a 0.5-sec window length with a moving step of 0.25-sec. Percentages of six patterns and two artifacts of eight control and eight experimental subjects are listed in Tables 4-2 and 4-3, respectively. To compare the global trend of a pattern-distribution histogram between two groups for the whole view, the percentage of each pattern was derived by (1) averaging the percentages of all 30 channels (removing the spatial factor), and (2) averaging the percentages of all the subjects within the same group (removing the inter-subject factor). Figure 4-7(a) displays the final pattern-distribution histograms of both groups. Based on the comparison of EEG pattern percentages between the two groups, the P value was calculated by the t-test for each pattern. We notice significant distinction between the two groups in four patterns, χ ($P<0.05$), δ ($P<0.01$), θ ($P<0.01$) and β ($P<0.01$). The large percentage of χ in the experimental group may be due to frequent transitions, during Zen meditation, between different consciousness states resulting in different brain dynamics. Higher δ and θ contents in the control group apparently correspond to the habitual drowsiness induced during the relaxation session. In regard to the β phenomenon, our previous study has shown significantly higher β activities for the meditation EEG. The above observation can be further verified by Fig. 4-7(b) that plots the pattern histograms for all sixteen subjects listed in Tables 4-2 and 4-3.

Table 4-2: The percentage of each pattern (control group).

Subject	ϕ	χ	δ	θ	α	β	B	I
c1	6.27	4.41	43.33	2.35	0.36	22.50	20.72	0.07
c2	2.62	13.01	59.64	3.74	0.16	15.94	4.57	0.32
c3	2.63	4.53	20.45	32.88	25.36	11.52	2.57	0.05
c4	10.56	7.00	30.54	18.90	13.61	16.33	2.42	0.61
c5	2.88	3.92	32.74	24.55	27.69	6.45	1.67	0.10
c6	6.24	1.11	49.40	25.23	10.91	1.43	5.66	0.03
c7	13.38	1.08	32.01	20.64	25.89	4.86	2.01	0.12
c8	2.97	10.81	57.85	2.81	1.92	20.66	2.94	0.04

ϕ : flat wave B: Baseline-drift I: EMG interference

Table 4-3: The percentage of each pattern (experimental group).

subject	ϕ	χ	δ	θ	α	β	B	I
e1	2.39	13.32	12.21	0.45	9.54	59.32	2.68	0.08
e2	20.92	23.10	9.56	0.60	5.56	39.45	0.79	0.01
e3	2.43	19.63	23.56	1.25	1.03	39.86	10.80	1.43
e4	5.20	57.28	3.71	1.12	1.46	31.06	0.06	0.11
e5	35.01	2.03	21.81	0.90	0.19	33.73	6.18	0.15
e6	1.78	64.02	3.64	0.46	3.50	26.14	0.16	0.29
e7	0.13	39.00	8.83	0.93	8.57	34.57	0.80	7.17
e8	2.21	2.20	7.47	7.08	59.14	20.66	0.99	0.25

ϕ : flat wave B: Baseline-drift I: EMG interference

	ψ	χ	δ	θ	α	β	B	I
□ experimental group	8.76	27.57	11.35	1.60	11.13	35.60	2.81	1.19
■ control group	5.95	5.73	40.75	16.39	13.24	12.46	5.32	0.17
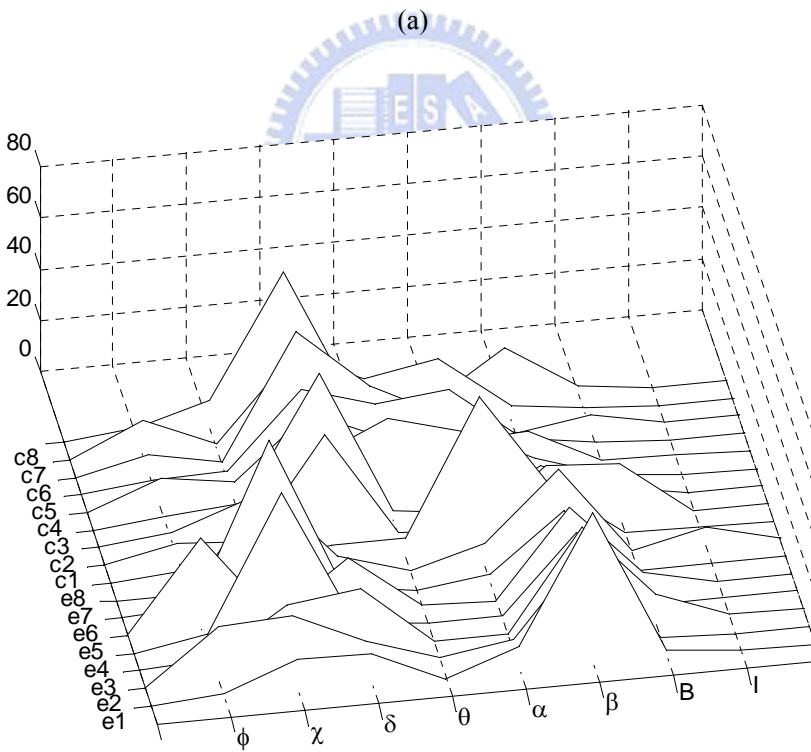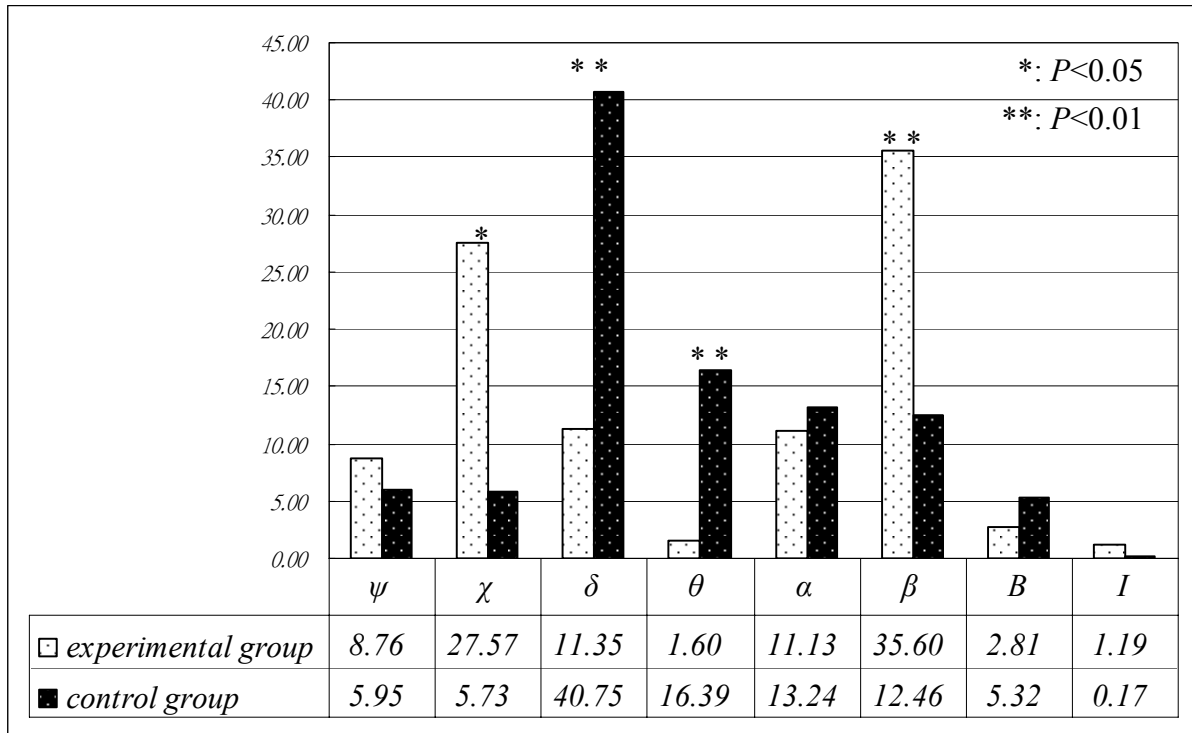
(a)

(b)

Figure 4-7: Mean percentage of each pattern: (a) for the experimental (light bars) and control (dark bars) group (*: *P*<0.05 and **: *P*<0.01), (b) for each individual subject (e1–e8: experimental subjects, c1–c8: control subjects).

56

When inspecting the individual variation in the experimental group, the flat wave is remarkable in subjects e2 and e5 (Table 4-3). According to our previous studies [Lo et al. 2003], the flat wave ϕ often emerges during deep meditation for some Zen meditators. Subjects e4 and e6 have prominent χ activities, indicating possibly the situation that their meditation scenarios involved a number of transitions from one consciousness state to another. Subject e8's EEG showing a lot of α activity is quite different from the others. According to her narration, she was in a very relaxed state and felt energy (Qi) flowing through her back during the meditation. We note that the artifacts identified are mostly the baseline drift for both groups.

We then investigated the time evolution of spatial characteristics of EEG rhythms. Figure 4-8 displays the interpretation results for two experimental subjects (e1 and e6) and one control subject (c2). They reveal three typical histograms of EEG spatiotemporal characteristics often observed in both groups: 1) β-dominant globally, 2) χ-dominant locally, and 3) δ-dominant all over the scalp.

The horizontal axis of gray-scale bar charts in Fig. 4-8 represents the time, while the vertical direction corresponds to the recording channels, from the top downwards, FP_1, F_7, FP_2, F_3, FC_3, FT_7, T_7, F_8, F_4, Fz, FCz, C_3, TP_7, FT_8, FC_4, Cz, CPz, CP_3, P_3, P_7, T_8, TP_8, C_4, P_8, CP_4, P_4, Pz, Oz, O_1, and O_2. Gray-scale mapping as illustrated in Figs. 4-4–4-6 is applied. The interpretation result of control subject c2 (Fig. 4-8(c)) reveals a large proportion of δ, θ and α activities in comparison with the result of experimental subjects e1 (Fig. 4-8(a)) and e6 (Fig. 4-8(b)). Results of control subject c2 reveal decreasing β and χ activities and increasing δ rhythm during the entire process. On the contrary, the δ rhythm is insignificant in both experimental subjects.
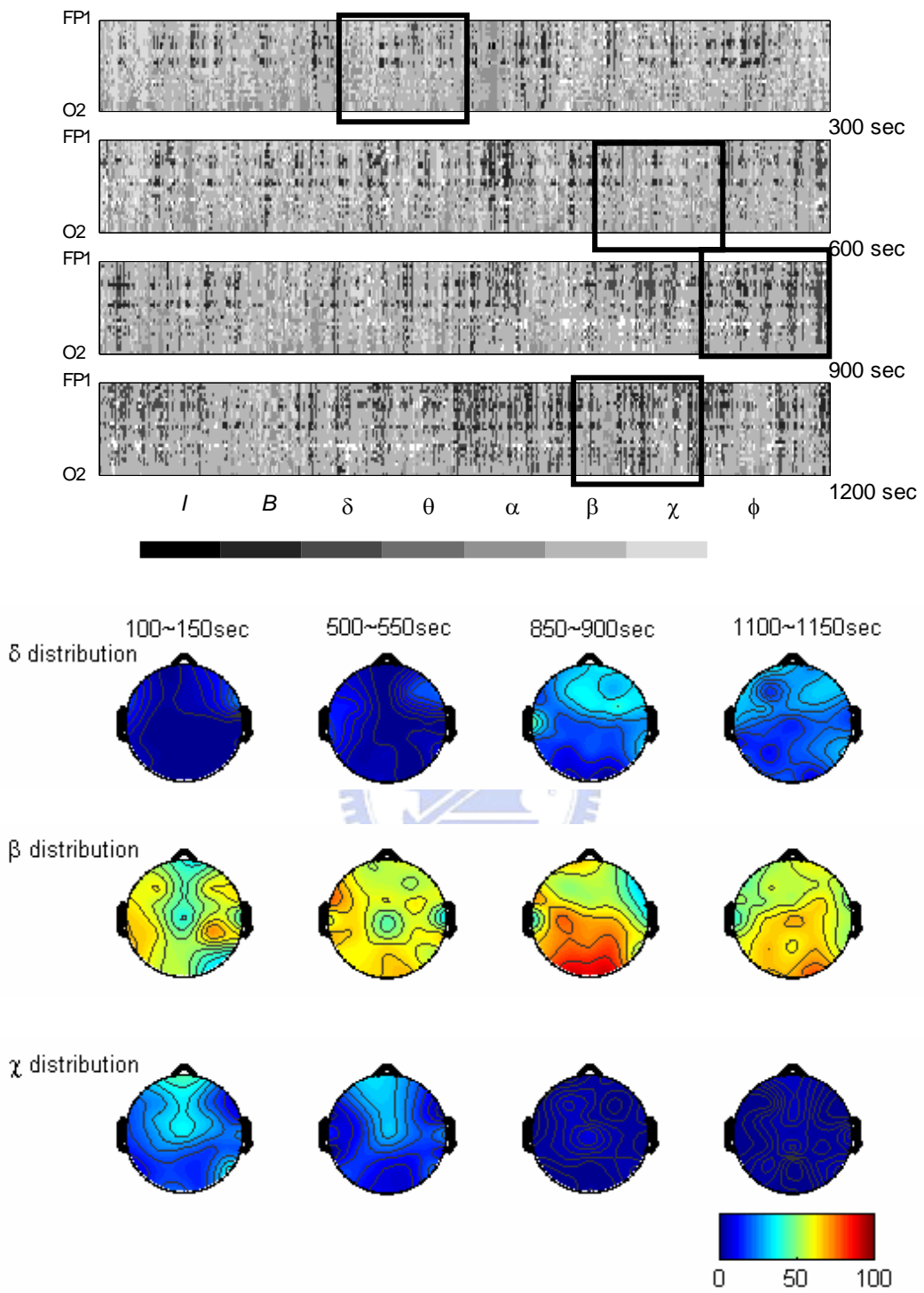
(a)

Figure 4-8: Interpretation results of (a) subject e1, (b) subject e6, and (c) subject c2, with four selected time ranges framed by squares.

FP1

O2

300 sec

FP1

O2

600 sec

FP1

O2

900 sec

FP1

O2

1200 sec

I B δ θ α β χ ϕ

δ distribution

100~150sec 425~475sec 850~900sec 1100~1150sec

β distribution

χ distribution

0 50 100
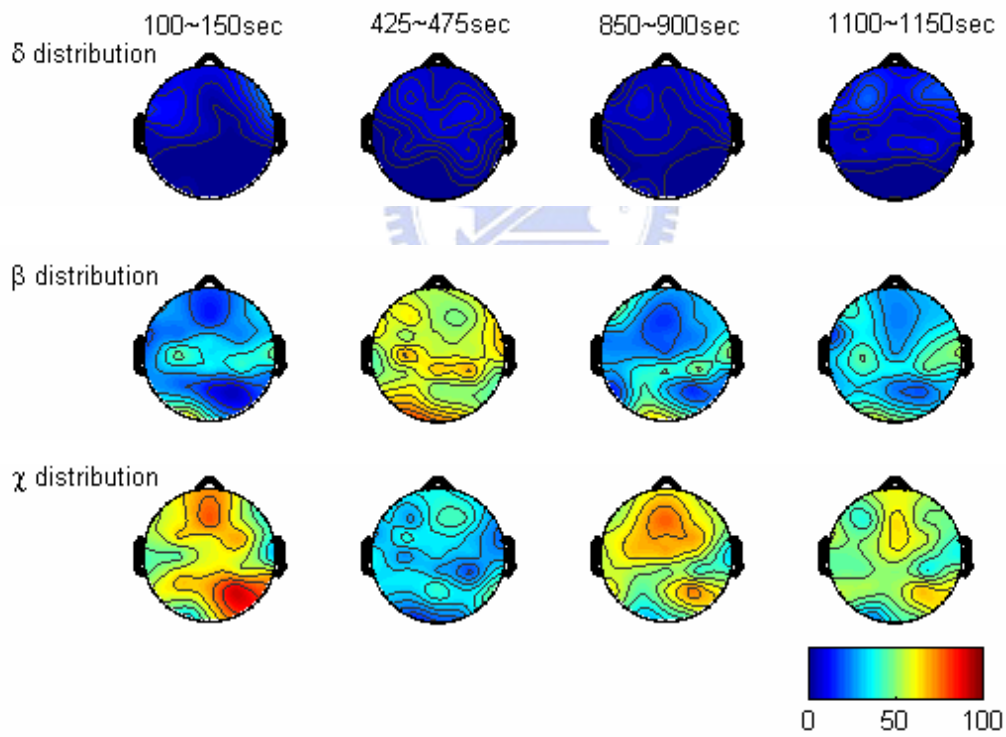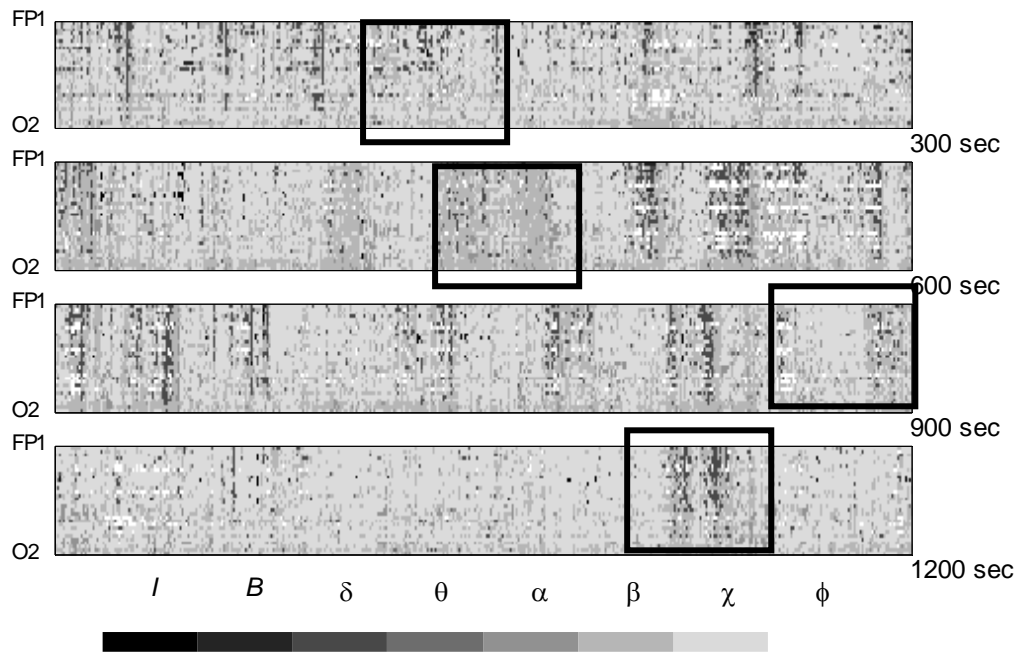
(b)

Figure 4-8 (Continued)
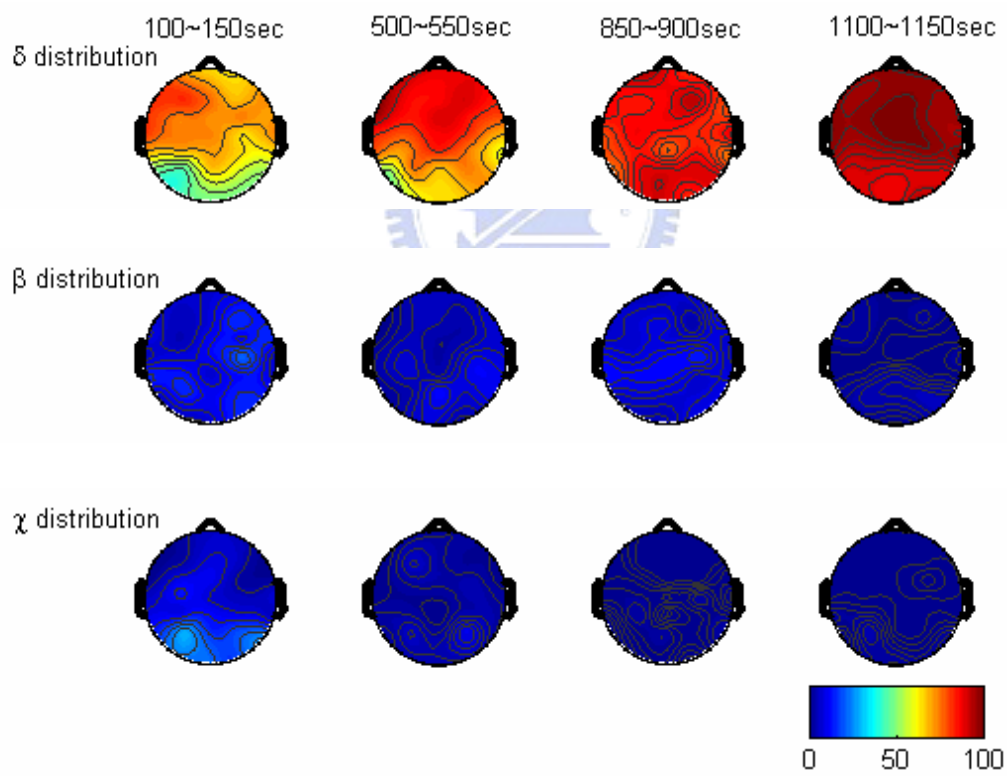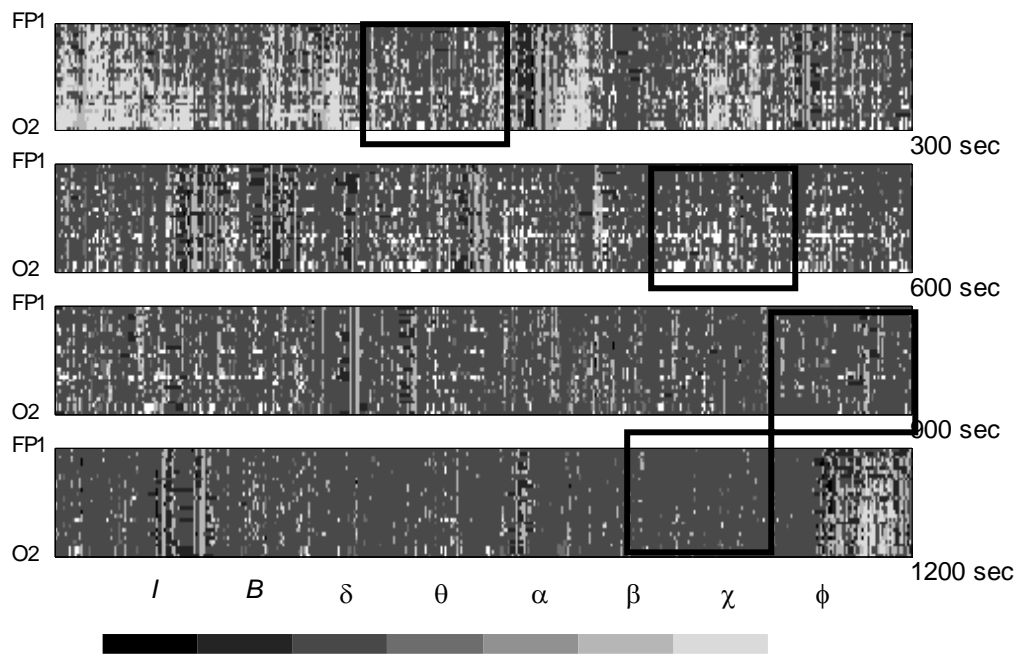
(c)

Figure 4-8 (Continued)

4.4.2. Temporal evolution of β brain mappings

As illustrated in Fig. 4-7, the β pattern plays a key role in discriminating EEG character-istics between the two groups. This part of the study was thus designed to explore the tempo-ral evolution of β spatial distribution. The "β% mapping" in Fig. 4-9 was constructed from the percentages of β activity of all 30 channels, based on a window size of 10 s. The time marked beneath each scalp plot is the beginning of each window under analysis. The β% mapping for subject e1 (Fig. 4-9(a)) demonstrates one typical case in the experimental group that their oc-cipital β activity spreads quickly towards the central and frontal regions and becomes a dif-fuse low-power, fast activity. Subject e6 has more focal, occipital β activity occurring inter-mittently (Fig. 4-9(b)). On the other hand, we can hardly identify any β activity from the β% mapping of control subject c2 (Fig. 4-9(c)).

(a)
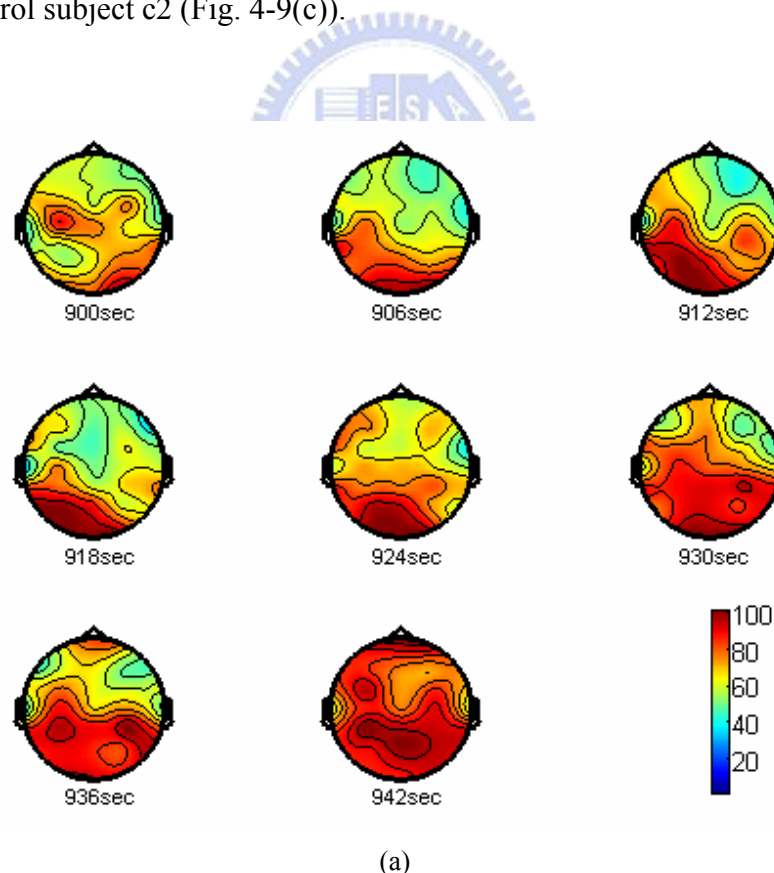
Figure 4-9: The β% mappings of two experimental subjects: e1 in (a) and e6 in (b), as well as one control subject c2 in (c). Each mapping displays the spatial distribution of percentages of β activity within a 10-second window beginning at the designated time.
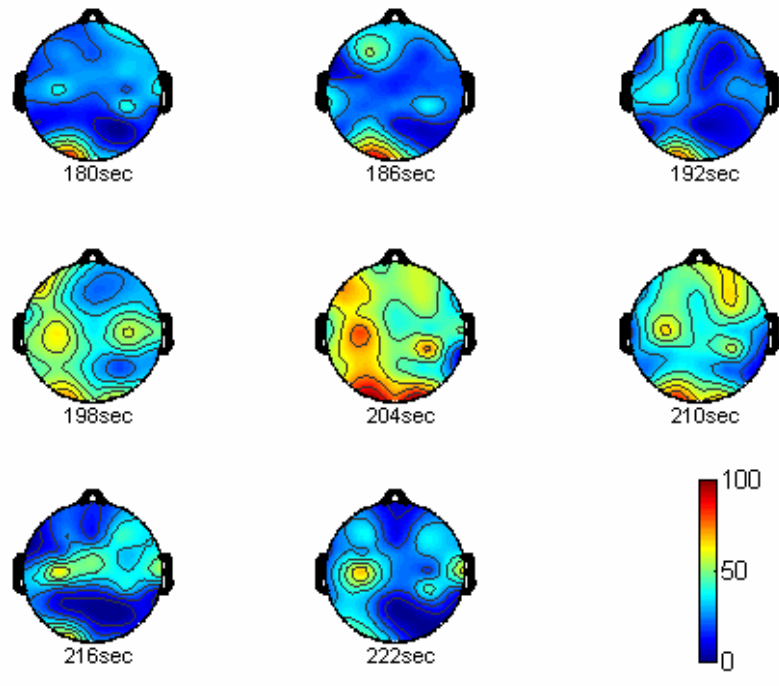
(b)
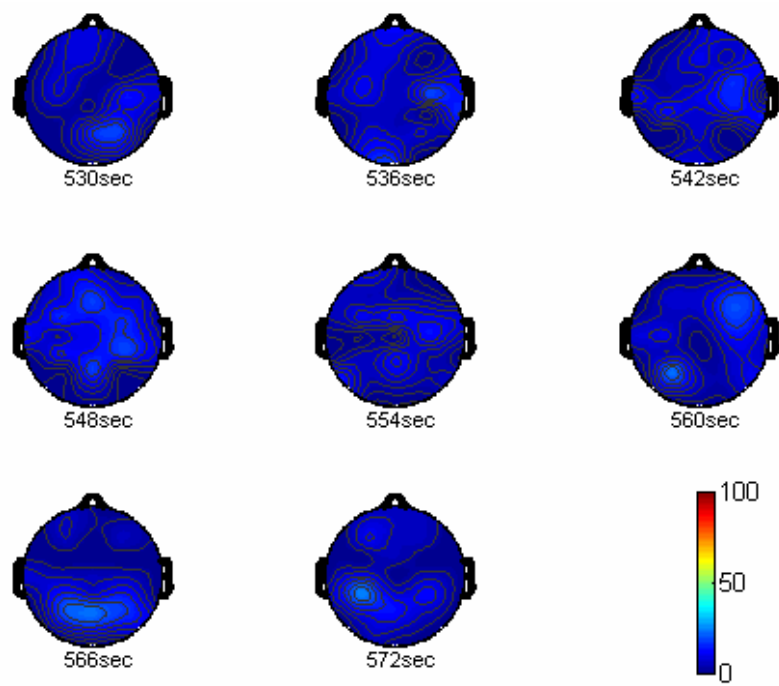
(c)

Figure 4-9 (Continued)

Chapter 5－
Study on EEG Local Spatiotemporal Synchronization Based on Multivariate AR Model

Instead of postulating that the brain constructs information from the input of a sensory nerve, we can suppose that the centers of the nervous system, including the brain, resonate to information.

~ James Jerome Gibson
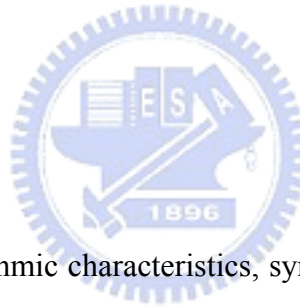
IN addition to the EEG rhythmic characteristics, synchronization among different brain areas has been another important issue of meditation-EEG study. This chapter presents an approach for synchronization measurement, Local spatiotemporal synchronization index (LSTS index). With an efficient algorithm, the LSTS measurement could be considered as a potential approach for investigating the spatiotemporal synchronization under particular mental states, such as the Zen meditation. The following section illustrates the method for computing LSTS index. And then performance of the method was evaluated by a finger-movement experiment. Finally, the index was applied to the meditation EEG, providing us with another view of brain dynamics under meditation.

5.1. Local spatiotemporal synchronization index (LSTS)

5.1.1. Multivariate Autoregressive (mAR) Model

In terms of an mAR model, multichannel EEGs **x** at time n can be modeled as the weighted summation of its p's previous observations plus a residual noise **e**, we obtain

$$\mathbf{x}_n = \mathbf{A}_1 \mathbf{x}_{n-1} + \mathbf{A}_2 \mathbf{x}_{n-2} + \cdots + \mathbf{A}_p \mathbf{x}_{n-p} + \mathbf{e}_n.$$ (5-1)

The column vector $\mathbf{x}_n$ is composed of m-channel EEG samples at time n with their mean removed, and $\mathbf{A}_i$ is an $m \times m$ coefficient matrix.

In the mAR model, noise covariance matrix $\mathbf{V}_e$ of a noise vector $\mathbf{e}_n$ can be regarded as the goodness of fitting a linear model to a set of data. Based on a specified dimension mp, we can achieve a good fitting for a system with better synchronization among state variables (channels), that results smaller fitting residuals. On the contrary, spatial desynchronization causes an increase in residuals. Thus, the LSTS index defined as

$$S_{ch} = \log_{10}\left[\det(\mathbf{V}_e)\right]$$ (5-2)

can reasonably represent the goodness of fitting neighboring EEGs to channel ch. With the same model order p, a large S represents weak spatiotemporal synchronization, that is, EEG activities at different channels behave dissimilarly in rhythmic aspects.

According to the algorithm Arfit [Schneider and Neumaier 2000, Neumaier and Schneider 2001], the noise covariance matrix $\mathbf{V}_e$ can be efficiently estimated. A pth order mAR model can be solved by formulating a linear regression model of which the parameters can be estimated by an ordinary least squares (OLS) method. Evaluation of N state vectors $\mathbf{x}_1, \cdots \mathbf{x}_N$ requires p's initial vectors $\mathbf{x}_{1-p}, \cdots \mathbf{x}_0$. Thus equation (5-1) can be reformulated as

$$\underbrace{\left[\mathbf{x}_1 \cdots \mathbf{x}_N\right]}_{\mathbf{b}} = \underbrace{\left[\mathbf{A}_1 \cdots \mathbf{A}_p\right]}_{\mathbf{a}} \underbrace{\begin{bmatrix} \mathbf{x}_0 & \cdots & \mathbf{x}_{N-1} \\ \vdots & \cdots & \vdots \\ \mathbf{x}_{1-p} & \cdots & \mathbf{x}_{N-p} \end{bmatrix}}_{\mathbf{X}} + \left[\mathbf{e}_1 \cdots \mathbf{e}_N\right] \tag{5-3}$$

that leads to the OLS solution of $\mathbf{a}$ as

$$\mathbf{a} = \mathbf{b}\mathbf{X}^T(\mathbf{X}\mathbf{X}^T)^{-1} \tag{5-4}$$

The least squares estimates can be computed from a QR factorization of the compound matrix

$\mathbf{K} = [\mathbf{X}^T \mathbf{b}^T]$, that is

$$\mathbf{K} = \mathbf{Q}\mathbf{R} \tag{5-5}$$

where $\mathbf{Q}$ is an orthogonal matrix and $\mathbf{R}$ is an upper triangular matrix

$$\mathbf{R} = \begin{bmatrix} \mathbf{R}_{11} & \mathbf{R}_{12} \\ 0 & \mathbf{R}_{22} \end{bmatrix} \tag{5-6}$$

Thus, the LSTS index S_{ch} is estimated by the noise covariance matrix $\mathbf{V}_e$ that can be efficiently derived without computing the coefficient matrices $\mathbf{A}_1 \cdots \mathbf{A}_p$ as shown below

$$\mathbf{V}_e = \frac{1}{N - mp} \mathbf{R}_{22}^T \mathbf{R}_{22} . \tag{5-7}$$

More details can be referred to [Neumaier and Schneider 2001].

5.1.2 Array of channel montage

To construct the multichannel autoregressive model, we need to determine the array of neighboring channels (number and montage). This study employed the standard 10/20, 30-channel recording montage. As illustrated in Fig. 5-1(a), the neighboring channels of Cz (called the "seed channel"), assuming a link distance d=1, are FCz, C3, C4, and CPz, denoted by $N_{Cz}(1)$ = {Cz, FCz, C3, C4, CPz}. Note that the link distance d=1 indicates those channels, in all directions, right adjacent to the seed channel considered (Cz). To derive the channel array obtain $N_{Cz}(2)$ for d=2, the five channels in $N_{Cz}(1)$ are used as seed channels to find their adjacent channels, as shown in Fig. 5-1(b).

65

$N_{Cz}(1) = \{Cz, FCz, C3, C4, CPz\}$

(a)
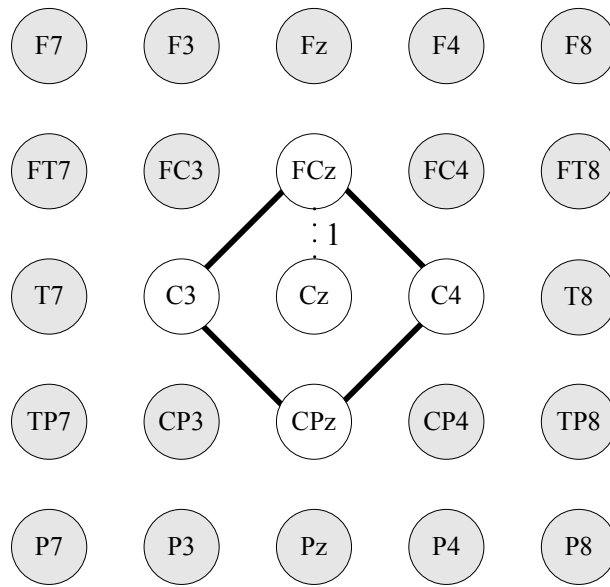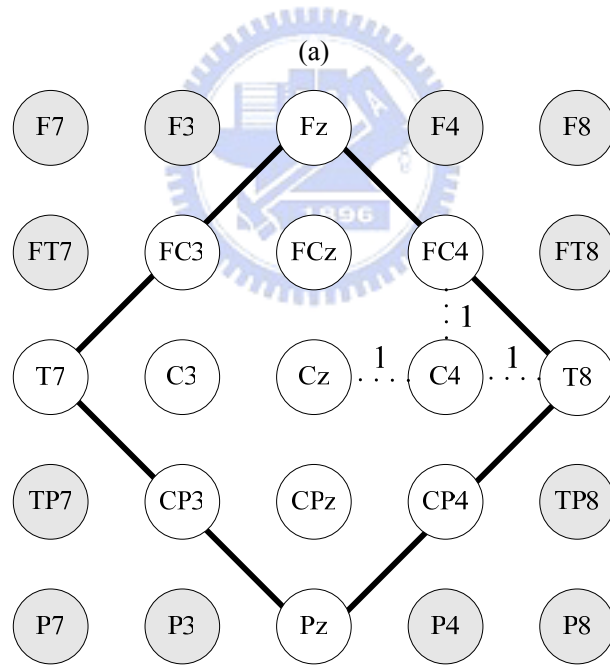
$N_{Cz}(2) = \{Cz, Fz, FC3, FCz, FC4, T7, C3,$
$C4, T8, CP3, CPz, CP4, Pz\}$

(b)

Figure 5-1: An illustration of array of neighboring channels. The array montage for seed channel Cz with link distance (a) d=1, (b) d=2.

5.2. An externally-paced finger-movement experiment

5.2.1. Data collection

Three right-handed, male subjects (s1, s2 and s3) at the mean age of 30±1 years participated in this experiment. EEG signals were recorded from standard 10/20, 30 electrode sites, that are fed into a 30-channel amplifiers (SynAmps, manufactured by NeuroScan, Inc.) connected to a Pentium4 1.5 (GHz) PC. Common reference of linked M1-M2 (mastoid electrodes) was used (Fig. 4-3). The analog EEGs were filtered by a bandpass filter with passband 0.3–30 Hz, and digitized at 200 Hz sampling rate.

In the finger-movement experiment, each subject was requested to perform two experimental runs, each with 20 trials (10 left-finger and 10 right-finger trials). The subject pressed a button using his right (left) index finger on the right-finger (left-finger) trials. A stimulation unit, g.STIMunit (manufactured by Guger Technologies OEG), was used to control the experimental procedure. The subject sat in a comfortable chair in front of the stimulation unit (Fig. 5-2(a)). Figure 5-2(b) illustrates the entire experimental protocol. Initially, a cross (+) was displayed in the screen center. At the 8th second, the cross vanished. At the 9th second, an arrow pointing to the right (or left) appeared for 5 seconds to instruct the subject to press the rightmost (leftmost) button on the keypad (Fig. 5-2(b)) using his right (or left) index finger. Each trial lasted 14 seconds and the span between two trials varied in the range of 4–4.5 seconds to avoid adaptation.
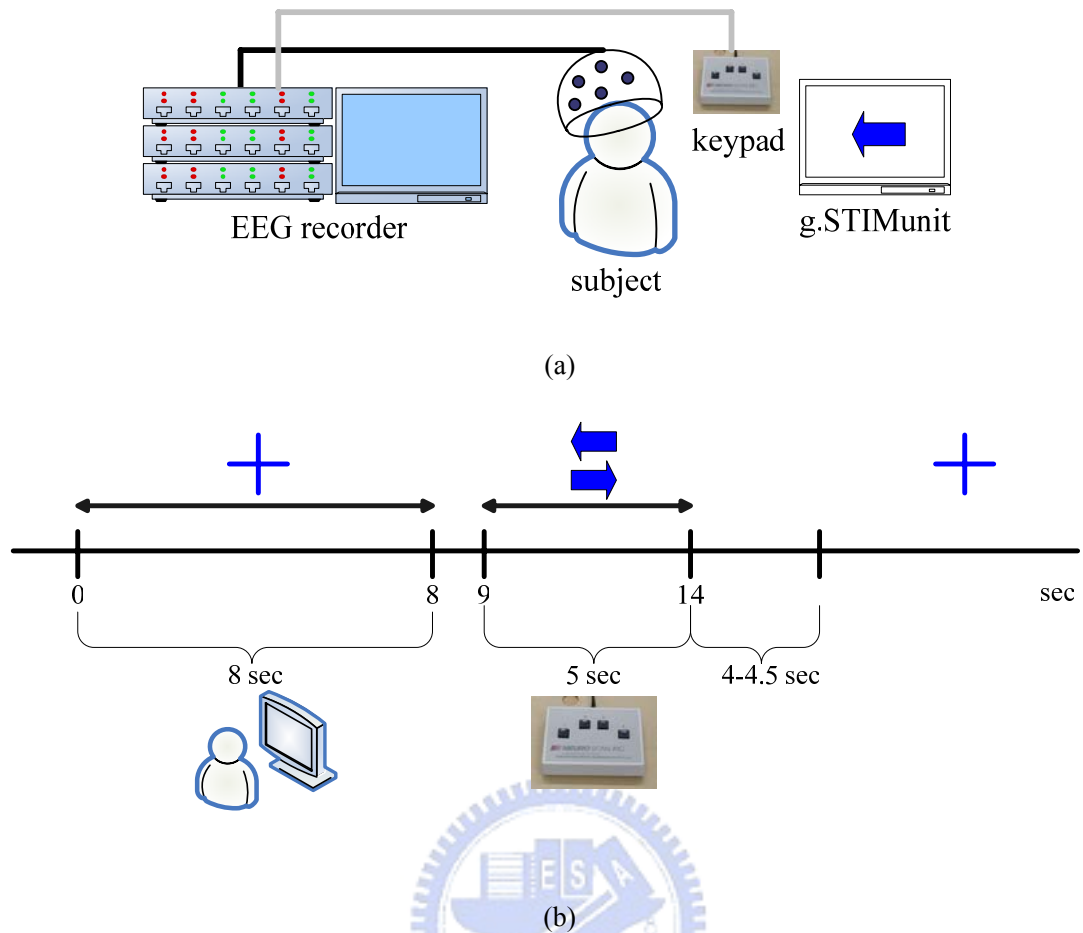
Figure 5-2: (a) The experimental setup and (b) the scheduling protocol in the externally-paced finger-movement experiment.

5.2.2. Determination of model order

To determine an appropriate order of the mAR model, Schwarz's [Schwarz 1978] Bayesian Criterion (SBC) was adopted in this study for its superior consistency [Lütkepohl 1993]. Order p of the mAR model needs to be optimally determined to encompass possible EEG activities. In the finger-movement experiment, 10-second EEGs were extracted from each trial for further analysis (will be illustrated in the following section). The mAR model was implemented on a 2-second epoch. Based on our analysis, the resulting model order drifts within a small range of 2. Figure 5-3 presents the maximum and minimum orders of 20 trials of subject s1. Accordingly, for each subject a constant model order was chosen as the

computed maximum value plus one in order to cover the possible model dynamics embedded.
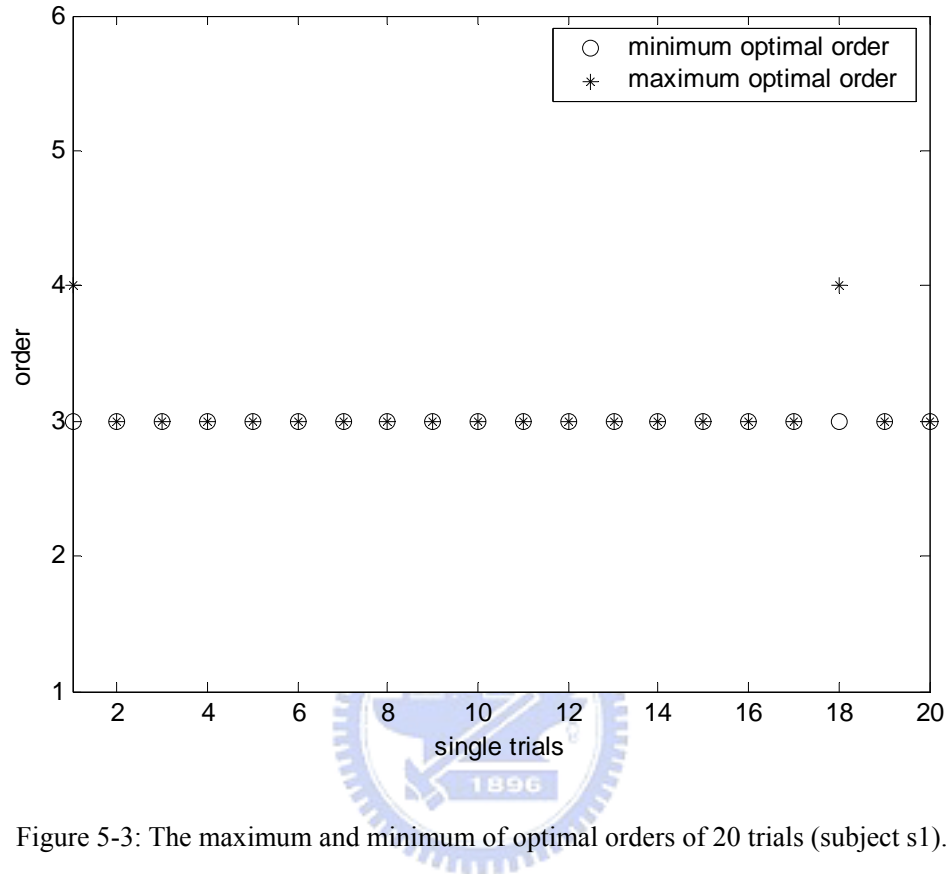
Figure 5-3: The maximum and minimum of optimal orders of 20 trials (subject s1).

5.2.3. Simulation

We firstly analyzed the LSTS index of a simulated 5-channel, 10-second EEG signal. Assuming a sampling rate of 200Hz, the "local synchronization" phenomenon can be simulated by simply placing the model pole at the same location ($0.98 \angle \pm 0.4$ as shown in Fig. 5-4(a)) for all five channels. Further, Gaussian noise n with little disturbance n_{1-5} (Fig. 5-5(a)) is injected into each channel. To mimic the time-varying behavior, the pole of $H_3(z)$ is shifted into beta band ($0.9 \angle \pm 0.63$ as shown in Fig. 5-4(b)) at the 7th second, with another uncorrelated Gaussian noise n_b added (Fig. 5-5(b)). The simulated signals are shown in Fig. 5-6(a). In the LSTS analysis, we implemented a 2-second running window with a moving step

of 1 second. Order of the mAR model is 3, which is the SBC optimal model order plus one. The LSTS index shown in Fig. 5-6(b) exhibits a burst value of S at the 7th second that corresponds to the pre-designed variation in channel 3.

5.2.4. Results

Each single-trial 10-second EEG was composed of one 7-second epoch before pressing the button and another 3-second epoch afterward (Fig. 5-7). Totally 40 trials were collected over two runs (20 "left-finger" and 20 "right-finger" trials). All trials were visually inspected to exclude epochs with artifacts. The model order $p=5$ for all subjects was determined by the strategy described in Section 5.2.3. As illustrated in Fig. 5-7, the running LSTS curve was derived using a moving window with length of 2 seconds and step size of 1 second. Each seed channel with its neighboring channels can form 9 S values for each single trial. The S sequences derived under the same task (right-finger or left-finger movement) were averaged by each channel. We took an average of the first 3 values as the baseline and calculated the relative changes in the following data analysis.
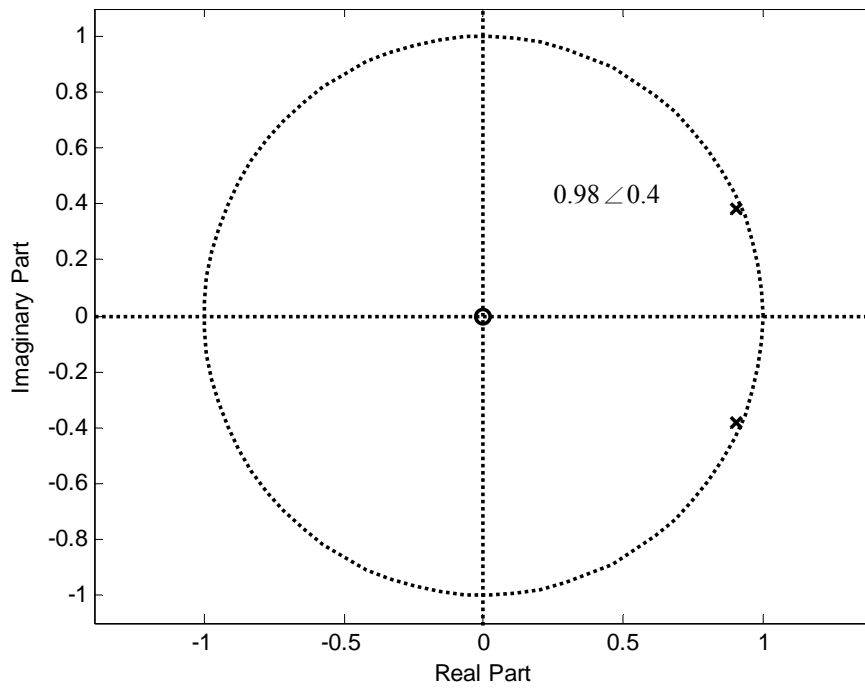
(a)
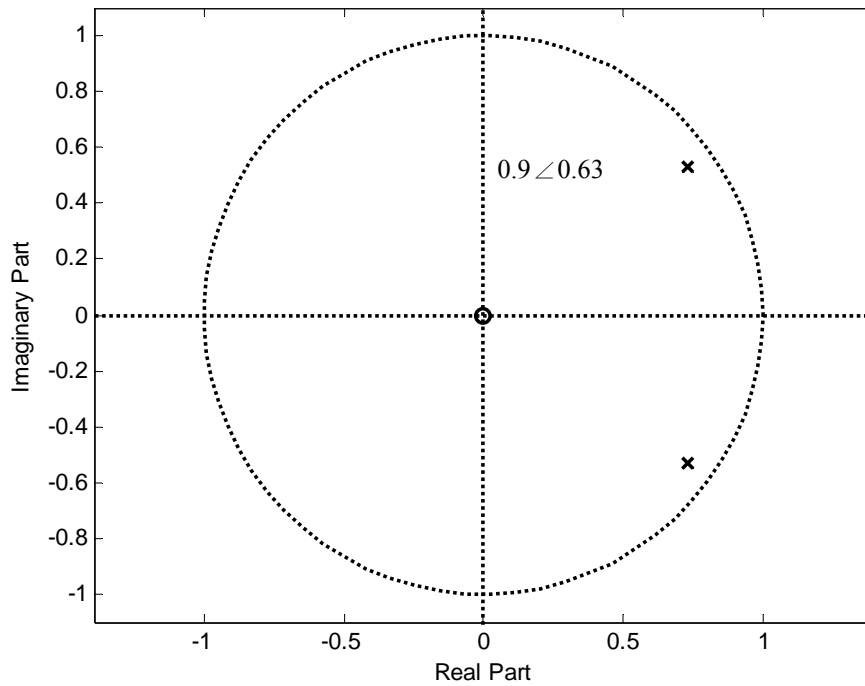
(b)

Figure 5-4: (a) Pole-zero plot of $H_{1,2,4,5}(z)$ and $H_3(z)$ for the first 7 seconds. (b) Pole-zero plot of $H_3(z)$ after the 7th second.
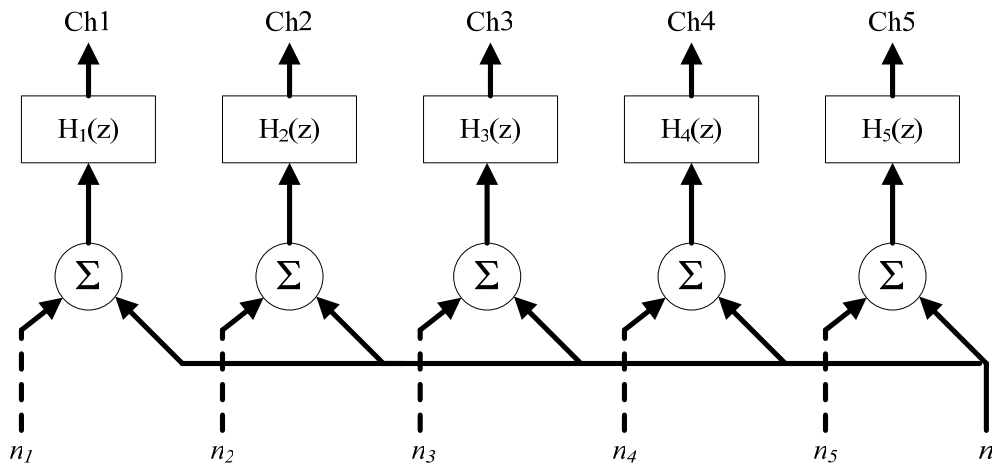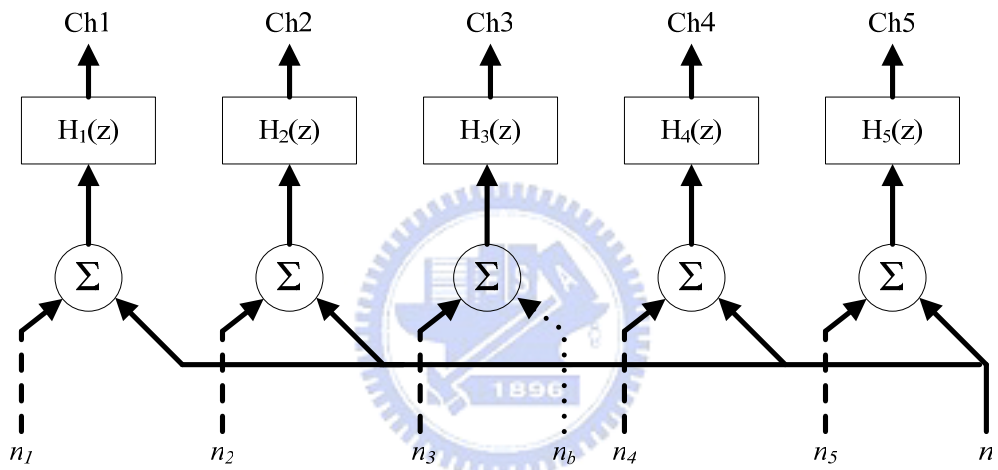
Figure 5-5: Model of the simulated signal for (a) the first 7 seconds, and (b) the last 3

seconds.
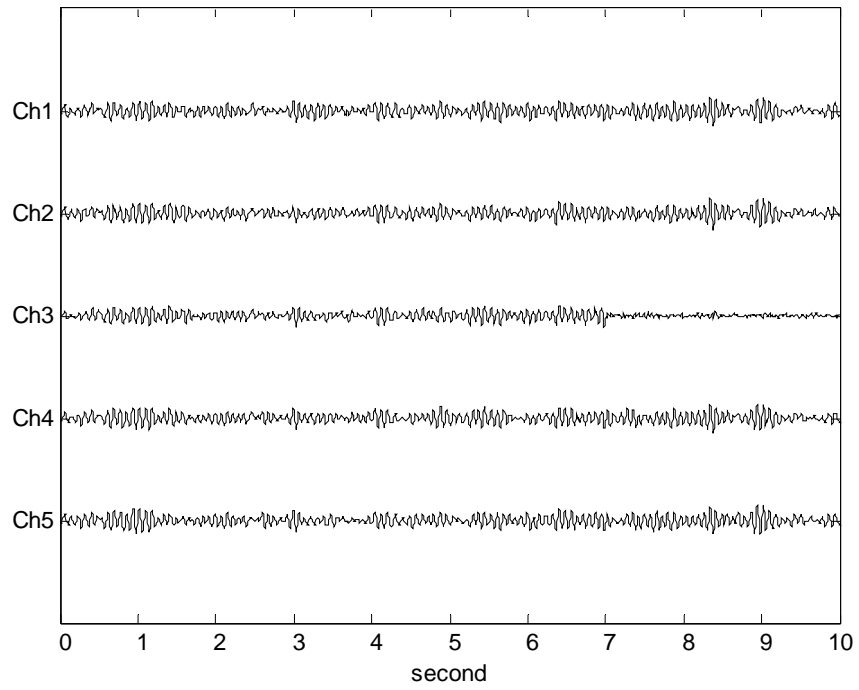
(a)
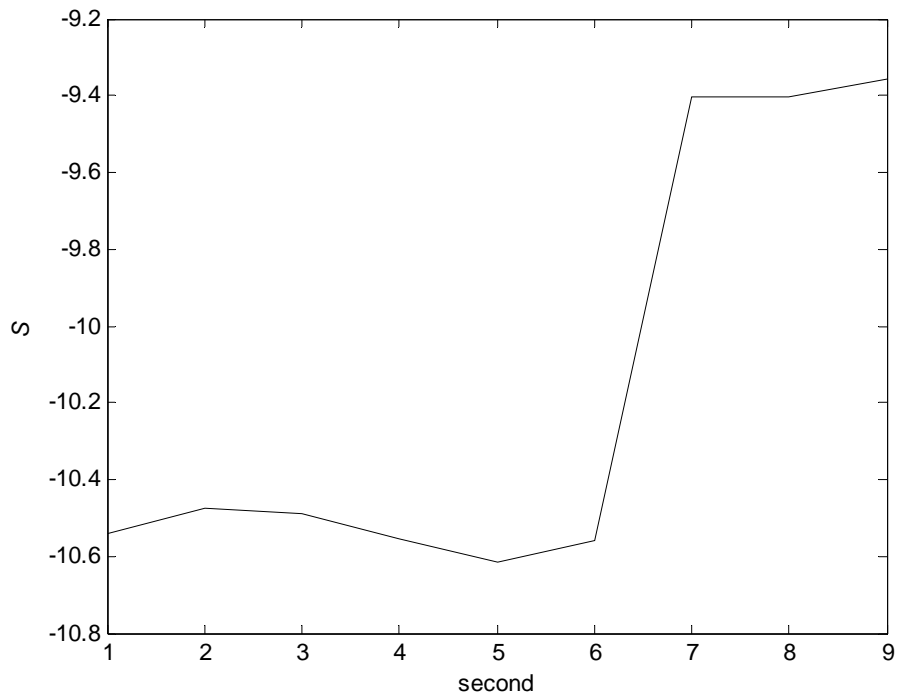
(b)

Figure 5-6: (a) The simulated signal, and (b) the time-varying LSTS index.
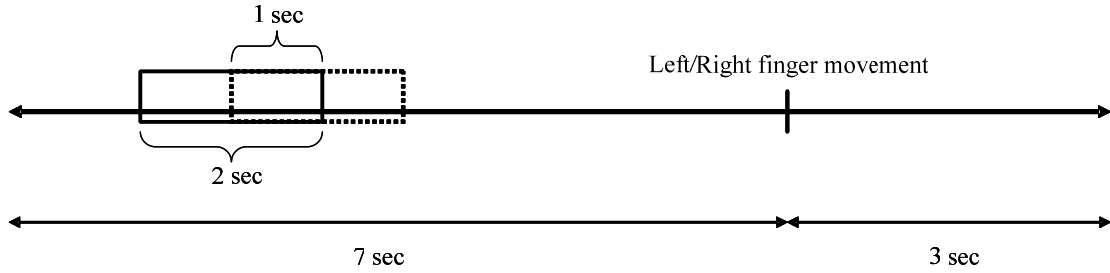
Figure 5-7: Illustration of the single-trial and the moving window used in the LSTS analysis.

Figure 5-8 presents an example of right-finger movement experiment conducted by subject s1. The figure plots S_{C3} (seed channel: C3) curves for orders p=3–5. Note that the actual time of starting to move the finger is earlier than that of pressing the button. Since primary motor area becomes desynchronous at movement, a significant increase (Table 5-1) at the 6th second (due to the 2-second window size) occurs. The results also demonstrate that order p=3 is insufficient for modeling the overall system complexity characterized by the selected five channels.

Despite the model order, the neighboring channels are another concern of computing LSTS index. Based on the same data set, Fig. 5-9 demonstrates the effect of various channel combinations (order p=5). The figure reveals that S_{C4} is much smaller than S_{C3}. To investigate spatiotemporal (de)synchronization, we constructed the brain mapping of S_{ch} using different colors to encode the levels of S_{ch}. Based on d=1 and d=2, Fig. 5-10 and 5-11 respectively plot the S_{ch} brain mappings evolving in a 10-second trial interval for subject s1. Warm hues indicate spatiotemporal desynchronization. Groups (a) and (b) in both figures refer to S_{ch} brain mappings for left-finger and right-finger tests, respectively. Using an array of channels at a smaller area (d=1), Fig. 5-10 reveals more localized spatiotemporal desynchronization than Fig. 5-11.
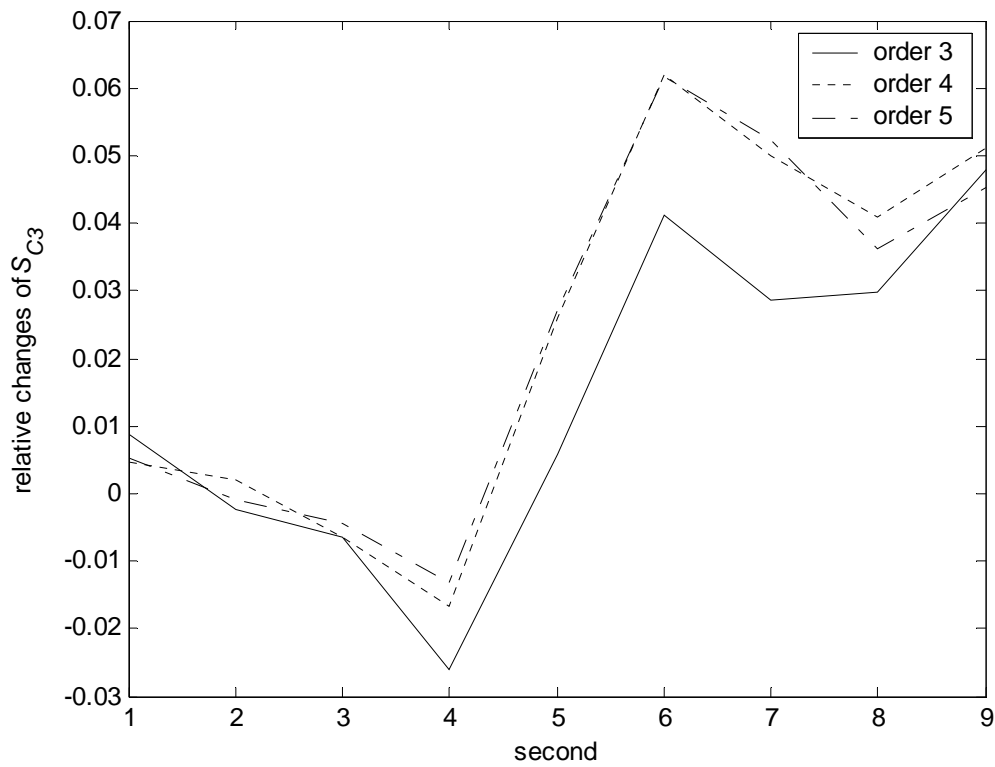
Figure 5-8: The time-varying S_{C3} (subject s1) using model orders 3 (solid), 4 (dotted),

and 5 (dash-dot) in the right finger movement study.

Table 5-1: Relative changes of S_{C3} at second 4 and 6 and their differences in different

model order.

	at second 4	at second 6	difference
Order 3	-0.026	0.041	0.067
Order 4	-0.017	0.062	0.079
Order 5	-0.013	0.062	0.075
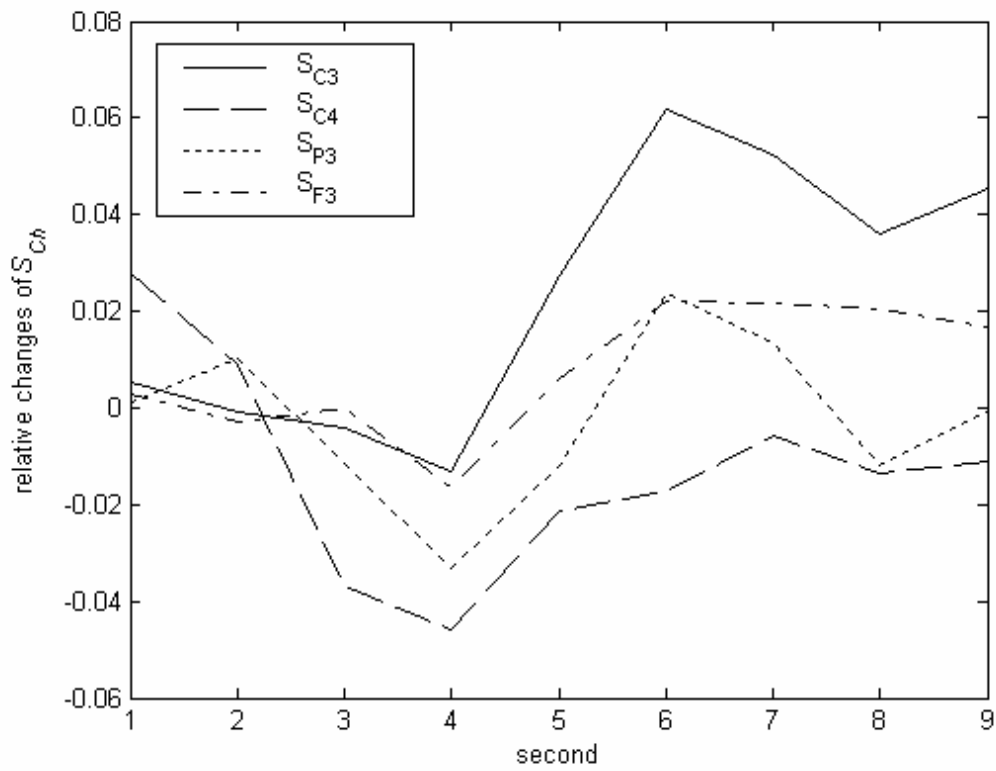
Figure 5-9: The time-varying S_{ch} (subject s1) using seed channel C3 (solid), C4 (dashed), P3 (dotted), and F3 (dash-dot) in the right finger movement study.

second 1-2　　　second 2-3　　　second 3-4

second 4-5　　　second 5-6　　　second 6-7

second 7-8　　　second 8-9　　　second 9-10

Press the button

(a)

second 1-2　　　second 2-3　　　second 3-4

second 4-5　　　second 5-6　　　second 6-7

second 7-8　　　second 8-9　　　second 9-10

Press the button
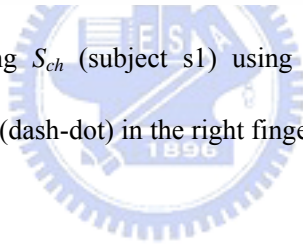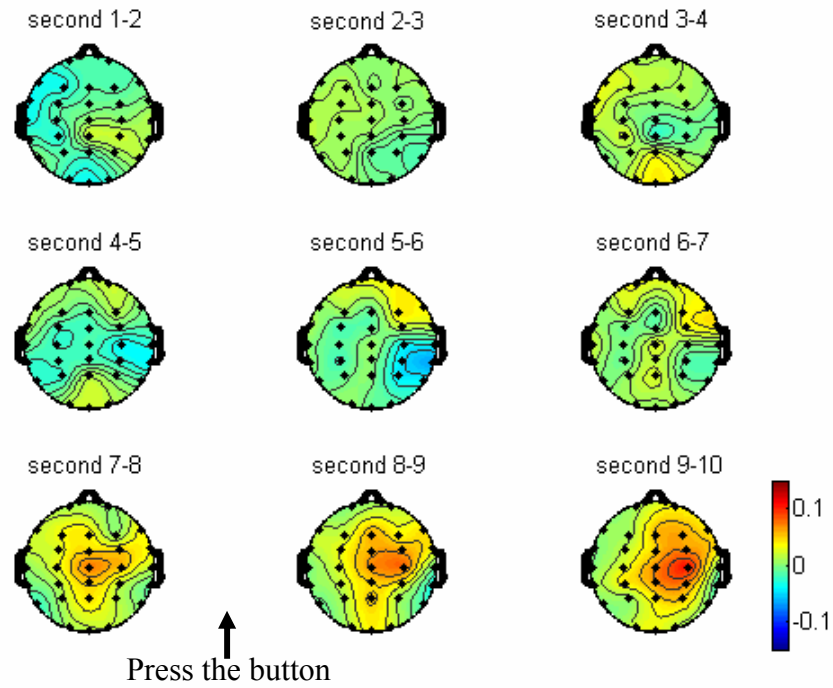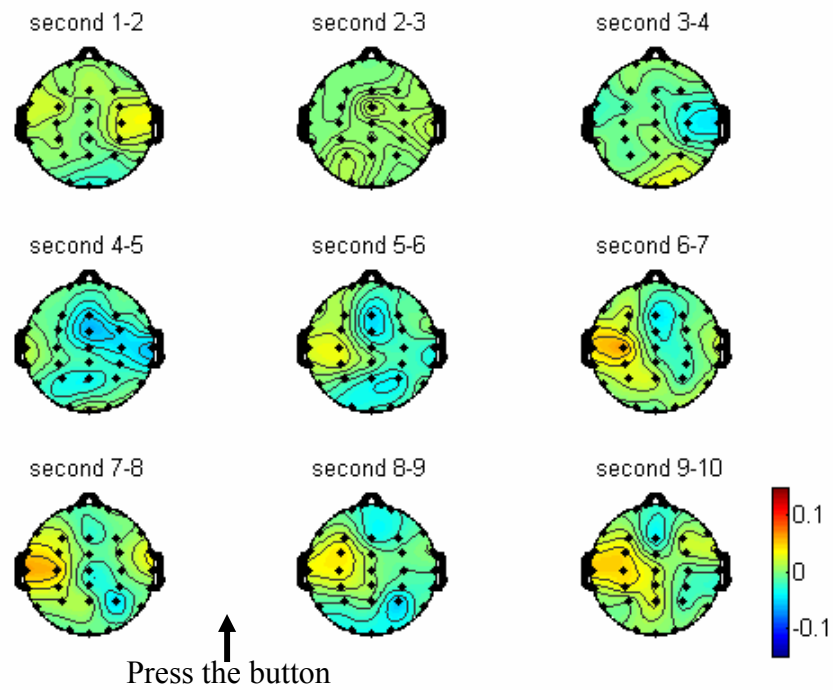
(b)

Figure 5-10: The S_{ch} brain mappings evolving in a 10-second trial interval for subject s1 using link distance d=1 in the study of (a) left index finger movement, and (b) right index finger movement.

77

second 1-2   second 2-3   second 3-4

second 4-5   second 5-6   second 6-7

second 7-8   second 8-9   second 9-10

0.1
0
-0.1

Press the button

(a)

second 1-2   second 2-3   second 3-4

second 4-5   second 5-6   second 6-7

second 7-8   second 8-9   second 9-10

0.1
0
-0.1

Press the button
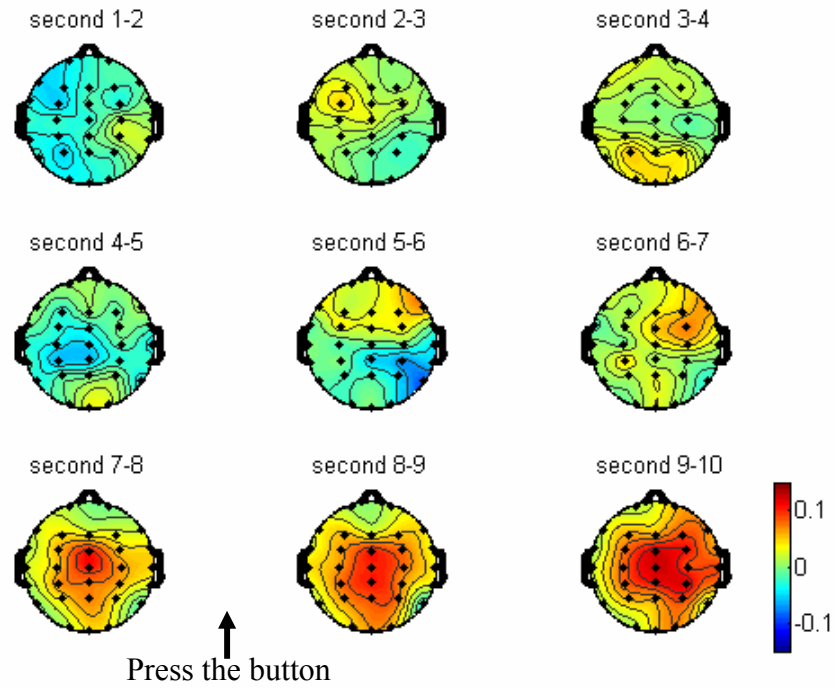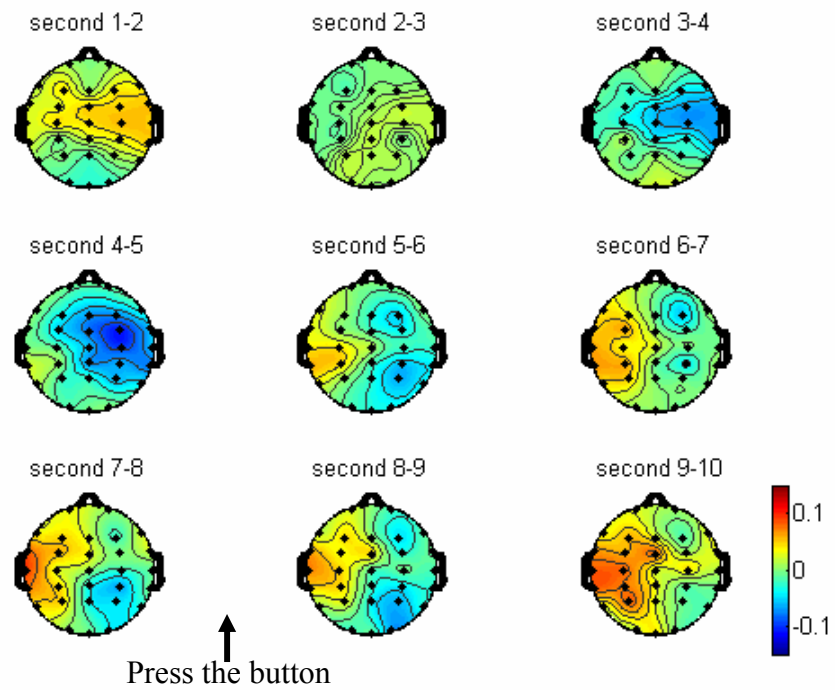
(b)

Figure 5-11: The S_{ch} brain mappings evolving in a 10-second trial interval for subject s1 using link distance d=2 in the study of (a) left index finger movement and (b) right index finger movement.

second 1-2 second 2-3 second 3-4

second 4-5 second 5-6 second 6-7

second 7-8 second 8-9 second 9-10

0.1
0
-0.1

Press the button

(a)

second 1-2 second 2-3 second 3-4

second 4-5 second 5-6 second 6-7

second 7-8 second 8-9 second 9-10

0.1
0
-0.1

Press the button
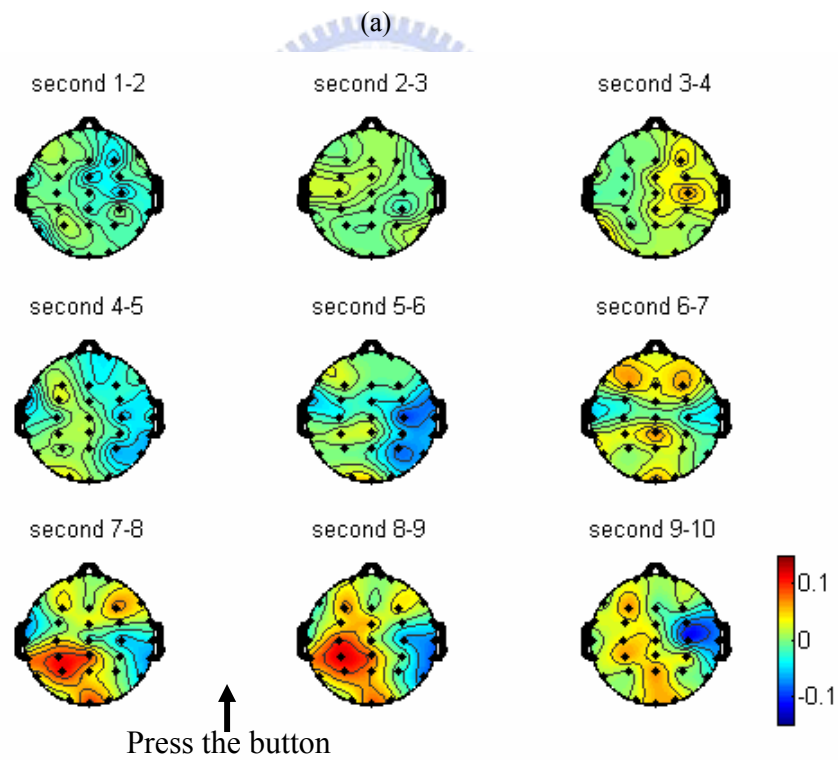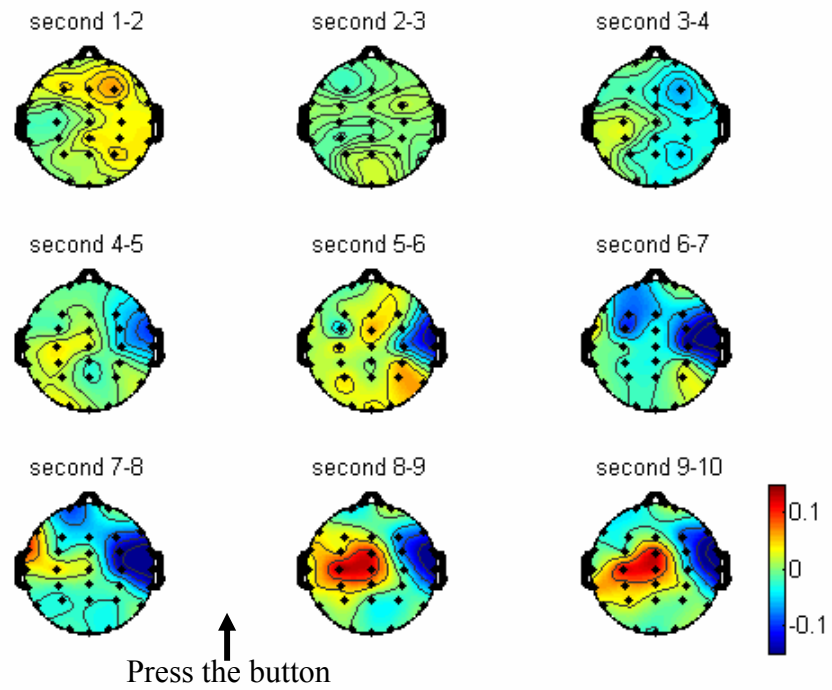
(b)

Figure 5-12. The 10-second S_{ch} brain mappings of (a) subject s2, and (b) subject s3 in the right index finger movement study (link distance d=1).

Figure 5-12 displays the S_{ch} brain mappings (d=1) in the 10-second trial interval for (a) subject s2 and (b) subject s3 at the right-finger movement tests. Both subjects exhibit spatiotemporal desynchronization near the corresponding primary motor area (C3). Another noticeable result was the spatial desynchronization emerging at the primary motor area *before* actually making a movement in Fig. 5-10(b). This phenomenon depicts the observation of advance desynchronization induced by mentally intended movement [Pfurtscheller 2001].

5.3. An application to meditation EEG

5.3.1. Data collection

The EEG recording setup was the same as the externally-paced finger-movement experiment. Two meditators and one control subject participated in the experiment. Both meditators have been practicing Zen-Buddhist meditation for more than eight years. Each meditation EEG recording lasted 30 minutes, including the first 10-minute background EEG (the subject sat in a normal relaxed position with eyes closed) and the rest 20-minute meditation EEG [Lo et al. 2003]. The second-phase recording for control subject collected the awake, resting EEG with eyes closed.

5.3.2. Results

Unlike the previous experiment, the EEGs collected in this study cannot be correlated with any a priori event or reference. In meditation EEG analysis, we focused on the variation of LSTS index relative to some specific EEG patterns. Base on the same signal processing scheme, a baseline was first derived as the average of the first 3 LSTS indexes obtained by applying a 2-second running window moving at a 1-second step. Order of the mAR model was determined by the SBC optimal model order plus one. Figure 5-13 (a) displays a typical

flat wave usually observed in meditation EEG, with the 10-second S_{ch} brain mappings (p=6) beneath. According to our previous study [Lo et al. 2003, Chang and Lo 2005, Liao and Lo 2006], flat wave often emerges during deep meditation for some Zen meditators. Apparently, synchronization increased upon the occurrence of flat-wave activities. Results of meditator e2 reveals similar, yet weaker, synchronization behavior (Fig. 5-13(b), p=9). According to the post-experimental interview, meditation practitioners often enter into a more detached state of consciousness or sensory perception in deep meditation, that is, they are more detached in sensory-organ stimuli. Our preliminary results of LSTS analysis might provide an evidence for the deep meditation state accompanying the global spatiotemporal synchronization of brain electrical activities. Conversely, control subject c1 had α rhythm dominant EEG during the entire recording. Upon the α bursting (suppressing), an increasing (decreasing) synchronization was observed in the frontal region (Fig. 5-13(c), p=11), which was contemplated as the situation that the subject was performing some high level cognitive processes.
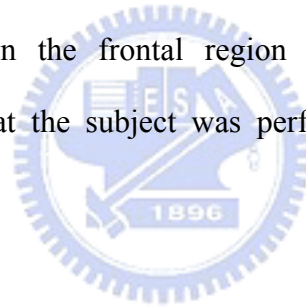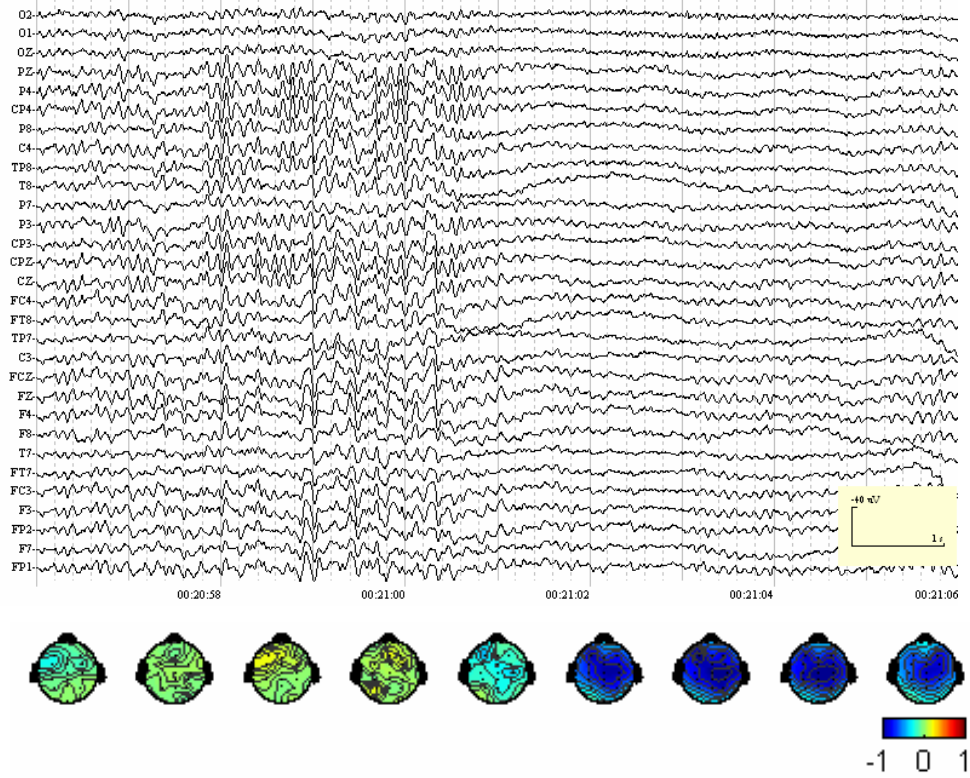
(a)
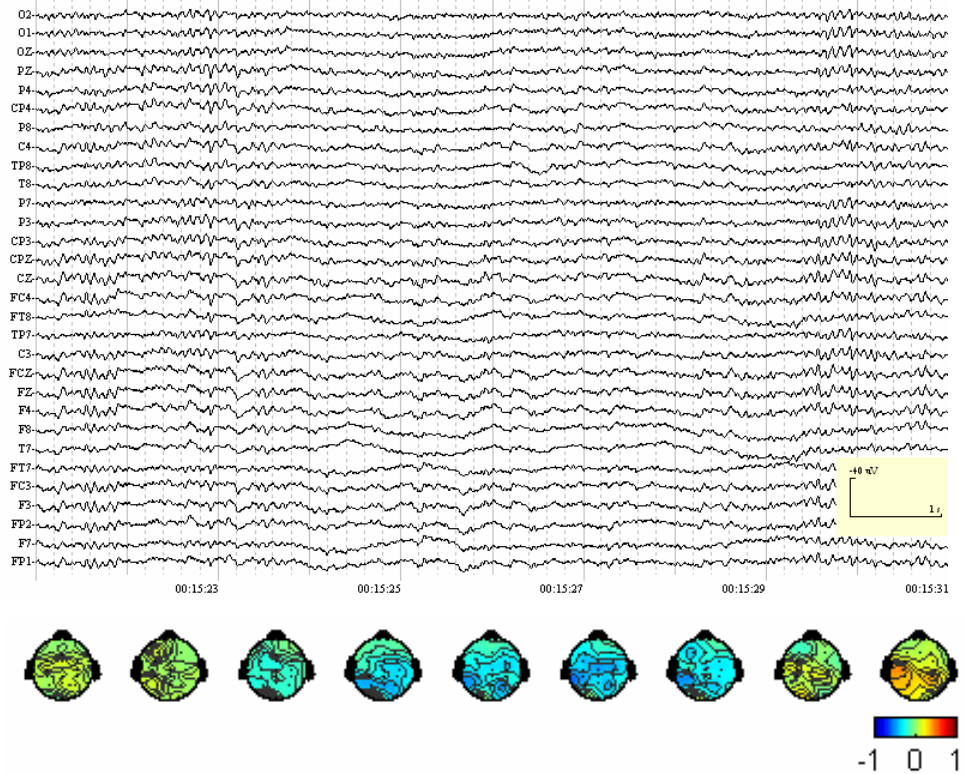
(b)

Figure 5-13: 10-second EEG signals and the evolving *S* brain mapping for (a) meditator

e1, (b) meditator e2, and (c) non-meditator c1.

(c)
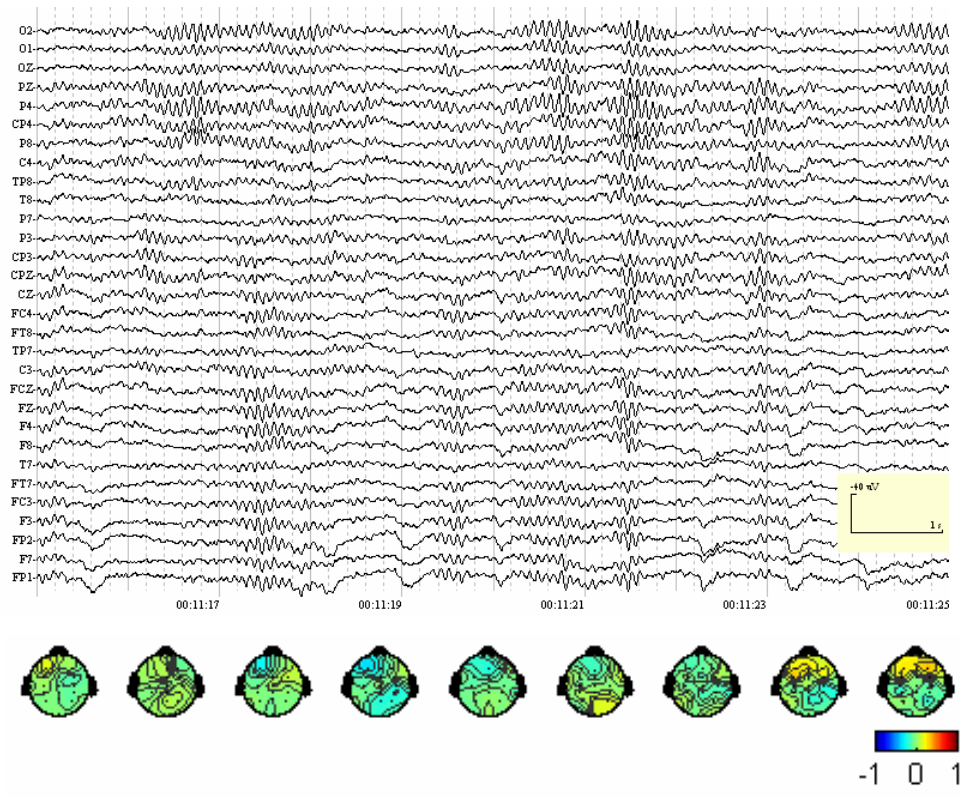
Figure 5-13 (Continued)

Chapter 6－

Discussion and Conclusion

The real end of science is the honor of the human mind.

~ Carl Jacobi

To explore and quantify the brain characteristics under Zen meditation, this dissertation presents methods and algorithms that were developed mainly on the basis of AR modeling, including both univariate and multivariate models. The proposed *Subband-AR-EEG Viewer* and LSTS index provide the quantitative characterization for the *Zen-meditation brain* in different aspects. The following content sums up results of this study and organizes into three key subjects.

6.1. Meditation EEG overview based on subband features quantified by AR model

In order to explore the meditation scenario, contents of the long-term EEG recorded during meditation need to be analytically quantified. Chapter 2 presented a systematic strategy for developing algorithms for automatic EEG interpretation. Based on the concepts of subband filtering and parametric modeling, a generalized computation scheme, called *Subband-AR-EEG Viewer*, was modified and adapted for different application purposes. With appropriate logic for examining the characteristic frequency, the *Subband-AR-EEG Viewer* could be further reduced to improve computational efficiency without affecting the performance. In

addition, the proposed scheme requires no implementing parameter. Another noticeable advantage is its feasibility for real-time, hardware realization and implementation. Since an order-2 AR model is employed, computational load is very light. For the example of slow α-rhythm detection in Section 2.3, the algorithm involved approximately $3.75N$ real multiplications (N: number of samples), which was a significant reduction in arithmetic operations compared with the fast Fourier transform (FFT) algorithm for rhythmic analysis. A spot evaluation of execution time required to determine $f_{r,1}$ - $f_{r,4}$ (based on one-channel, 0.5-sec EEG segment) is 0.008 sec on a Pentium4 1.8G, Windows-based computer. As a consequence, the algorithm proposed in this paper can process almost 60-channel EEG data in real time ($0.5/0.008 \cong 62$).

With the modification of *Subband-AR-EEG Viewer*, *meditation EEG interpreter* was presented in Chapter 4 and was applied to the exploration of spatiotemporal behavior of meditation EEG. The interpreter provides a systematic strategy for automatic EEG interpretation. By integrating the subband architecture with the AR model, various EEG rhythms can be effectively extracted. With empirically designed criteria implementing sound logic, the meditation EEG interpreter is able to identify even the low-power β pattern which is often cloaked in large-amplitude activities. In addition, those low-frequency rhythms with irregular waveform shape can be estimated more efficiently. Another noticeable advantage is its feasibility for hardware realization and real-time implementation with just a few implemention parameters.

Zen meditation EEG differs significantly from the normal relaxation EEG, with eyes closed, in the spatiotemporal characteristics of EEG spectra. According to the pattern histograms, we have noticed a significant distinction between two groups in four patterns, χ, δ, θ, and β. Meditation EEG exhibited relatively larger percentages of both χ and β activities that have been found to correlate highly with different consciousness states during Zen meditation [Lo et al. 2003]. The β% mapping demonstrated substantial occipital-β phenomena for the experimental subjects.

6.2. Visual perception under Zen-Meditation

In Chapter 3, we have reported an alternative strategy to investigate the effects of Zen-meditation on human brain. Alpha-dependent F-VEP analysis was suggested as a standardized and consistent scheme for investigating the event-related response dependency on oscillatory features of the meditation EEG. Without any access into the real system dynamics of the brain, scientific study requires manipulating the experiment under pre-specified conditions. Accordingly, alpha-dependent F-VEPs were collected under the consistent alpha-dominating background EEG that increased significantly during Zen meditation process. Based on the same scheme, the online α-detection algorithm could be modified for investigating the brain evoked response under given background EEG activity associated with other brain states, for example, theta- or beta-dominating background rhythms.

Our study has shown a great difference in the amplitudes of F-VEPs between the experimental and control group. Apparently, the meditation process modulates the amplitudes of F-VEPs under frontal α-rhythm emergence, especially components P1-N2 and N2-P2. These three peaks P1, N2 and P2, emerge respectively at about 80, 120 and 190 ms after photic stimulation. Moreover, such F-VEP amplitude variations for Zen-meditation practitioners were more consistent at the electrode locus Cz than at Fz. Since subjects mostly focused on the Zen Chakra (the third ventricle) during Zen meditation, we thus infer that meditation *focusing* changes the brain dynamics and the sensory responses to the external stimulus.

According to the literatures of visual function research, P1 component is generated from the major striate area, and N2 and P2 are generated from V4 which might be related to selective attention [Ducati et al. 1988, Tsutsui 1987, Skrandies 1995]. The increase of F-VEP amplitude indicates that Zen meditation, differing from normal relaxation, may cause some effects on primary visual cortex, central cortex, and frontal cortex. The study may assist in further understanding the intrinsic mechanism of such evidence as improving efficiency of the

concept learning and integrating the brain function via Zen-meditation that has been reported.

6.3. Spatiotemporal synchronization during meditation

To quantify the spatiotemporal synchronization subtly embedded in multi-channel EEG signals, a novel approach based on the evaluation of LSTS index was proposed and reported in Chapter 5. Note that high correlation among neighboring channels increases model predictability. Therefore the fitness of an mAR model for a set of multi-channel EEGs reflects the probability of predicting a channel from others. A small value of S (LSTS index) indicates a better fitness of the model for the empirical data.

To verify the feasibility of proposed approach for EEG spatiotemporal study, we conducted the externally-paced finger-movement experiments and reported the increasing S of the corresponding primary motor area while desynchronization took over. Development of this approach particularly was to disclose the unknown brain dynamics under Zen meditation. In our preliminary findings, flat-wave activities emerging during deep meditation exhibited globally spatiotemporal synchronization.

Unlike coherence or other event-related (de)synchronization analysis, the LSTS index evaluation does not require the pre-defined frequency ranges. Accordingly, the LSTS index might provide a quick inspection of EEG spatiotemporal characteristics and thus augment the understanding of brain dynamics under Zen meditation.

6.4. Summary

In this dissertation, both univariate and multivariate AR models are applied on the meditation EEG research. The scheme *Subband-AR-EEG Viewer* mainly based on univariate AR modeling and subband filtering was presented. Two applications, online α-detection and the

meditation EEG interpreter, were inferred from the scheme. The online α-detection algorithm assisted in the Alpha-dependent F-VEP collection. In comparison of F-VEP amplitudes between experimental and control groups, we hypothesized, according to the significant amplitude difference, that meditation process modulated the amplitudes of F-VEPs upon emergence of the frontal α-rhythm.

According to the results of the meditation EEG interpreter, significant larger percentages of both χ and β activities are identified in Zen-meditation scenario, especially in the occipital region. This phenomenon was considered to be highly correlated with specific consciousness states induced by Zen meditation. In addition to univariate AR model, the LSTS index based on multivariate AR model was proposed to investigate the spatiotemporal synchronization embedded in multi-channel meditation EEG. A globally spatiotemporal synchronization was discovered for the flat-wave activities, which might provide scientific evidence for the detached state of consciousness or sensory perception in deep meditation.
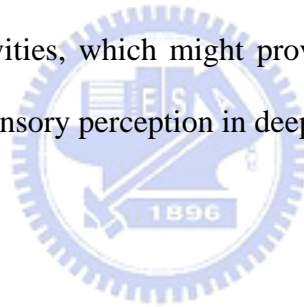
6.5. Future work

By using *Subband-AR-EEG Viewer*, we could derive algorithms to assist meditation EEG analysis. But due to inter-subject variations of physiological conditions are always complicated, the procedure and setup of experiments should be further readjusted or redesigned. In order to investigate into brain dynamics under specific meditation states, subjects should be limited to perform a specific meditation task during EEG recording, ex: focusing on Zen Chakra or counting breaths. Therefore, a strong correlation between meditation states and EEG characteristics might be revealed.

Beside experimental setup, an improved meditation EEG interpreter with high accuracy should be further derived. With this improved interpreter, we might be able to identify more meditation EEG patterns and different meditation scenarios. We could use LSTS index to ob-

serve synchronization phenomena of other meditation EEG patterns. Moreover, the catego-

rized scenarios could be used as a criterion to give stimuli while subjects are practicing medi-

tation. Thus we could inspect event-related potentials under specific meditation scenarios.

Then we might have a more comprehensive understanding of brain dynamics during medita-

tion.

Bibliography

Aftanas L.I., and Golocheikine S.A., "Human anterior and frontal midline theta and lower alpha reflect emotionally positive state and internalized attention high-resolution EEG investigation of meditation," *Neuroscience Letters*, vol. 310, pp. 57–60, 2001.

Agarwal R., Gotman J., Flanagan D., and Rosenblatt B., "Automatic EEG analysis during long-term monitoring in the ICU," *Electroencephalogr. Clin. Neurophysiol.*, vol. 107, pp. 44–58, 1998.

Agarwal R., and Gotman J., "Adaptive segmentation of electroencephalographic data using nonlinear energy operator," *Proc. IEEE ISCAS'99*, pp. 199–202, 1999.

Amir N. and Gath I., "Segmentation of EEG during sleep using time-varying autoregressive modeling," *Bio. Cybern.* vol. 61, pp. 447–455, 1989.

Anderson C.W., Stolz E.A., and Shamsunder S., "Multivariate autoregressive models for classification of spontaneous electroencephalographic signals during mental tasks," *IEEE Trans. Biomed. Eng.*, vol. 45, no. 3, pp. 277–286, 1998.

Banquet J.P., "Spectral analysis of the EEG in meditation," *Electroencephalogr. Clin. Neurophysiol.*, vol. 35, pp. 143–151, 1973.

Brodsky B.E., Darkhovsky B.S., Kaplan A.Y., and Shishkin S.L., "A nonparametric method for the segmentation of the EEG," *Comput. Meth. Prog. Bio.*, vol. 60, pp. 93–106, 1999.

Cahn B.R., and Polich J., "Meditation states and traits: EEG, ERP, and neuroimaging studies," *Psychol. Bull.*, vol. 132, no. 2, pp. 180–211, 2006.

Chang K.M., and Lo P.C., "Hurst exponents and linear regression with an application to low-power beta characterization in meditation EEG," *Am. J. Electroneurodiagnostic Technol.*, vol. 45, no. 2, pp. 130–138, 2005.

Creutzfeld O.D., Bodenstein G., and Barlow J.S., "Computerized EEG pattern classification

by adaptive segmentation and probability density function classification. Clinical evaluation," *Electroencephalogr. Clin. Neurophysiol.*, vol. 60, pp. 373–393, 1985.

Ding M., Bressler S.L., Yang W., and Liang H., "Short-window spectral analysis of cortical event-related potentialsby adaptive multivariate autoregressive modeling: data preprocessing, model validation, and variability assessment," *Biol. Cybern.*, vol. 83, pp. 35–45, 2000.

Ducati A., Fava E., and Motti E.D.F., "Neuronal generators of visual evoked potentials: intracerebral recording in awake humans," *Electroenceph. Clin. Neurophysiol.*, vol. 71, pp. 89–99, 1988.

Duckrow R.B., and Zaveri H.P., "Coherence of the electroencephalogram during the first sleep cycle," *Clin. Neurophysiol.*, vol. 116, pp. 1088–1095, 2005.

Elson B.D., Hauri P., and Cunis D., "Physiological changes in Yoga Meditation," *Psychophysiology*, vol. 14, no. 1, pp. 52–57, 1977.

Franaszczuk P.J., and Bergey G.K., "An autoregressive method for the measurement of synchronization of interictal and ictal EEG signals," *Biol. Cybern.*, vol. 81, pp. 3–9, 1999.

Gath I., and Michaeli A., "Two channel segmentation of EEG," *IEEE Engineering in Medicine and Biology Society 11th Annual International Conference*, vol. 5, pp. 1690, 1989.

Guger C., Schlögl A., Neuper C., Walterspacher D., Strein T., and Pfurtscheller G., "Rapid protyping of an EEG-Based Brain-computer Interface (BCI)," *IEEE Trans. Neural. Syst. Rehabil. Eng.*, vol. 9, pp. 49–58, 2001.

Güler İ., Kiymik M.K., Akin M., and Alkan A., "AR spectral analysis of EEG signals by using maximum likelihood estimation," *Comput. Biol. Med.*, vol. 31, no. 6, pp. 441–450, 2001.

Hayes M.H., *Statistical Digital Signal Processing and Modeling*. Canada: John Wiley and Son, 1996.

Hebert R., and Lehmann D., "Theta bursts: An EEG pattern in normal subjects practicing the Transcendental Meditation technique," *Electroencephalogr. Clin. Neurophysiol.*, vol. 42,

pp. 397–405, 1977.

Hughes J.R., Kuruvilla A., and Fino J.J., "Topographic analysis of visual evoked potentials from flash and pattern reversal stimuli: evidence for 'traveling waves'," *Brain Topogr.*, vol. 4, pp. 215–228, 1992.

Inouye T., Toi S., and Matsumoto Y., "A new segmentation method of electroencephalograms by use of Akaike's information criterion," *Cognitive Brain Res.*, vol. 3, pp. 33–40, 1995.

Jansen B.H., Hasman A., and Lenten R., "Piecewise analysis of EEGs using AR-modeling and clustering," *Comput. Biomed. Res.*, vol. 14, pp. 168–178, 1981.

Jevning R., Wallace R.K., and Beidebach M., "The physiology of meditation: A review. A wakeful hypometabolic integrated response," *Neurosci. Biobehav. Rev.*, vol. 16, pp. 415–424, 1992.

Kasamatsu A., and Hirai T., "An electroencephalographic study on the Zen meditation (Zazen)," *Folia Psychiatrica et Neurologica Japonica*, vol. 20, pp. 315–336, 1966.

Klimesch W., "Memory processes, brain oscillations and EEG synchronization," *Int. J. Psychophysiol.*, vol. 24, pp. 61–100, 1996.

Knyazev G.G., Savostyanov A.N., and Levin E.A., "Anxiety and synchrony of alpha oscillations," *Int. J. Psychophysiol.*, vol. 57, pp. 175–180, 2005.

Kraut M.A., Arezzo J.C., and Vaughan H.G. Jr, "Intracortical generators of the flash VEP in monkeys," *Electroencephalogr. Clin. Neurophysiol.*, vol. 62, pp. 300–312, 1985.

Kuś R., Kamiński M., and Blinowska K.J., "Determination of EEG activity propagation: pair-wise versus multichannel estimate, " *IEEE Trans. Biomed. Eng.*, vol. 51, no. 9, pp. 1501–1510, 2004.

Liao H.C., and Lo P.C., "Meditation EEG overview based on sub-band features quantified by AR model," *J. Intl. Soc. Life. Info. Sci.*, vol. 24, no. 1, pp. 19–28, 2006.

Liu C.Y., and Lo P.C., "Flash visual evoked potentials in Zen-Buddhist meditation," *in 3rd Eur. Med. Biol. Eng. Conf.*, Prague, 2005.

Lo P.C., Huang M.L., and Chang K.M., "EEG alpha blocking correlated with perception of inner light under Zen-Buddhism meditation," *Am. J. Chin. Med.*, vol. 31, no. 4, pp. 629–942, 2003.

Lo P.C., and Leu J.S., "Adaptive baseline correction of Meditation EEG," *Am. J. END. Technol.*, vol. 41, pp. 142–155, 2001.

Locatelli T., Cursi M., Liberati D., Franceschi M., and Comi G., "EEG coherence in Alzheimer's disease," *Electroencephalogr. Clin. Neurophysiol.*, vol. 106, pp. 229–237, 1998.

Lütkepohl H., *Introduction to Multiple Time Series Analysis*. 2nd ed, Berlin: Springer-Verlag, 1993, pp. 132–133.

Michael D., and Houchin H., "Automatic EEG analysis: a segmentation procedure based on the autocorrelation function," *Electroencephalogr. Clin. Neurophysiol.*, vol. 46, pp. 232–235, 1979.

Möller E., Schack B., Arnold M., and Witte H., "Instantaneous multivariate EEG coherence analysis by means of adaptive high-dimensional autoregressive models." *J. Neurosci. Meth.*, vol. 105, pp. 143–158, 2001.

Murata T., Takahashi T., Hamada T., Omori M., Kosaka H., Yoshida H., and Wada Y., "Individual trait anxiety levels characterizing the properties of Zen meditation," *Neuropsychobiology*, vol. 50, pp. 189–194, 2004.

National Center for Complementary and Alternative Medicine, "What is complementary and alternative medicine," http://nccam.nih.gov/health/whatiscam/, 2002.

Neumaier A., and Schneider T., "Estimation of parameters and eigenmodes of multivariate autoregressive models," *ACM Trans. Math. Softw.* vol. 27, no. 1, pp. 27–57, 2001.

Newberg A., Alavi A., Baime M., Pourdehnad M., Santanna J., and d'Aquili E., "The measurement of regional cerebral blood flow during the complex cognitive task of meditation: a preliminary SPECT study," *Psychiatry Res.: Neuroimaging Section*, vol. 106, pp. 113–122, 2001.

Niedermeyer E., and Lopes da Silva F., *Electroencephalography: basic principles, clinical applications and related fields*, 5th ed, Baltimore: Williams and Wilkins, 2004, pp.167–192.

Odom J.V., Bach M., Barber C., Brigell M., Marmor M.F., Tormene A.P., Holder G., and Vaegan, "Visual evoked potentials standard," *Doc. Ophthalmol.*, vol. 108, pp. 115–123, 2004.

Oppenheim A.V., Schafer R.W., and Buck J.R., *Discrete-Time Signal Processing*, 2nd ed, New Jersey: Prentice Hall, 1998.

Pagano R.R., Rose R.M., and Stivers R.M., and Warrenburg S., "Sleep during Transcendental Meditation," *Science*, vol. 191, pp. 308–310, 1976.

Pardey J., Roberts S., and Tarassenko L., "A review of parametric modeling techniques for EEG analysis," *Med. Eng. Phys.*, vol. 18, no. 1, pp. 2–11, 1996.

Pei X.M., and Zheng C.X., "Feature extraction and classification of brain motor imagery task based on MVAR model," *Proceedings of the International Conference on Machine Learning and Cybernetics*, Shanghai, pp. 3276–3730, 2004.

Peters B.O., Pfurtscheller G., and Flyvbjerg H., "Automatic differention of multichannel EEG signals," *IEEE Trans. Biomed. Eng.*, vol. 48, no. 1, pp.111–116, 2001.

Pfurtscheller G., Brunner C., Schlögl A., and Lopes da Silva F.H., "Mu rhythm (de)synchronization and EEG single-trial classification of different motor imagery tasks," *Neuroimage*, vol. 31, pp. 153–159, 2006.

Pfurtscheller G., and Lopes da Silva F.H., "Event-related EEG/MEG synchronization and desynchronization: basic principles," *Clin. Neurophysiol.*, vol. 110, pp. 1842–1857, 1999.

Pfurtscheller G., and Neuper C., "Motor imagery and direct brain–computer communication," *Proc. IEEE*, vol. 89, no. 7, pp. 1123–1134, 2001.

Philips W., "Adaptive noise removal from biomedical signals using warped polynomials," *IEEE Trans. Biomed. Eng.*, vol. 43, no. 5, pp. 480–92, 1996.

Schneider T., and Neumaier A., "Algorithm 808: ARfit—A Matlab package for the estimation of parameters and eigenmodes of multivariate autoregressive models," *ACM Trans. Math. Softw.*, vol. 27, pp. 58–65. 2000

Schwarz G., "Estimating the dimension of a model," *Ann. Statist.*, vol. 6, pp. 461–464, 1978.

Skrandies W., "Visual information processing: topography of brain electrical activity," *Biol. Psychol.*, vol. 40, pp. 1–15, 1995.

Takahashi T., Murata T., Hamada T., Omori M., Kosaka H., Kikuchi M., Yoshida H., and Wada Y., "Changes in EEG and autonomic nervous activity during meditation and their association with personality traits," *Int. J. Psychophysiol.*, vol. 55, pp. 199–207, 2005.

Thatcher R.W., North D., and Biver C., "EEG and intelligence: Relations between EEG coherence, EEG phase delay and power," *Clin. Neurophysiol.*, vol. 116, pp. 2129–2141, 2005.

Theodoridis S., and Koutroumbas K., *Pattern Recognition*. 2nd ed, San Diego: Academic Press, 1999.

Travis F., "Autonomic and EEG patterns distinguish transcending from other experiences during Transcendental Meditation practice," *Int. J. Psychophysiol.*, vol. 42, pp. 1–9, 2001.

Tsutsui J., "Dynamic topography of the visual evoked potentials," *Rinsh Noha*, vol. 29, pp. 445–449, 1987 (in Japanese).

Vaidyanathan P.P., *Multirate systems and Filter Banks*. 1st ed, New Jersey: Prentice Hall, 1993.

Vuckovic A., Radivojevic V., Chen,A.C.N. and Popovic D., "Automatic recognition of alertness and drowsiness from EEG by an artificial neural network," *Med. Eng. Phys.*, vol. 24, pp. 349–360, 2002.

Wallace R.K., *Neurophysiology of Enlightenment*, Iowa: Maharishi University of Management Press, 1986.

Wallace R.K., "Physiological effects of transcendental meditation," *Science*, vol. 167, pp.

1751-1754, 1970.

Wallace R.K., Benson H., and Wilson A.F., "A wakeful hypometabolic physiologic state," *Am. J. Physiol.*, vol. 221, pp. 795–799, 1971.

Watts A., *The way of Zen*, New York: Vintage, 1957.

Weiss S., and Rappelsberger P., "Long-range EEG synchronization during word encoding correlates with successful memory performance," *Cogn. Brain Res.*, vol. 9, pp. 299–312, 2000.

West M.A., "Meditation and the EEG," *Psychol. Med.*, Vo. 10, pp. 369–375, 1980.

Wolpaw J.R., Birbaumer N., McFarland D., Pfurtscheller G., and Vaughan T.M., "Brain-computer interfaces for communication and control." *Clin. Neurophys.*, vol. 113, pp. 767–791, 2002.

Woolfolk R.L., "Psychophysiological correlates of meditation," *Arch. Gen. Psychiatry*, vol. 32, pp. 1326–1333, 1975.

Xu M., Tomotake M., Ikuta T., Ishimoto Y., and Okura M., "The effects of qi-gong and acupuncture on human cerebral evoked potentials and electroencephalogram," *J. Med. Invest.*, vol. 44, pp. 163–171, 1998.

Zhang J.Z., Zhao J., and He Q.N., "EEG findings during special psychical state (Qi Gong state) by means of compressed spectral array and topographic mapping," *Comput. Biol. Med.*, vol. 18, no. 6, pp. 455–463, 1988.

Zhang W., Zheng R., Zhang B., Yu W., and Shen X., "An observation of Flash Evoked Cortical Potentials and qigong meditation," *Am. J. Chin. Med.*, vol. 21, pp. 243–249, 1993.

Vita and Publication List

Hsien-Cheng Liao received his B.S. degree in Electrical Engineering from National Chung-Hsing University, Taiwan, in 1998 and his M.S. and Ph.D. degrees in Electrical and Control Engineering from National Chiao-Tung University, Taiwan, in 2000 and 2007, respectively. His research interests include biomedical signal processing, statistical signal processing, machine learning, pattern recognition and classification. Please visit his homepage http://hsiencheng.liao.googlepages.com/ for more information.

Journal:

Liao, H.-C. and Lo, P.-C., "Meditation EEG Overview Based on Subband Features Quantified by AR Model," *the Journal of International Society of Life Information Science*, vol. 24, no. 1, 2006.

Liao, H.-C., Liu, C.-Y. and Lo, P.-C., "Investigation of Visual Perception under Zen-Meditation based on Alpha-dependent F-VEPs," *Journal of Biomedical Engineering Research*, vol. 27, no. 6, 2006.

Liao, H.-C. and Lo, P.-C., "Investigation on Spatiotemporal Characteristics of Zen-Meditation EEG Rhythms," *the Journal of International Society of Life Information Science*, vol. 25, no. 1, 2007.

Liao, H.-C. and Lo, P.-C., "Study on EEG Local Spatiotemporal Synchronization Based on Quantified Residuals of Multivariate AR Model," submitted to *Computational Intelligence and Neuroscience*, 2007 (revised).

Wu, L.-W., Liao, H.-C., Hu, J.-S., and Lo, P.-C., "Brain-Controlled Robot Agent: an EEG-Based eRobot Agent," submitted to *Computational Intelligence and Neuroscience*, 2007 (revised).

Conference:

Liao, H.-C. and Lo, P.-C., "Long-term Meditation EEG Interpretation Based on Subband AR Coefficients," *Proceeding of 2002 Annual Symposium of The Biomedical Engineering Society of ROC*, pp.E1.48-49, Dec. 2002.

Liao, H.-C. and Lo, P.-C., "Meditation EEG Classification by Subband Decomposed AR Coefficients," *Conference on Health and Management,* 2002. (In Chinese, with English abstract.)

Huang, C.-C., Liao, H.-C. and Lo, P.-C., "Development of Real-time HRV Analyzer and its Application to the Biofeedback System," *Proceeding of 2006 Annual Symposium of The Biomedical Engineering Society of ROC*, Dec. 2006.

Patent:

Wu, L.-W. and Liao, H.-C., "Architecture of an Embedded Internet Robot System Controlled by Brain Waves," ROC patent (Invention No. I 257214), June 21, 2006.

Wu, L.-W. and Liao, H.-C., "Architecture of an Embedded Internet Robot System Controlled by Brain Waves," US Patent Application No. 11/296,217 (allowed for issuance as a patent, April 26, 2007)

Honors and Activities:

- Honorable mention, National Chiao-Tung University's Architecture Photography Contest, 2006.
- 09/2003 ~ 08/2004: Scholarship for "Sandwich Programme" (Research visits to German universities or research institutes. The scholarship is supported by the German Academic Exchange Service and the National Science Council, Taipei)
- Honorable mention, National Chiao Tung University's Lotus Photography Contest, 2002.
- 09/2000 ~ 06/2002: The fellowship of the ring, Department of Electrical and Control Engineering, National Chiao Tung University
- 09/1996 ~ 06/1997: The president of the Chinese Original Quiet Sitting Club, National Chung-Hsing University